© Copyright by Balakrishnan Raja 2014
All Rights Reserved

IMMUNOLOGICAL AND MOLECULAR TECHNIQUES FOR POINT-OF-CARE DIAGNOSTICS

A Dissertation

Presented to

the Faculty of the Department of Chemical and Biomolecular Engineering

University of Houston

In Partial Fulfillment

of the Requirements for the Degree

Doctor of Philosophy

in Chemical and Biomolecular Engineering

by

Balakrishnan Raja

December 2014

IMMUNOLOGICAL AND MOLECULAR TECHNIQUES FOR POINT-OF-CARE DIAGNOSTICS

_____

(Balakrishnan Raja)

Approved:

_____

Chair of the Committee
Richard C. Willson, Professor,
Chemical and Biomolecular Engineering

Committee Members:

_____

Jacinta C. Conrad, Assistant Professor,
Chemical and Biomolecular Engineering

_____

Navin Varadarajan, Assistant Professor,
Chemical and Biomolecular Engineering

_____

Paul Ruchhoeft, Associate Professor,
Electrical and Computer Engineering

_____

Wei-Chuan Shih, Assistant Professor,
Electrical and Computer Engineering

_____

Suresh K. Khator, Associate Dean,
Cullen College of Engineering

_____

Michael Harold, Professor and Chair,
Chemical and Biomolecular Engineering

IMMUNOLOGICAL AND MOLECULAR TECHNIQUES FOR POINT-OF-CARE DIAGNOSTICS

An Abstract

of a

Dissertation

Presented to

the Faculty of the Department of Chemical and Biomolecular Engineering

University of Houston

In Partial Fulfillment

of the Requirements for the Degree

Doctor of Philosophy

in Chemical and Biomolecular Engineering

by

Balakrishnan Raja

December 2014

ABSTRACT

The development of technologies that enable early and accurate diagnosis is critical to the management of infectious diseases, especially with highly transmissible pathogens or in cases where the early administration of the right antibiotics could be life-saving. Demonstrating the presence of the relevant pathogen, rather than looking for serological markers, is the surest and fastest way of confirming an infection and diagnosing a disease. In this biosensing approach, pathogenic bacteria, viruses and protozoa, along with their secreted proteins and constituent nucleic acids are the principal analytical targets. Rapid screening tests, suitable for use as point-of-care (POC) devices by minimally trained personnel in decentralized laboratories and in the field, can be useful in diagnosing patients presenting with non-specific symptoms and in expediting control measures to manage emerging infectious diseases or in the unfortunate event of a bioterror attack. In this work, two POC-friendly technologies have been developed and evaluated analytically and/or clinically.

The first assay used embedded, microfabricated linear retroreflectors as bio-sensing surfaces and micron-sized magnetic particles as light-blocking labels in a semi-homogeneous format, resulting in a highly sensitive diagnostic immunoassay. The magnetic properties of the particle labels were useful in sample pre-concentration to increase sensitivity, while fluidic force discrimination was used to increase specificity of the assay. This assay, which was readout by an automated sample capture and imaging approach, was determined to have a limit of detection of less than 4000 *R. conorii* per mL from buffer.

Also, a panel of rapid assays based on Recombinase Polymerase Amplification, an isothermal nucleic acid amplification technique, were developed for the detection of urinary tract infection (UTI) causing bacteria. The five assays developed as part of this panel detected 100 genomes per reaction or less in around ten minutes, and showed no cross-reactivity with high concentrations of non-specific gDNA. The assay panel's overall clinical sensitivity, as determined from a 25-sample cohort of culture-positive urine samples, was 84%, and the clinical specificity, determined using a 10-sample cohort of culture-negative urine samples, was 100%.

TABLE OF CONTENTS

LIST OF FIGURES

LIST OF TABLES

CHAPTER 1 – INTRODUCTION

In vitro diagnostics

Human diseases can be broadly categorized, based on the mechanisms underlying them, into infections, cancers, auto-immune diseases, inflammations, degenerative diseases and those caused by accidents or poisoning[1]. For all these types of diseases, accurate diagnosis is a critical step in disease management and enabling positive outcomes for patients. In addition to obtaining a detailed medical history and performing a physical examination, physicians often require the assistance of diagnostic tests or procedures to identify the cause of a patient's signs and symptoms. Diagnostic tests, often called diagnostics, include *in vivo* procedures on the patient and *in vitro* testing of patient samples, and can be invasive, non-invasive or minimally invasive in nature. For the purposes of this dissertation, "diagnostic tests" will refer to *in vitro* diagnostic tests (IVDs) – tests that are performed on samples taken from the patient's body. Besides diagnosis, IVDs are used to guide healthcare decision-making in areas including risk assessment, disease staging and prognosis, therapeutic selection and treatment monitoring, and long-term disease management (Table 1)[3-4]. IVDs are also used as screening tests, which refer to a single test or a series of tests performed on individuals that might not be symptomatic, but are part of a defined risk group of the population based on their age, sex, occupation, etc. Screening tests are generally used to aid the prevention of disease, and can also help monitor disease prevalence or gain epidemiological data. Based on 2007 data from the Centers for Medicare and Medicaid (CMS) and Online Survey, Certification, and Reporting (OSCAR) databases, the Centers

for Disease Control and Prevention (CDC) estimates that approximately 6.8 billion IVDs are performed annually in the United States[3].

Table 1. Different uses of *in vitro* diagnostics (IVDs)

IVD test use	IVD test purpose and/or benefit	Examples
Screening and risk assessment, and early detection	Screening asymptomatic individuals for risk factors and developing or latent disease. Often credited with reducing incidence rates of disease.	• Breast cancer (BRCA) gene analysis; identifies pre-disposition to breast and ovarian cancer • Chlamydia screening by PCR; annual screening recommended by the CDC for women under 25 years. • Papanicolaou test (Pap test or Pap smear) for cervical cancer
Diagnosis	Typically used in symptomatic patients. Helps "rule in" or "rule out" a particular disease or condition.	• Brain natriuretic peptide (BNP) levels in plasma to assess recent heart failure. • PCR test for Dengue fever in patient presenting with fever in Dengue-endemic region.
Disease staging and prognosis	Used to determine the extent of progression of the disease and its severity, and the probability of recurrence.	• Oncotype DX™ - genetic test that quantifies the probability of breast cancer recurrence • Blood clotting tests for pre-surgical risk assessment
Therapeutic selection, treatment and monitoring	Allows targeted dosage and treatment, and monitoring of treatment efficacy.	• Viral load, CD4 count, complete blood count, and blood chemistry for assessing treatment response in patients with HIV • Alpha-fetoprotein (AFP) tests are used to monitor the effectiveness of therapy for cancers of the liver, testes or ovaries
Long-term monitoring	To understand disease course (usually for chronic diseases) and change treatment plans.	• Blood glucose and/or HbA1c testing for diabetes monitoring. • Cholesterol tests for patients with coronary artery disease.

Table 1 provides an overview, with examples, of the different applications of IVDs across the patient care continuum. Some of the examples provided might fit into

more than one category. IVDs are typically based on biosensors that detect the presence of one or more biomarkers from a sample of a body fluid. 'Biomarkers', in the diagnostic context, refer to measurable analytes indicative of the diseased state of a patient. In a diagnostic or screening test, these biomarkers serve as the analytical "target" for the biosensing technology that underlies the test. These analytical targets include proteins, nucleic acids, metabolites, drugs, dissolved ions and gases, human cells and microbes, found in blood, saliva, urine or other bodily fluids or (semi)solids[5]. Examples of IVDs include over-the-counter pregnancy test kits or blood glucose tests; laboratory tests for infectious disease, such as HIV or Tuberculosis, and tests performed in the doctor's office for Group A *Streptococcus* or Influenza A/B infections; and nucleic acid amplification or sequencing-based tests for various genetic diseases or conditions. More recently, specific IVDs, called companion diagnostics, are beginning to be used to select the right therapy, dosage and time of administration based on a patient's individual biology - this is often referred to as personalized medicine[6].

Infectious diseases and their diagnosis

Around 15 million (> 25%) of the 57 million annual deaths worldwide are estimated to be directly related to infectious diseases[7]. They are caused by pathogenic organisms such as bacteria, viruses, fungi and parasites; they may be transmitted, directly or indirectly, from one person to another. With the advancement of biosensing technologies over the last few decades, a physician's assessment of infectious diseases has evolved from a syndromic approach based on personal experience to being focused on the scientific method, and evidence-based treatment[8]. The systematic clinician's approach to diagnosing infectious diseases includes, in general chronological order:

1. Clearly understanding disease pathogenesis and mechanisms.
2. Identifying the patient's chief complaint and obtaining a chronologically accurate medical history.
3. Formulating a differential diagnosis using a combination of the chief complaint and medical history.
4. Conducting physical examination maneuvers that will support or contradict the differential diagnoses.
5. Ordering appropriate diagnostic and laboratory tests and interpreting the results in relation to the differential diagnosis.
6. Implementing an appropriate treatment plan

Infectious diseases are diagnosed by demonstrating the presence of the pathogen itself, or a surrogate marker of infection. Traditional clinical microbiological techniques, still widely practiced for the diagnosis of certain infectious diseases, include microscopy (pathogen identification based on morphological characteristics and gram staining) and culture (specific identification after using artificial growth media to grow bacteria or fungi, and tissues for virus propagation) techniques. These techniques are generally highly specific to the pathogen being tested for (depending on the skill of the microbiologist), but suffer from having long turnaround times (days to weeks from sample to result) and having their sensitivity be reliant on sample storage and transport conditions. Alternatively, diagnostic immunology (immunoassays) and molecular diagnostics are two broad categories of techniques that are used in IVDs for infectious diseases; they almost always have a faster time-to-result than culturing techniques irrespective of the format of use. Immunoassays are based either on the direct detection

of a microbial antigen specific to the infection, or the detection of the patient's serological response to an infection. On the other hand, molecular diagnostics are based on the detection of specific nucleic acid sequences from a microbial genome, either directly or following amplification.

Point-of-care testing for infectious diseases

The primary aim of point-of-care (POC) diagnostic tests is to reduce the turnaround time between sample collection and test results, thereby allowing clinicians and patients to make a quick clinical decision. Diagnostic laboratories are mostly centralized facilities requiring highly trained staff and specialized, expensive equipment that need regular maintenance by skilled technicians. Consequently, several laboratory-based tests have slow turnaround times in addition to being cost-prohibitive and inaccessible to patients in resource-limited areas of developed countries and a majority of the population in developing countries. The timely initiation of appropriate therapy, usually contingent upon the result of a diagnostic test, is especially vital in the clinical management of infectious diseases. According to some estimates, effective POC tests for only four infections (bacterial pneumonia, syphilis, malaria, and tuberculosis) could prevent more than 1.2 million deaths each year in developing countries[9-11].

The introduction of the rapid blood glucose test in 1962[12] followed by the rapid pregnancy test in 1977[13] heralded the era of POC testing, with tests having been developed for several diseases and medical specialties in the decades that followed[2, 14]. POC tests have been given dozens of definitions in the literature that vary slightly from each other, and have no accepted universal definition. Examples include: "a diagnostic test that is performed near the patient or treatment facility, has a fast turnaround time, and

may lead to a change in patient management"[15], and "any test that is performed at the time at which the test result enables a clinical decision to be made and an action taken that leads to an improved health outcome"[16]. The key elements of all definitions of POC tests are the 'near patient' aspect and rapid turnaround time (a few minutes to a few hours) that help expedite clinical decisions, typically leading to follow-up actions in the same clinical encounter.

In addition to these key elements, POC tests should have features specific to the target purpose, target user, and target setting. For example, POC tests intended to be used by (a) lay people for home-based self-testing, (b) healthcare workers to monitor disease prevalence in Zambia, and (c) physicians in intensive care units, can be expected to have radically different features. It is widely believed that all POC tests should satisfy most or all of the "ASSURED" criteria (**A**ffordable, **S**ensitive, **S**pecific, **U**ser-friendly, **R**apid and robust, **E**quipment-free and **D**eliverable to end users) laid out by the World Health Organization (WHO)-led Sexually Transmitted Diseases Initiative in 2006[17]. While the ASSURED criteria provide a good framework for the evaluation of new POC tests, attempting to strictly adhere to them imposes restrictions on the concept of POC testing. In the right context, POC tests that require hand-held or benchtop equipment or those that are not as cheap as dipstick tests could be cost-effective and have positive outcomes. POC tests should therefore be developed and evaluated on a case-by-case basis using a framework such as the one proposed by Pai et al., which encourages the viewing of POC testing as a spectrum of technologies (simple to more sophisticated), users (lay persons to skilled technicians), settings (homes to hospitals) and purposes (triage and referral, diagnosis, treatment, monitoring) (Figure 1).

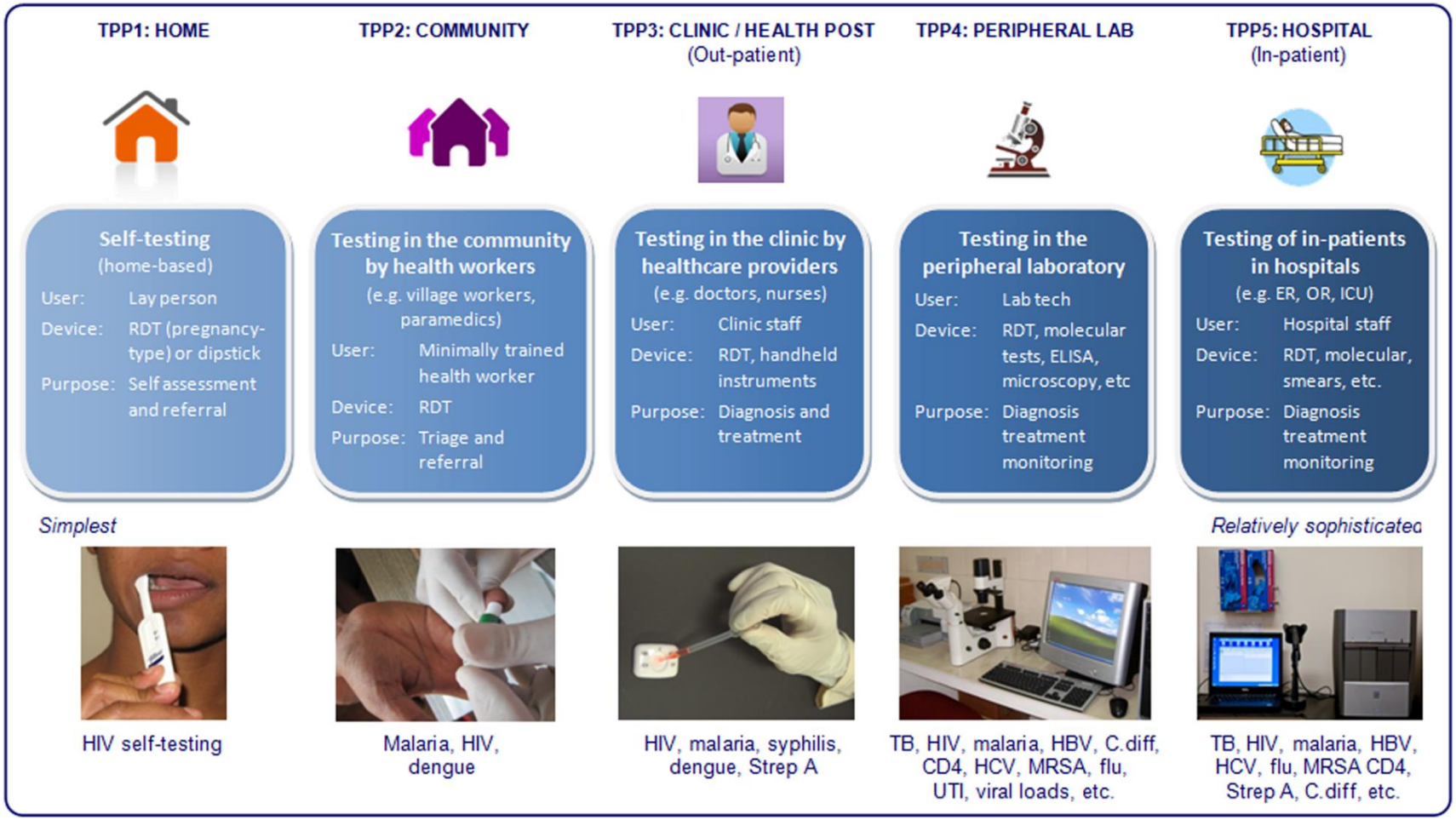

Figure 1. The wide spectrum of POC settings and user training dictates the acceptable level of test format complexity. HBV, hepatitis B virus; HCV, hepatitis C virus; UTI, urinary tract infection; MRSA, methicillin-resistant staphylococcus aureus; C. diff, clostridium difficile; RDT, rapid diagnostic test; Strep A, group A *Streptococcus*; TPP, target product profile. Figure re-used from PLOS Medicine article;[2] doi:10.1371/journal.pmed.1001306.

Performance evaluation of diagnostic tests

The accuracy and reliability of diagnostic tests for infectious diseases are most commonly measured using the broad terms ‘sensitivity’ and ‘specificity’. There are two kinds of sensitivity and specificity: analytical, and clinical (or diagnostic). Despite there being important differences between analytical sensitivity and clinical sensitivity, these terms are often interchangeably used without explicitly distinguishing them by their adjectives. The same error is also made with analytical specificity and clinical specificity[18]. The loose and incorrect use of these terms leads to confusion, like when a “highly sensitive” test ends up having a high rate of false negatives or a “highly specific” test gives false-positive results. For example, in prospective clinical studies, up to 15% of patients who were seropositive for human immunodeficiency virus type 1 (HIV-1) infection tested negative with the “ultrasensitive” polymerase chain reaction (PCR) assay[19-20].

Analytical sensitivity

The analytical sensitivity of an assay, synonymous with limit of detection (LOD), is the assay’s ability to detect a particular low concentration of analyte in a particular sample matrix. Analytical sensitivities are expressed as concentrations in a particular biological sample (for example, 50 genome copies per mL blood or 2 ng per L serum). Analytical sensitivity is also used, albeit less commonly, to indicate an assay’s ability to detect a change in concentration of analyte. The smaller the change detected, the better the analytical sensitivity. The analytical sensitivity of an assay is determined one of two ways: empirically, by testing serial dilutions of well-characterized samples with known

analyte concentrations; or statistically, by testing multiple 'blank' or 'negative' samples to establish a baseline signal and picking a value 3 or more standard deviations above that baseline as the lower limit of detection.

Analytical specificity

The analytical specificity of an assay is its ability to exclusively detect and/or identify the target analyte rather than similar-but-different substances in a sample. Examples include the detection of HIV-1 and not HIV-2, or detecting *Enterococcus faecalis* rather than *Enterococcus faecium*. A comprehensive evaluation of analytical specificity would call for testing an exhaustive number of well characterized samples with varying concentrations of similar-but-different analytes and/or interfering substances.

Clinical sensitivity and specificity

An assay has to be tested using real patient samples, in comparison to a reference or "gold" standard test, to determine its clinical sensitivity and specificity. The reference test is used to determine the number of "truly" infected and uninfected patients. The clinical sensitivity of an assay is the probability that an individual that tests positive is truly infected, while the clinical specificity is the probability that an individual that tests negative is truly uninfected. These numbers are usually expressed as proportions or percentages. The clinical sensitivity, by definition, does not correlate with the ability to detect very low concentrations of an analyte (analytical sensitivity). On the other hand, an assay that has high analytical specificity could end up having low clinical specificity (leading to false positives) because of the detection of contaminants, interfering substances, or carryover analyte from previous experiments. The latter is especially true

of assays such as PCR, which are extraordinarily sensitive analytically – the slightest carryover of analyte can result in a falsely positive result. Diagnostic predictive values (positive predictive values and negative predictive values) can sometimes be more important than clinical sensitivities or specificities (which are operational characteristics) from a clinician's perspective; this is because they account for the prevalence of the disease in specific populations. For example, a diagnostic test with a seemingly high clinical specificity of 95% would most likely be unsuitable for screening a population with a disease prevalence of only 1%. The number of false positives would be five times the number of true positives, resulting in a positive predictive value of only 17%.

Outline of work

This dissertation details the development and validation of two POC assays: a microfluidic assay, based on optical detection, for the immunological detection of *R. conorii* bacteria (Chapter 2), and an assay panel for the molecular detection of urinary tract infection (UTI) causing bacteria (Chapter 3). In their final envisioned forms, these assays will fit target product profiles 4 and 5 of the POC spectrum illustrated in Figure 1. Also, in collaboration with a centralized laboratory in Houston (Medical Center Laboratories), the assays developed in Chapter 3, along with other molecular techniques, were used in the clinical evaluation of a POC benchtop molecular diagnostic platform, the FilmArray system, for UTI diagnostics (Chapter 4).

Chapter 2 discusses the development of an amplification-independent immunodiagnostic platform for pathogen detection. The platform is based on using superparamagnetic microparticles for sample preparation and concentration, and as light-blocking optical labels, in a microfluidic chip-based immunoassay. Embedded

microretroreflectors, fabricated using an easily scalable process, served as the solid phase in the sandwich immunoassay, and assay readout was carried out using an automated, calibration-independent difference imaging approach that is demonstrated by using *R. conorii* bacteria as a model analyte.

Chapter 3 describes the development of a panel of molecular diagnostic assays based on Recombinase Polymerase Amplification (RPA), an isothermal nucleic acid amplification technique (NAAT). RPA has shown great promise as a potential POC NAAT in recent years; in this work, real-time RPA assays (< 15 min to result) for the top six urinary tract infection (UTI) pathogens (*Escherichia coli, Proteus mirabilis, Pseudomonas aeruginosa, Klebsiella pneumoniae, Enterococcus faecalis* and *Enterococcus faecium*) were developed and validated using reference genomic DNA and well-characterized, archived clinical samples.

Chapter 4 details the clinical evaluation of the FilmArray system's Blood Culture Identification (BCID) Panel (Biofire Diagnostics, Salt Lake City, UT) for the detection of pathogens from patients suspected of having UTIs. Urine samples were tested using the FilmArray BCID panel and conventional microbiological gold standard culture methods by Medical Center Laboratories (Houston, Texas). The true bacterial ID of the discordant samples generated as part of this study was determined by a combination of PCR, Sanger sequencing, and the real-time RPA methods developed in Chapter 3.

CHAPTER 2 – AN EMBEDDED MICRORETROREFLECTOR-BASED MICROFLUIDIC IMMUNODIAGNOSTIC PLATFORM

Introduction

Immunoassays

Immunoassays are a commonly used technique for the detection of proteins, hormones, antibodies, bacteria, viruses, food contaminants and other molecules. They are a very important protein analysis technique, and have been a routine practice in medicine since the pioneering work on radioimmunoassays for insulin detection by Yalow and Berson in the 1950s[21]. They rely on the ability of antibodies, which are proteins produced by the immune system of animals in response to foreign invasion, to bind specifically to one or more regions (epitopes) of an analyte (antigen). Immunoassays do not involve analyte amplification and typically involve the labeling of analyte-specific antibodies with a dye, fluor, enzyme or particle to produce a detectable signal. The antibodies used in immunoassays, which bind specifically and with high affinity to target analytes, are manufactured by first immunizing animals (rabbits, mice, sheep, etc.) and harvesting their serum or spleen cells (depending on whether the antibodies are monoclonal or polyclonal), followed by further processing and purification. Alternately, they are selected from phage display libraries. From a structural perspective, antibodies commonly used in immunoassays are of the Immunoglobulin G isotype (IgG). IgGs are protein complexes composed of four peptide chains (two identical heavy chains and two identical light chains) arranged in a Y-shape, with dimensions[22] of roughly 15 nm H x 8

nm L x 4 nm W (Figure 2). The avidity of antibody-antigen binding is brought upon by a combination of the structural "lock and key" mechanism and non-covalent interactions including hydrogen bonding, electrostatic interactions, and hydrophobic interactions. The different applications of biosensors based on immunoassays include biodefense, medical diagnostics, and environmental monitoring, which often demand highly sensitive and selective systems with operational complexity and cost requirements specific to the application.

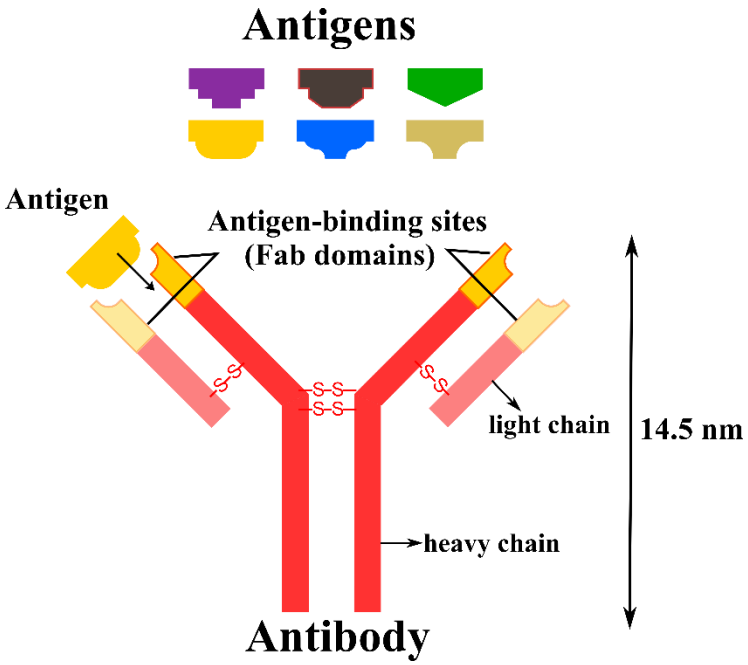

Figure 2. Illustration of an IgG antibody molecule. The light and heavy peptide chains are held together by disulfide bonds. Fab domains are responsible for specific antigen-binding.

Solid-phase sandwich immunoassays

A typical sandwich immunoassay, illustrated in Figure 3, uses an antibody-modified solid-phase to capture the analyte from a sample, and a secondary antibody modified with a highly detectable label for signal transduction. Examples of solid-phase sandwich immunoassays include enzyme-linked immunosorbent assays (ELISAs) and lateral flow assays (LFAs), which use polystyrene microtiter plates and porous

nitrocellulose membranes as the solid phase, respectively. ELISAs use enzymes, such as peroxidases or phosphatases, as labels. LFAs, the most common examples of which are home pregnancy tests that detect the hormone human chorionic gonadotropin from urine, use gold nanoparticles as labels. The signal from the label is representative of the amount of analyte originally present in the sample.

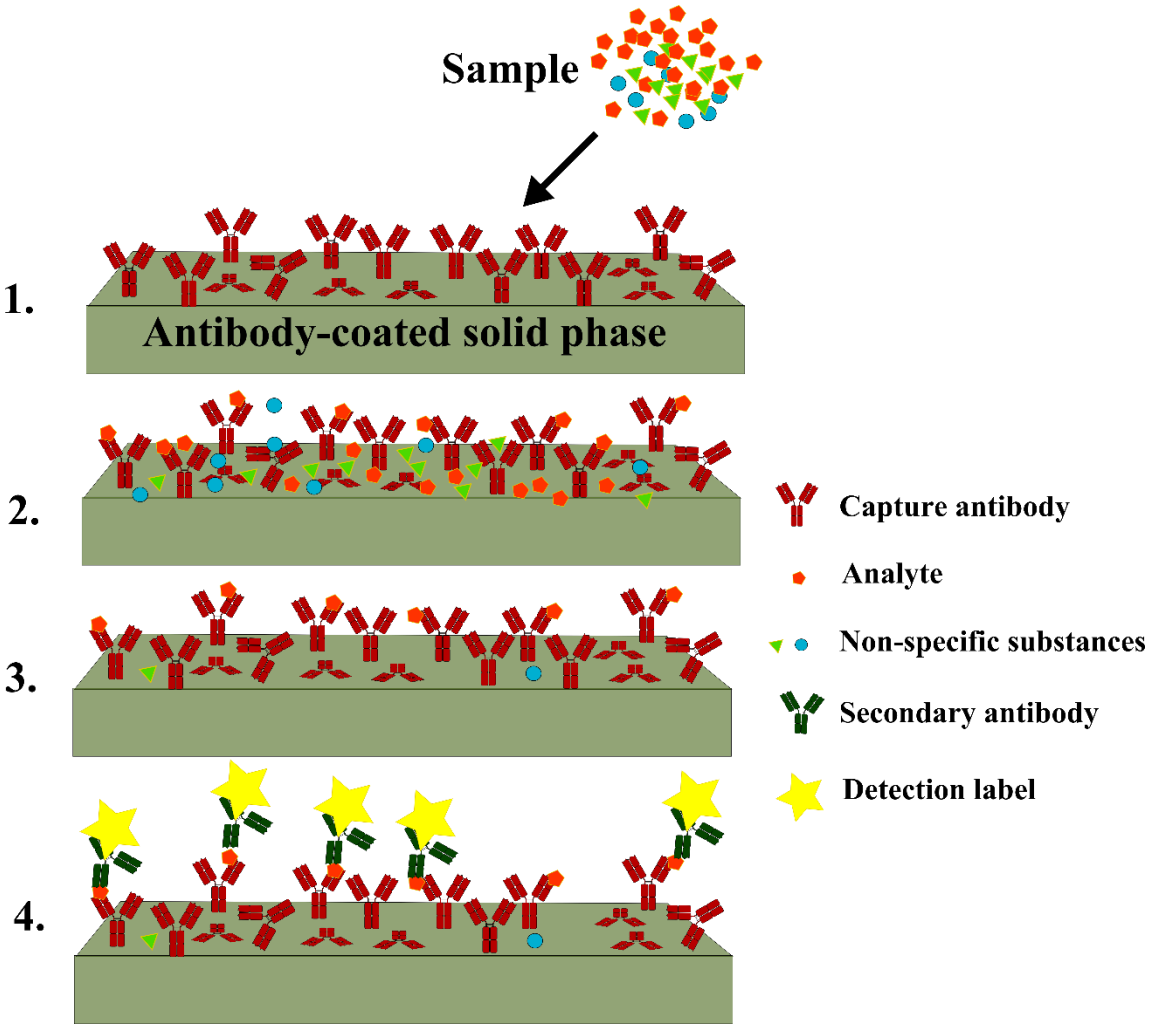

Figure 3. Sequential solid-phase sandwich immunoassay. 1. Sample addition and incubation; 2. Specific and non-specific (van der Waals, electrostatic) interactions; 3. After washing; 4. Completion of the immuno-sandwich.

ELISAs are not easily adaptable to POC use because they require elaborate, expensive instrumentation that is difficult to miniaturize, and suffer from signal

quenching and photobleaching of unstable labels. On the other hand, the low analytical sensitivity, subjective interpretation, and the limited quantitative or multiplexing ability of LFAs limits their application to a wide range of diagnostic problems.

Microfluidic immunoassays

Traditional immunoassays (ELISAs, for example) rely on macroscopic liquid handling systems such as microtiter plates. Microfluidic technology, the origins of which can be traced to high-precision analytical methods such as high-pressure liquid chromatography and continuous inkjet printing[23], has given assay developers a plethora of tools and techniques that enable immunoassay development in POC-friendly formats for several detection modalities. The advantages of assays performed in microfluidic channels, which have dimensions of tens to hundreds of micrometers, include: smaller device footprints and sample or reagent quantities; shorter assay times; well-defined and precisely controllable laminar flow; more robust statistics from redundant, miniaturized detection regions; faster heat or mass transfer; and the dominance of surface phenomena over volume phenomena[24]. The degree of integration of microfluidics into immunoassays intended for POC use can vary from having disposable microfluidic chips that require external equipment to operate (pumps, reader device), to fully integrated chips that can report test results after processing and analyzing samples. The selection criteria for the degree of integration include the desired device portability and cost per test, which tie back to the envisioned target product profile (Figure 1).

At the broadest level, microfluidic chips used for immunoassays have two generic components. The first component is a method of introducing samples and reagents to the chip and moving them around in a controlled manner – this is done by methods including

pressure-driven laminar flow (using syringe pumps), capillary flow, electrokinetic flow, and centrifugal flow. The second component of microfluidic chips enables labeling-induced signal transduction or a label-free readout strategy – an example of the former is simply the surface modification of the channel with analyte-specific antibodies, while the latter includes the fabrication of field effect transistors[25-26], cantilevers[27] or resonant optical waveguides[28-29], and the exploitation of phenomena such as surface plasmon resonance[30] and surface acoustic waves[31].

Label-based analyte detection in microfluidic assays

Optical detection is the most common label-based analyte detection method in microfluidic immunoassays. Fluorescence is a commonly exploited phenomenon – the analyte is labeled using a detection antibody or antibody fragment carrying fluorophores, fluorescent proteins, quantum dots, or other fluorescent nanoparticles, and typically read out using a combination of magnifying optics that have direct or engineered optical paths that enhance signal, and CCD cameras[32-35]. Miniaturization is difficult for absorbance-based or colorimetric detection due to the long optical paths required for signal accumulation. Chemiluminescence, which is independent of an excitation source and therefore involves a simpler optical path, has been integrated into microfluidics[36], but involves specialized reagents and enzymes. Fluorescent readout hardware is typically complex, expensive and difficult to maintain, while chemiluminescence assays require multiple liquid handling steps to introduce several chemical reagents. In contrast, the use of reflective labels such as silver precipitates, the formation of which is catalyzed by gold nanoparticle-labeled detection antibodies, can be read with a standard optical disk reader.[37] Another example of reflection-based detection is the use of nanoparticles to

frustrate total internal reflection of antibody-modified surfaces; this method has been shown to detect picomolar protein concentrations[38]. Electrochemical detection has been used as a successful non-optical detection modality. Electrochemical microfluidic assays typically use enzyme-labeled capture or detection antibodies along with hydrogen peroxide as the substrate[39-40].

Magnetic bead-based analyte detection in microfluidic assays

Magnetic "beads" are nanometer or micrometer-sized particles that have well-characterized compositions and surfaces in addition to being widely commercially available with many different functional groups. Immunoassay procedures including analyte capture, concentration and purification are greatly facilitated by magnetic beads, which can be easily manipulated and separated using an inexpensive permanent magnet. Magnetic beads used in immunoassays are typically superparamagnetic and therefore do not aggregate in the absence of a magnetic field (due to zero magnetization), adding to the attractiveness of using them for analyte capture. They can be used as an analyte-capture substrate only, as label only, or as both substrate and label. Microfluidic assays that use magnetic beads solely as analyte-capture substrates have been developed for electrochemical detection[41], electrochemiluminescence[42-43], mass spectrometry[44] and surface-enhanced Raman scattering[45-46], and have been commercialized by the Luminex xMAP platform that uses fluorescent detection[47].

The autofluorescence and electrochemical background of complex sample matrices such as whole blood, which are problems that plague fluorescent or amperometric labels, do not pose a problem when magnetic beads are used as labels. Microfluidic assays that use magnetic beads as both substrates and labels have been

developed as either agglutination-monitoring assays[46, 48] or "surface coverage" assays[49-51]. The former is usually the microfluidic adaptation, with the added advantage of magnetic manipulation, of a popular macroscopic POC assay format in which the visual observation of analyte-induced aggregates of latex or gold nanoparticles serves as the readout.

"Surface coverage" assays are very frequently observed in the published literature – the differences between them usually come down to the techniques used to sense magnetic bead labels bound to the surface. In the semi-homogeneous, non-sequential version of these assays, capture antibody-modified magnetic beads are used for sample preparation and/or concentration to capture analytes, followed by flowing them into the channel (pressure-driven or electrophoretic flow) for completion of the immunosandwich. In the sequential version of these assays, the analyte is initially introduced into capture antibody-modified microfluidic channels for capture and followed by secondary antibody-modified magnetic beads to complete the immunosandwich. In both versions, the "bead count" after assay completion, expected to represent the number of specifically bound, analyte-sandwiching beads bound to the sensor surfaces, serves as readout.

The techniques that have been used thus far to obtain "bead counts" in such assays include (i) direct inspection and counting using an optical microscope, which has been used to detect, for example, human IgG from exhaled breath condensate[52], Tumor Necrosis Factor-α[53] and staphylococcal enterotoxin B[54]; (ii) surface plasmon resonance to quantify the shift in reflectivity dip – for example, in the detection of human chorionic gonadotropin[55] or prostate specific antigen[50]; (iii) magnetoresistive sensing technologies such as the compact bead array sensor system (cBASS)[54] and the bead array counter

(BARC)[56] for the detection of proteins[54] and nucleic acids[57]; (iv) mass-based detection using measurements of the shift in resonant frequency of a MEMS resonator, which has been demonstrated for PSA detection from bovine serum[58]; and (v) nuclear magnetic resonance for the detection of bacteria[59]. In a few of the aforementioned examples, following incubation of magnetic beads to form the sandwich, nonspecifically bound beads are removed by Fluidic Force Discrimination (FFD) – the application of controlled laminar flow induced viscous forces to lower the background "bead count" – resulting in a lower limit of detection[52-54, 57, 60].

There are several examples of impressive limits of detection (in the femtomolar to attomolar range) for proteins and nucleic acids being achieved using magnetic bead "surface coverage" assays in the published literature. The readout strategies range from direct counting using an optical microscope to using magnetoresistance-based sensors. However, these readout strategies require significant user training in their current form, and are inherently difficult to automate. For example, for direct bead counting using an optical microscope, the actual enumeration of beads is easy to automate, but an experienced operator would still be needed to adjust the focus for each assay area and/or microfluidic channel. The assays cited above claim an assay time of between 5 and 20 minutes, but discount the significant user involvement in the readout process. Automation is a pre-requisite feature for any POC application, and it is easy to see that biosensing platforms that lack it will likely fail to translate into actual products with a public health impact.

Outline of work

In this work, the development and analytical evaluation of a novel optical biosensor platform based on embedded microretroreflectors is described. This platform, which has been developed in a microfluidic format, is based on a semi-homogeneous sandwich immunoassay. Antibody-modified magnetic microparticles were used for sample capture and concentration, following which they were introduced into a microfluidic channel to serve as optical light-blocking labels by completing the "surface coverage" immunosandwich. Non-specifically bound particles were removed by controlled fluidic force discrimination, following which the "bead count", which correlated with the concentration of analyte in the original sample, was measured. The detection of whole *R. conorii* bacteria was used as the model system to evaluate the performance of this platform.

The embedded microretroreflector platform, in its final envisioned form, is intended to fit target product profile 4 of the POC device spectrum depicted in Figure 1. More specifically, it is meant to be used as a "yes/no" assay for the high throughput testing of patient samples in a format conducive to untrained personnel. The primary requirement during development, therefore, was a clear distinction between the signals (bead count) measured from "blank" or "negative" samples (absence of analyte) and the bead counts measured from all "positive samples". The limit of detection was defined as the analyte concentration below which this distinction could no longer be made. The selected target user profile required that automated readout be another feature that drove design. The primary innovation introduced through this work – the use of microfluidic embedded microretroreflectors as the solid phase of the immunosensor – enabled

automated image capture and analysis using an inexpensive, in-lens illuminated, low numerical aperture camera.

Retroreflectors

Retroreflectors are structures that efficiently reflect light back to its source from many viewing angles. They typically consist of three mutually perpendicular reflective surfaces (corner cube retroreflectors), or are transparent high refractive index spheres partially coated with a reflective surface. Arrays of spherical or corner-cube retroreflectors with dimensions on the order of 100 µm and above find applications in road markings and personnel or vehicle conspicuity (as retroreflective tape or paint)[61-62], remote sensing of air pollutants[63], lunar laser ranging[64], and as components of laser interferometers[65].

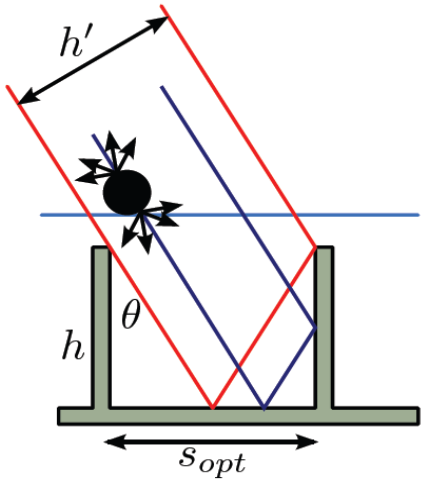

Figure 4. Embedded microretroreflector. Cartoon showing linear retroreflectors embedded into a transparent polymer layer and the 35° angle (from the vertical) at which they are illuminated. The presence of a light-scattering object appears as a dark spot on the retroreflected image.

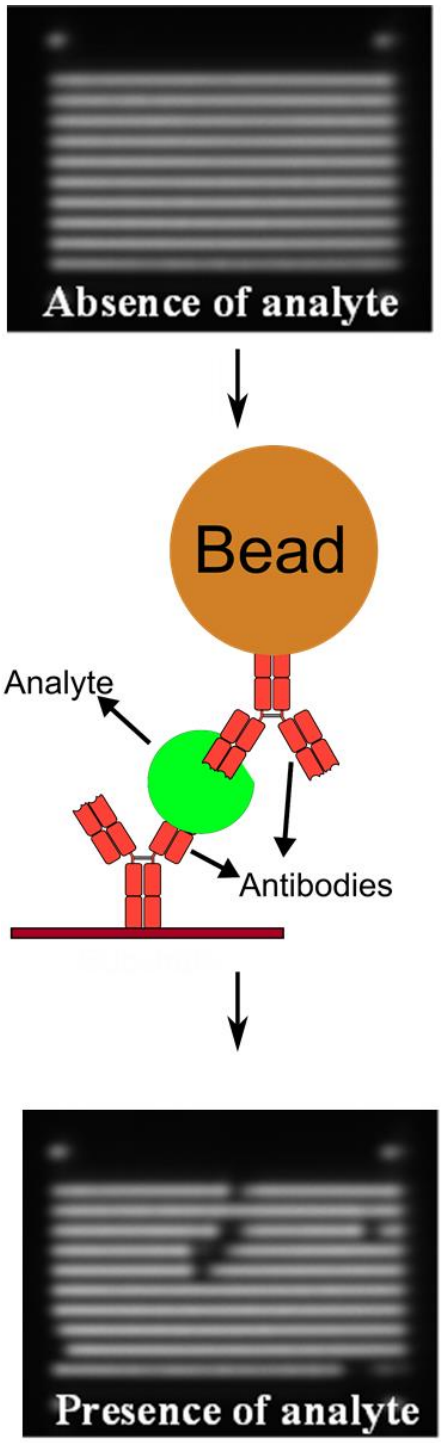

Figure 5. Immunoassay detection principle using magnetic beads as labels and embedded microretroreflectors as the solid phase.

Embedded microretroreflectors and detection principle

Linear retroreflectors have one less reflective surface than corner cube reflectors and are brightest from one viewing angle when arranged as densely packed arrays. In this work, several thousand micron-scale linear retroreflectors (typical dimensions 100 μm long × 3 μm wide × 5 μm tall) were fabricated with precise positioning on a microfluidic chip and embedded in a transparent polymer (Figure 4), resulting in a machine-registerable pattern of bright lines when viewed through an in-lens illuminated objective connected to a camera. As shown in Figure 5, the detection principle involves the analyte-dependent blocking of retroreflectors through a sandwich immunoassay in which the embedded retroreflector surface is the solid phase, and light-scattering magnetic particles are optical labels.

Materials and methods

Rickettsia conorii

Rickettsia conorii are Gram-negative, obligate intracellular, rod-shaped, pathogenic bacteria that are the causative agents of Mediterranean spotted fever[66] (also called Boutonneuse fever), which is transmitted by ticks. *Rickettsiae* are NIAID Category C priority pathogens, and flagged as potential bioterror agents due to the possibility of aerosolized release causing severe disease; attempts to weaponize *Rickettsiae* have been reported[67]. They are categorized as biosafety level-3 (BSL-3) agents owing to their highly infectious nature (infectious dose less than 10 organisms). For use in this work, a heat-sterilized, non-infectious version of *R. conorii* and rabbit polyclonal antibodies against it were supplied by Dr. Juan Olano of University of Texas Medical Branch, Galveston for use in experiments under BSL-2 containment at UH. The heat sterilized form retains its

structural integrity (tested by characterizing size using the Izon qNano) and is therefore expected to mimic the epitopes of the live form. ELISAs confirmed the functionality of the anti-*R. conorii* antibodies.

R. conorii (Malish strain) were grown in Vero cell monolayers in 150 cm^2 tissue culture flasks, cultured in Modified Eagle Medium (MEM; Gibco, Paisley, UK), supplemented with 4% fetal calf serum (FCS) and 2 mM L-glutamine. Heavily infected cells (5 days post-inoculation) were harvested with sterile glass beads and pelleted by centrifugation at 10,000g for 15 minutes. Bacteria were purified using sucrose gradients, and heat-inactivated organisms were obtained by heating at 60°C for 30 minutes[68]. The Olano lab determined the concentration of bacteria by quantitative real-time PCR – this was independently verified using the Izon qNano as described below.

To raise polyclonal rabbit anti-*R. conorii* antibodies, New Zealand rabbits, housed in a biosafety level-3 facility at UTMB Galveston were immunized with 10^6 Rickettsial organisms intravenously every 3 weeks until antibody titers by IFA reached 1:2096. The rabbits were sacrificed humanely according to IACUC protocols and blood was harvested. The serum was affinity purified using Protein A columns and re-suspended in PBS buffer at a concentration of around 1 mg/mL.

Magnetic beads

Magnetic beads ranging in size from tens of nanometers to several microns have been used for used for capturing bacteria from a sample, but for optical detection from sensing surfaces several hundred microns in size, they need to be micrometer sized. Commercially available Sera-Mag SpeedBeads (Thermo Scientific, Rockford, IL) with a nominal size of 1 µm and ProMag beads (Bangs Laboratories, Fishers, IN) with a

nominal size of 3 µm were used as labels in this work. They are both polystyrene-based and superparamagnetic (zero magnetization in the absence of an external magnetic field), and were obtained with NH_2, COOH or streptavidin functionalities on their surface. They are superparamagnetic by virtue of having several < 20 nm sized Fe_3O_4 nanoparticles embedded in them.

Bead and bacteria characterization using the IZON qNano

The format of the described assay's readout requires that the beads be reasonably monodisperse. The size distribution of beads and reproducibility of antibody immobilization were measured using the qNano instrument (Izon Science, New Zealand) which simultaneously measures particle size, surface charge and concentration with single-particle resolution by TRPS (Tunable Resistive Pulse Sensing). As illustrated in Figure 6, the qNano instrument consists of two fluid cells separated by an elastomeric polyurethane membrane into which a conical nanopore has been mechanically punched. A voltage is applied across the membrane, and the increase in electrical resistance from particles electrophoretically traversing the nanopore is observed as a decrease in current. The magnitude, frequency and duration of these "blockade" events, along with size standards, help measure size distributions, concentrations and relative surface charge (by electrophoretic mobility) of nanoparticles, respectively[69-72].

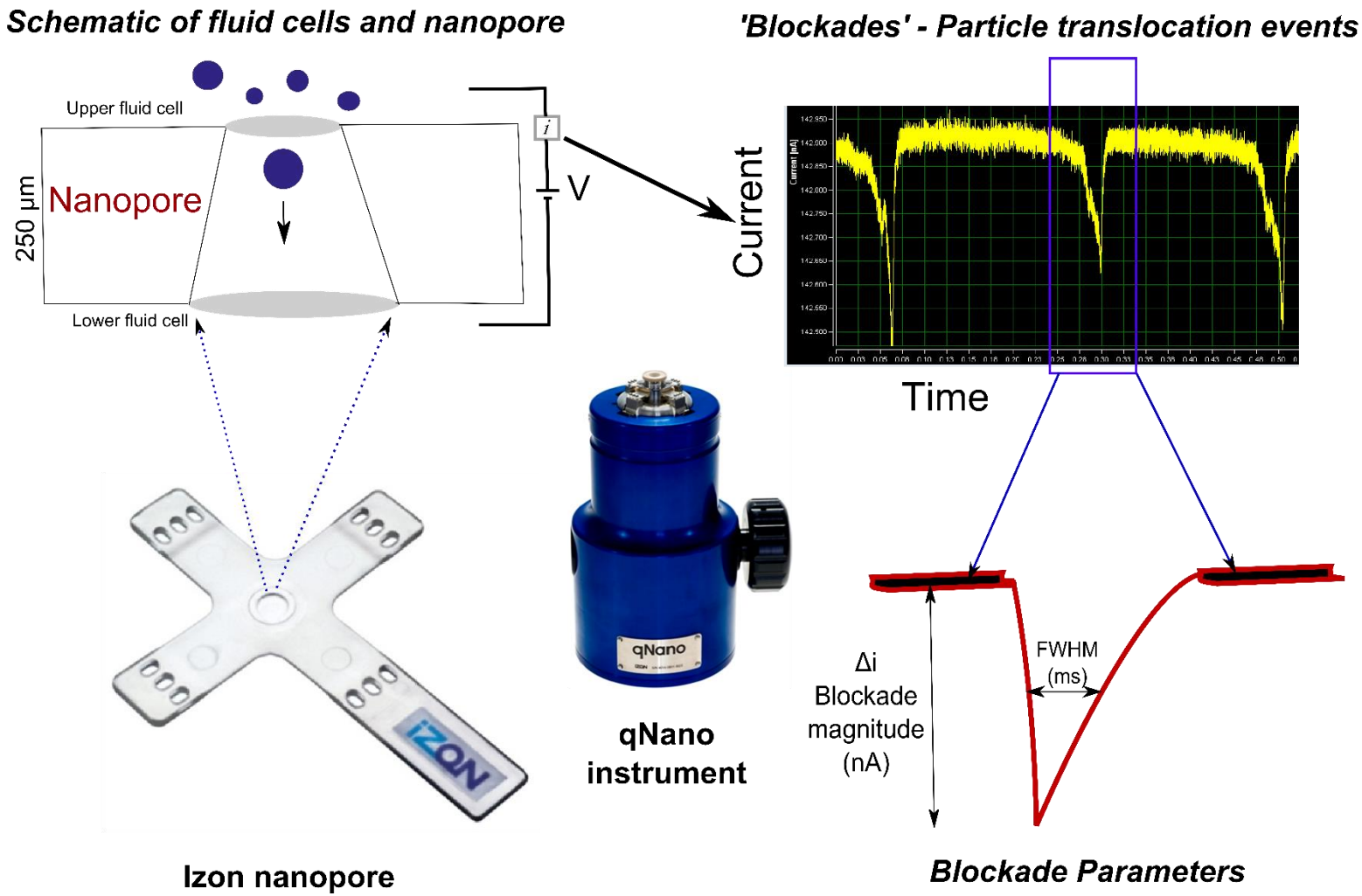

Figure 6. Izon qNano – Tunable Resistive Pulse Sensing (TRPS)

A comparison of the full width at half maximum (FWHM) blockade duration distributions of beads before and after antibody immobilization qualitatively measured the extent and uniformity of surface coverage. For example, if the beads were initially negatively charged from COOH surface functionality, successful antibody modification would be expected to lessen the negative charge on the surface and thereby increase the blockade duration. Experiments were performed using 40 μL volumes of 100-fold dilutions of magnetic beads were made in phosphate buffered saline (PBS) using the stock beads as purchased and after antibody modification for comparison. At least 500 particles were measured to generate FWHM distributions. IZON nanopore NP4000 was used for bead characterization.

The qNano was also used to characterize the size distribution and concentration of *R. conorii* bacteria received from UTMB Galveston. 40 μL volumes of 400-fold dilutions of *R. conorii* were analyzed using IZON nanopore NP1000, and at least 1000 bacteria were measured to generate distributions.

Embedded microretroreflectors fabrication

The embedded microretroreflectors used as microfluidic substrates were fabricated by one of two lithographic methods. In the first method (Figure 7; work done by David Shakarisaz), a 5 μm thick layer of SU-8 5 (Microchem, MA) was first spin-casted onto a 4 inch Si wafer and cured by exposure to UV, followed by thermal evaporation of 220 nm of Cu and spin-casting of a 70 nm layer of polystyrene (MW 76500, 1.5 wt% in toluene) at 1700 rpm for 1 minute. The polystyrene layer was exposed to the linear retroreflector array pattern through a silicon nitride membrane using a high resolution helium ion-beam lithography process[73]. After patterning, the polystyrene layer

was developed in toluene for 45 seconds to remove the unexposed regions of the layer, rinsed in toluene for 15 seconds and dried under a stream of N_2. The Cu layer was them isotropically wet etched in a solution of citric acid for 8 minutes. An in-house, magnetically enhanced CF_4 + O_2 (0.9 mTorr O_2, 0.1 mTorr CF_4, 1 hour etch time) reactive ion etch process[73] was used to transfer the pattern into the SU-8 layer, leaving behind the copper protected retroreflector patterns. To form the reflective layer, 300 nm of aluminum was angle-evaporated in a thermal evaporator to coat the top and sides of the patterned areas. The linear retroreflectors manufactured using this method were 5 μm tall, 2 μm wide and 100 μm long, and were spaced by an 8 μm pitch. The structures were planarized by spin-casting a solution of 20% w/v PMMA in Anisole at 1000 rpm for 45 seconds and baking on a hot plate at 180 °C for 10 min to get a layer thickness of 8 μm. Using this process, each 4-inch Si wafer yielded five chips (1.5" L x 1" W) with seven rows of six 0.8 mm^2 arrays of embedded linear retroreflectors to be used as described later.

The second method for embedded retroreflector fabrication involved fewer steps than the process described above, and was based on easily scalable contact photolithography techniques (Figure 8; work done by Carmen Pascente). As in the first method, 5 μm thick layer of SU-8 was first spin-cast onto an ozone-cleaned silicon wafer and pre-baked at 95°C for 4 minutes. This is followed by exposure to UV light through an opaque photomask and a post-bake at 95°C for 3 minutes to crosslink the retroreflector pattern. Following development in 1-methoxy-2-propanol acetate for 90 seconds to remove the unexposed regions and rinsing with IPA, silver was e-beam evaporated onto the structures at a 30° angle to the horizontal from both sides to a

thickness of 120 nm, and at a 90° angle to a thickness of 60 nm. The linear retroreflectors manufactured using this method were 5 μm tall, 3 μm wide and 100 μm long, and were spaced by an 8 μm pitch. The planarization layer to embed the now-retroreflective surfaces had two sub-layers, the first of which was created by spin-casting SU-8 2005 at 800 rpm for 1 minute (followed by baking at 95°C for 4.5 minutes, UV cross-linking for 10 minutes and baking again at 95°C for 3 minutes) to a thickness of 6 μm. The planarization layer was completed by spin-casting PMMA C9 at 2000 rpm for 30 seconds and baking at 180°C for 10 minute, resulting in an overall planarization layer thickness of 8 μm.

The PMMA-planarized linear retroreflectors manufactured using either method described above were directly used for the surface chemistry steps ultimately resulting in antibody immobilization. Before PMMA was chosen to be a viable option for antibody-modification and planarization, during the initial stages of assay development, the use of a thermally evaporated transparent layer of gold over SU-8 planarized linear retroreflectors was considered as an option for making the microfluidic substrates biofunctionalizable. In those early stages, silicon wafers were also directly coated with SU-8 (spin-casting followed by UV exposure and baking) before thermally evaporating 15 nm gold onto them to simulate the envisioned stack of layers and aiding assay development and optimization.

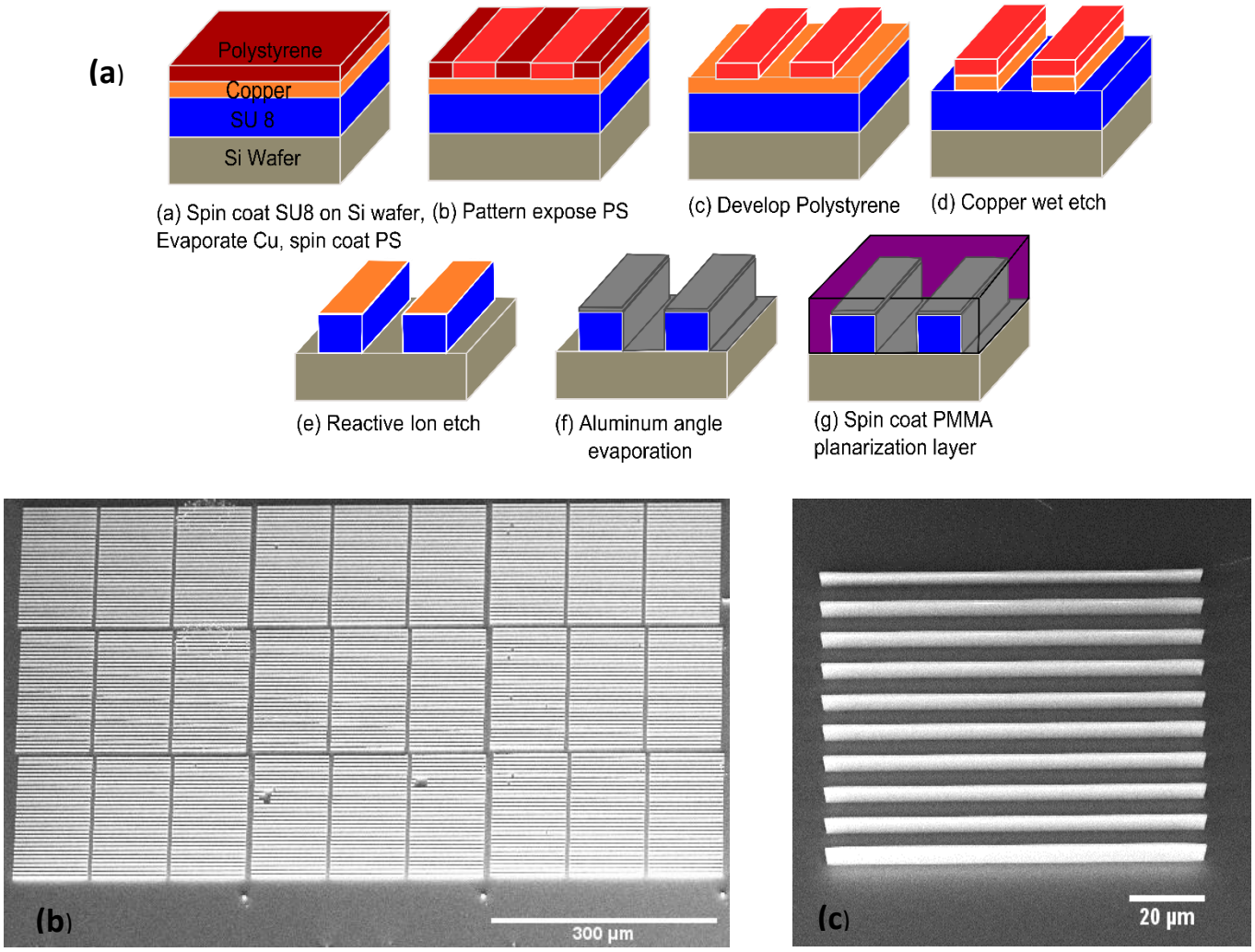

Figure 7. Embedded microretroreflectors fabrication process using ion beam lithography and reactive ion etching. (a) Schematic of process; (b) and (c) SEM images of microretroreflectors fabricated by this process before planarization.

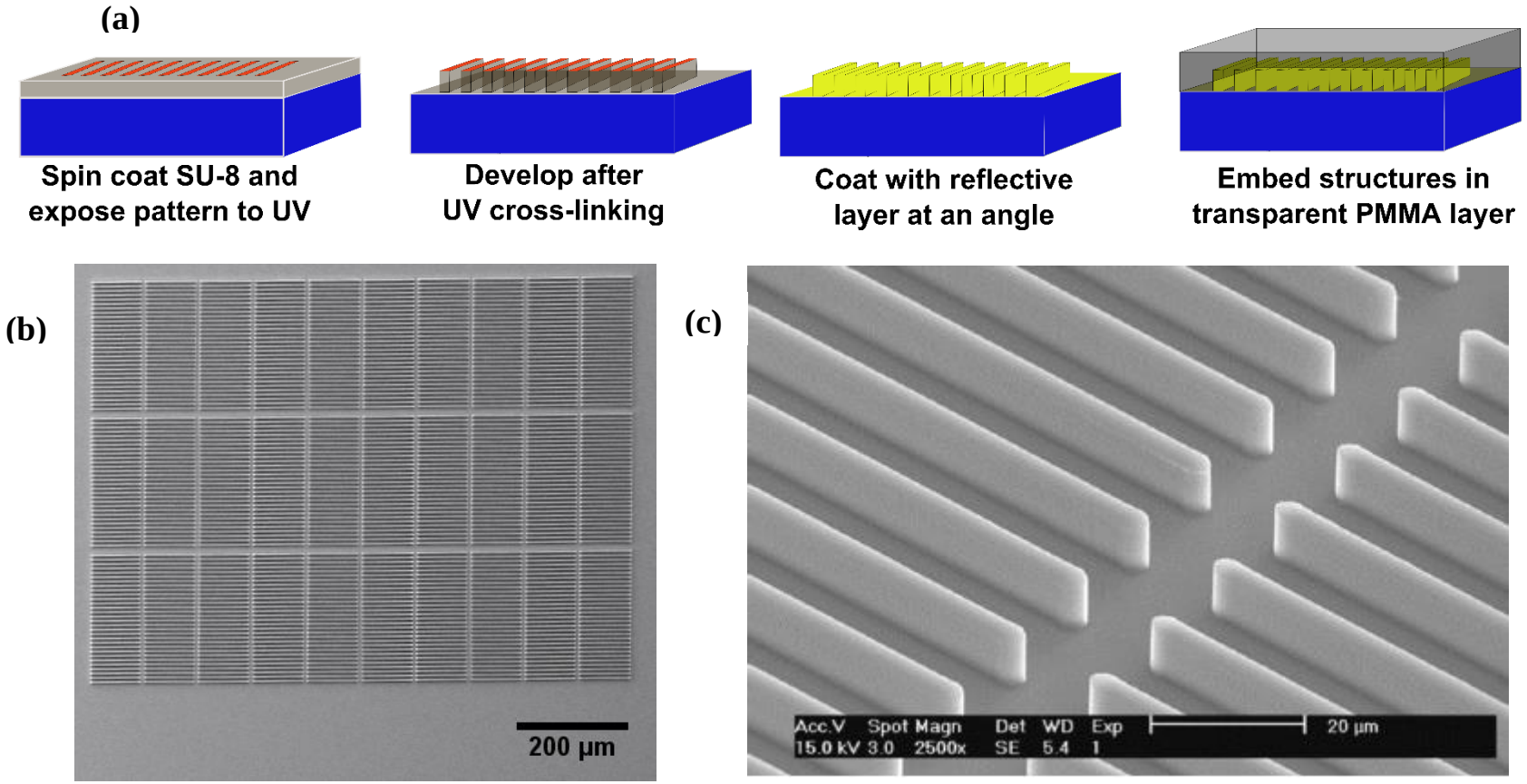

Figure 8. Embedded microretroreflector fabrication by contact printing. (a) Schematic of embedded microretroreflector fabrication process by photolithography; (b) and (c) SEM images of microretroreflectors fabricated by this process before planarization.

Antibody immobilization on sensing surfaces

"Sensing surfaces", in this context, refers to the two ends of the immunosandwich – the embedded retroreflector surfaces forming the bottom of microfluidic channels, and the surface of the magnetic beads. During assay development, various surface chemistries were considered and evaluated for the covalent immobilization of rabbit Anti-*R. conorii* (Anti-Rc) polyclonal antibodies to these sensing surfaces. The chemistries were chosen based on their purported ability to enhance sensitivity or lower non-specific binding. They included the following methods described below.

Antibody modification of gold-coated surfaces by PEGylation. This protocol was used to antibody-modify microfluidic substrates. More specifically, it was used on SU-8 surfaces coated with 15 nm Au by thermal evaporation. Briefly, the surfaces were first cleaned by immersion in 50 mL 100% ethanol and probe ultrasonication for 30-45 seconds. They were then rinsed in dimethyl sulfoxide (DMSO) and immersed in 4 mg/mL dithiobis[succinimidyl propionate] (DSP, Thermo Scientific) dissolved in DMSO for 75 min. Reacting gold surfaces with DSP creates a self-assembled monolayer, with SH-Au bonds at one end and the highly amine-reactive N-hydroxysuccinimide (NHS) esters at the other end. Following another rinse with DMSO and an extensive PBS wash, the surfaces were immersed in PBS containing a mixture of PEGylation reagents – 0.8 mg/mL heterobifunctional carboxy$(PEG)_{24}$amine and MW 1000 amine-PEG (Thermo Scientific) for 3 hours. The stack, which now terminated with carboxylic acid groups, was activated using 10 mg/mL 1-ethyl-3-(3-dimethylaminopropyl)carbodiimide (EDC) and 15 mg/mL NHS in 50 mM 2-(N-morpholino)ethanesulfonic acid (MES) buffer at pH 6 for 15 minutes. The COOH groups activated this way are highly amine-reactive, and

were coupled to 0.2 mg/mL Anti-Rc antibodies in PBS for 3 hours. The unreacted groups were quenched by incubation with a mixture of 2% bovine serum albumin (BSA) and 500 mM hydroxylamine in PBS for 2 hours at 37ºC or overnight at 4ºC, following which they were thoroughly rinsed with PBS and DI water, and either used immediately or stored at 4ºC.

Directed antibody immobilization on beads and embedded microretroreflector surfaces. This protocol was used to modify both magnetic beads and PMMA-coated surfaces, and required that the antibodies be subjected to some pre-treatment. The presence of glycosylated residues in the F_c portion of rabbit IgGs[74] enabled their immobilization on sensing surfaces in a favorably directed manner. A previously described method[75] was adapted to oxidize the carbohydrates and create aldehyde groups in the antibodies' F_c region. Briefly, 10 µL of 0.2 M sodium periodate (Sigma-Aldrich) in water was added to 100 µL of 1 mg/mL antibody in PBS and allowed to react in the dark for 2 h at 4ºC. The antibody was filtered out of the reaction mixture using Amicon 100 K microcentrifuge filters and re-suspended in PBS to a concentration of 1 mg/mL, verified using absorbance at 280 nm.

3 µm amine-modified magnetic beads, when used as assay labels, were covalently modified with F_c-oxidized polyclonal Anti-Rc antibodies. Briefly, 400 µL of amine magnetic particles as obtained from the manufacturer were washed and suspended in cyanoborohydride coupling buffer (0.02 M sodium phosphate, pH 7.5, 0.2 M sodium chloride and 3.0 g/L sodium cyanoborohydride) along with 100 µg of F_c-oxidized antibodies to a final reaction volume of 1 mL, and incubated at room temperature for 4 hours. The antibody-modified particles were then washed twice with PBS using a

magnetic stand and passivated by incubating with 1.5% BSA in PBS for 2 hours at room temperature. They were then washed and stored suspended in PBS at 4°C.

The sensing areas of the retroreflector chips were antibody-functionalized by first introducing primary amines on the embedding PMMA surface[76] followed by the reductive amination of the Schiff bases formed by their reaction with aldehydes on F_c-oxidized polyclonal rabbit Anti-Rc antibodies. Briefly, the chips were cleaned by bath sonication (5 min) in 200-proof ethanol followed by thorough rinsing with MilliQ water, dried under an N_2 stream, and immersed in a solution of hexamethylenediamine (10% in 100 mM borate buffer, pH 11.5) for 2 hours at room temperature to introduce covalently bound primary amines at the surface by nucleophilic addition-elimination. After washing with MilliQ water, the chips were dried at 40°C for 10 min, followed by manual spotting of 6 μL of a 140 μg/mL solution of F_c-oxidized Anti-Rc antibodies in cyanoborohydride coupling buffer on each 6-array row of retroreflectors and incubation in a humidified chamber at room temperature for 4 hours. The antibody-functionalized chips were washed thoroughly with PBS and passivated by immersion in 1.5% BSA for 2 hours at room temperature. The chips were washed with MilliQ water, dried under a nitrogen stream and stored at 4°C until further use.

Antibody modification of beads and embedded microfluidic surfaces by PEGylation. When 3 μm streptavidin Promag beads were used as assay labels, a PEGylation protocol was used for antibody modification. Briefly, 50 μL aliquots of stock beads as received were washed thrice with PBS, following which they were incubated with 2 mg/mL biotin-PEG-COOH (MW 3400; Nanocs, New York, NY) in PBS for 4 hours. They were then washed twice with MES buffer (50 mM, pH 5) and reacted with 200 μL of a mixture

of 10 mg/mL EDC and 5 mg/mL NHS in MES buffer for 15 minutes at room temperature to activate the now carboxyl-terminated beads. After two washes using PBS, 50 μg Anti-Rc was added and allowed to react at room temperature for 4 hours. The beads were passivated after removing unreacted Anti-Rc (and washing) by incubating them with a mixture of 500 mM NH_2OH and 4% BSA in PBS overnight at 4°C. After passivation, the beads were washed thrice and re-suspended in PBS and stored at 4°C.

PMMA-planarized embedded retroreflector surfaces were PEGylated by nucleophilic aminolysis after an initial cleaning step in which they were immersed in isopropyl alcohol for ten minutes followed by rinsing with water. A 100 mg/mL solution of PEG bis(amine) (MW 3000; Sigma-Aldrich), dissolved in highly basic borate buffer (100 mM, pH 11.9), was spotted on the microfluidic substrates for two hours at room temperature. The aminated PMMA, which now had a free primary amine from the use of a homobifunctional PEG molecule, was immersed in 2.5% glutaraldehyde (by volume, in PBS) at room temperature for 2 hours. Anti-Rc antibody, at 0.25 mg/mL in PBS with 250 mM sodium cyanoborohydride (for Schiff base reduction) was then spotted manually on the sensing areas and incubated in a humidified environment for between 4 and 6 hours. The passivation step was performed using 500 mM hydroxylamine and between 20 and 40 mg/mL BSA in PBS (100 mM $NaCNBH_3$) for 2 hours at 37°C or overnight at 4°C. The functionalized and passivated microfluidic substrates were then cleaved from the wafer (if necessary), assembled into chips, and either used immediately or stored at 4°C until use.

Microfluidic device assembly

The assay for *R. conorii* detection was carried out in a microfluidic format, developed in collaboration with Anson Hatch at Sandia National Laboratories (Livermore, CA), to enhance reproducibility. A picture of the laboratory setup is shown in Figure 9. The pressure-driven laminar flow that delivered fluid to the channels was precisely controlled by a 10-channel syringe pump (Chemyx, Stafford, TX), capable of both infusion and withdrawal, using 1 mL plastic BD syringes (Beckton Dickinson, East Rutherford, NJ); the syringe pump was controlled either manually, through its touch interface, or through a LabView program.

The actual microfluidic "chip" was assembled by simply sandwiching double-sided adhesive tape (300 LSE, 3M), into which the microfluidic channels (7 channels per chip; 15 mm L x 1.5 mm W) were laser-cut, between the microfluidic substrate (embedded microretroreflectors cleaved to appropriate dimensions) and a transparent optical lid with inlet and outlet via holes that allowed fluid flow (Figure 10). As shown in Figure 10, a re-usable microfluidic manifold, into which the chip was assembled by compression using fasteners, was used to interface fluid flow in the microchannels to the syringe pump using standard components including plastic ferrules and adapters, and polyetheretherketone (PEEK) tubing obtained from IDEX Corporation (Lake Forest, IL).

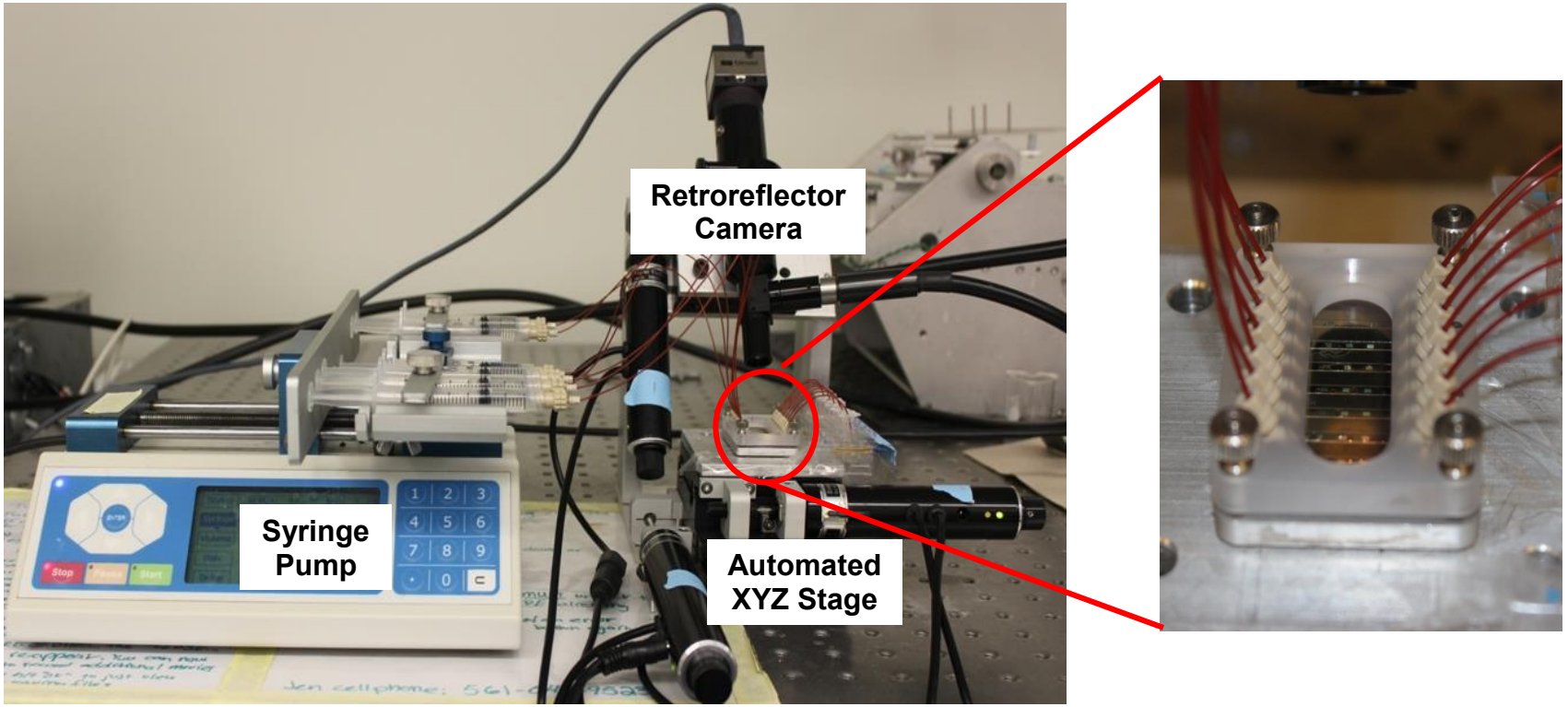

Figure 9. Picture of experimental setup showing microfluidic manifold, syringe pump, automated stage, and imaging optics. A zoomed-in picture of the microfluidic manifold is shown to the right.

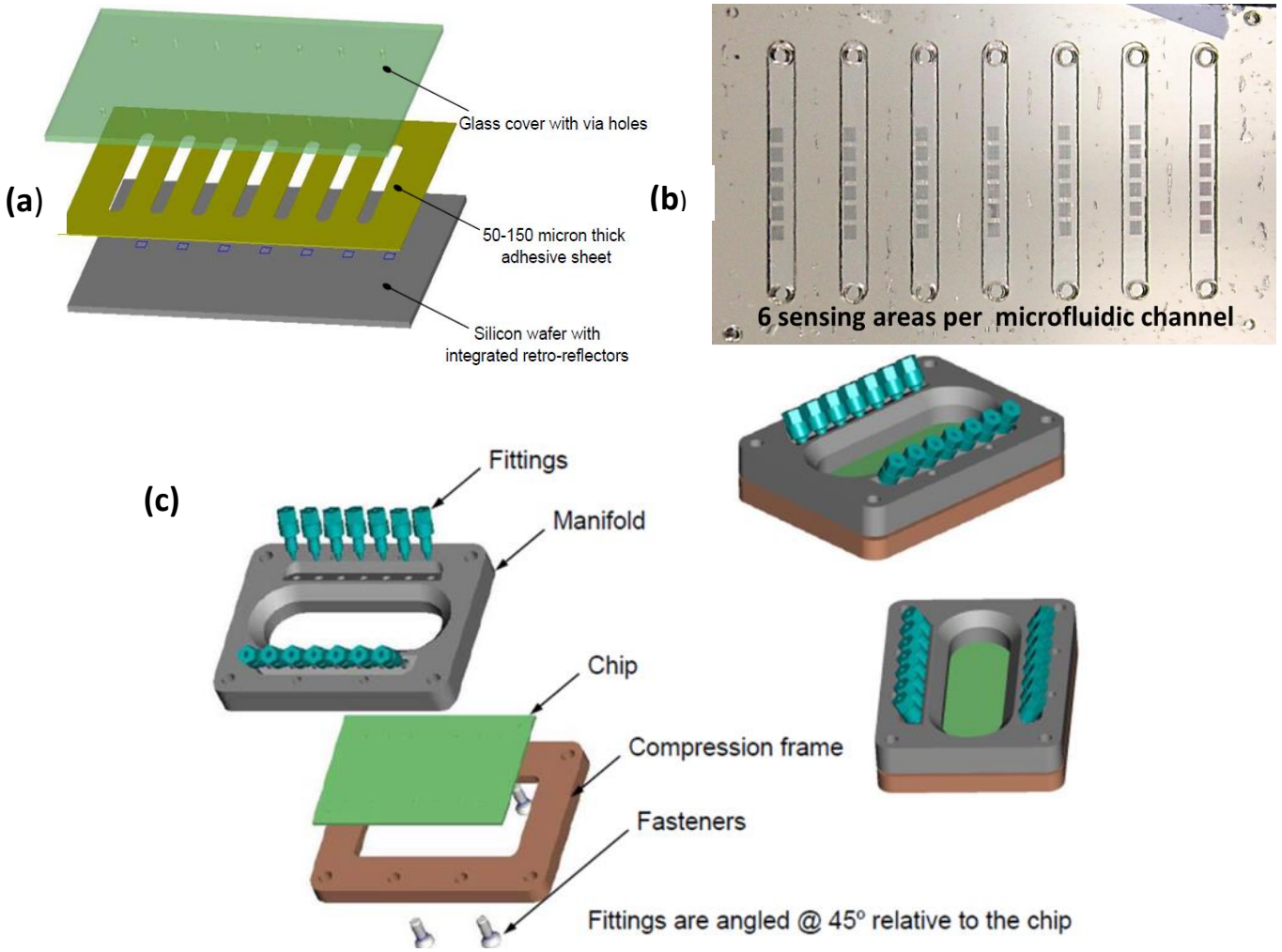

Figure 10. Microfluidic chip and manifold. (a) Components of the microfluidic chip; (b) a picture of an assembled microfluidic chip showing 6 sensing areas per channel; this design was later modified to include 7 areas per channel; (c) components of the microfluidic manifold, which interfaces microfluidic flow to the syringe pump.

The height of the microfluidic channels was defined by the thickness of the double-sided adhesive tape. In this case, the manufacturer's specifications for the triple-layer adhesive tape (two layers of 300LSE adhesive and an ultrathin, stabilizing polyester carrier sandwiched between them) added up to 175 μm. The actual height of the channels was lower due to the adhesive layers being compressed during assembly, and was measured using electronic calipers to be 150 ± 1 μm. During assay development, the transparent lid, which contained via holes for fluid flow and alignment holes at the edges for device assembly, evolved from being made of microscope slide glass (~1 mm thick) to cover slip glass (~100 μm thick) and finally, a cyclic olefin copolymer (~200 μm thick). There was no significant optical difference between these materials for the imaging purposes of the assay. The inlet/outlet via holes had a diameter of 0.8 mm in all these materials.

Optics and imaging

The optics used to image retroreflectors comprised a Dolan-Jenner MI-150 Fiber Optic Illuminator as the light source and an EO-5012M ½" Monochrome Camera (CMOS; USB 2.0) mounted on an Infinitube FM-200 in-line assembly system (with 4x internal magnification) that ended in a 1x objective lens and interfaced, on the side, with the illuminator through a 48" long fiber optic light guide. The ultimate field-of-view (FOV) of the acquired image, for retroreflective imaging, was 1.6 mm x 1 mm. The Infinitube system was mounted on a machined structure that held it at a constant 35° angle from the vertical and allowed the illumination and imaging of retroreflectors. Alternately, for top-down imaging, a PixelLink CCD camera was mounted on a Standard Infinitube 1.5x magnification in-line assembly system (6x total magnification) , and used

in conjunction with a 10x Mitutoyo infinity-corrected long WD objective and the same light source, resulting in 60x total magnification. All optical components were obtained from Edmund Optics (Barrington, NJ).

A LabView program was used to control the automated XYZ-stage (Zaber Technologies, Vancouver, Canada) onto which the microfluidic manifold was placed, at the same location for each experiment, using pre-drilled alignment holes and fastening screws. The first sensing region in the first microfluidic channel was manually positioned before each experiment, following which a script was used to manipulate the XYZ-stage and USB-camera and capture images of all other sensing regions on the chip when required. Three images (with 0.15 mm differences in z-focus) were acquired for each sensing region. The image acquisition process was rapid - for example, in experiments involving 49 sensing regions from 7 microfluidic channels, 149 total images were acquired and saved as PNG files in less than 3 minutes. Top-down images, obtained using the 10x objective using a similar LabView program as that used for retroreflective imaging, were analyzed using ImageJ (National Institutes of Health) software.

Assay procedure – sample capture

R. conorii was spiked into PBS or diluted human serum at varying concentrations (10^3 per mL to 10^9 per mL) for use as the "sample." Samples were incubated using 360° mixing for 1 to 3 hours with varying concentrations of differently-functionalized Anti-Rc modified magnetic beads. A magnetic separation stand (Thermo Scientific) was then used to magnetically concentrate the beads. The original sample was typically replaced with 15 to 20 μL assay buffer (PBS, 0.01% Tween-20), thereby concentrating the beads (and captured analyte) by 10 – 40 fold.

Assay procedure – microfluidic loading and imaging

In the following text, "assay buffer" refers to PBS with 0.01% Tween-20, and "wash buffer" refers to PBS with 0.25-1% Tween-20. In all microfluidic experiments, the channels were initially washed with assay buffer at volumetric flow rates between 50 and 100 μL/min after assembling the chip onto the manifold and verifying proper flow.

The results presented in this work from initial assay development not involving retroreflective surfaces (Au-coated SU-8 surfaces) were obtained from experiments using 1 μm beads as labels. In these experiments, samples and wash buffer (after assay completion) were loaded by infusion from the syringe pump side of the microfluidic manifold. This arrangement did not allow for more than 10-fold magnetic sample concentration, because the syringe used for infusion and the tubing leading to the chip had a combined dead volume of at least 40 μL. A typical experiment was performed as follows: Samples with analyte-captured beads were loaded into the channels at 15 μL/min for 4 minutes following which the flow was ceased and the beads were allowed to settle for 10 minutes. The wash buffer was then loaded and infused at between 40-60 μL/min for between 5 and 10 minutes to perform FFD, following which several assay areas from each microchannel were imaged manually using the top-down camera.

Sample and wash buffer loading in all retroreflective-imaging based experiments presented in this work were performed by withdrawal. Samples were loaded at the end of the microfluidic channel not connected to the syringe pump, typically by directly plugging a pipette tip into the ferrules of the microfluidic manifold. This protocol allowed for the use of much smaller sample volumes (5 - 15 μL) compared to loading by infusion. A set of "before" images of all sensing regions on the chip were acquired using the image

capture script before all experiments. The magnetically concentrated samples containing bead-*Rickettsia* complexes or "blanks" (beads with no bacteria) were then introduced into the microfluidic channel at between 10 and 20 μL/min for up to 15 seconds, and allowed to settle for between 2 and 3 minutes. The Stokes settling velocity of the 3 μm beads used is roughly 2 μm/s; in a 150 μm tall channel, therefore, 3 minutes was sufficient time for even the beads originally at the top of the microfluidic channel to settle and interact with the surface. This initial settling period was followed by at least five cycles of introducing 2-4 μL sample and 30 s settling times in a "stop and drop" format to allow for the beads to interact in a Brownian motion-mediated manner with the antibody-functionalized surface. Wash buffer was then loaded at flow rates of 30 – 120 μL/min for ten minutes, via infusion or withdrawal, to perform FFD. It should be noted that FFD was likely completed in the first 30 seconds to 1 minute, but additional washing was required to clear out all residual beads. Following FFD, the same image capture script as used for capturing "before" images was then used to capture "after" images.

Difference imaging

The before and after images of each assay area were analyzed by an in-house Python-based image differencing program developed by Paul Ruchhoeft to obtain bead counts. A detailed description of the algorithm is beyond the scope of this work. Briefly, the algorithm employed by the program performs the following steps in sequence for an image pair labeled "before" and "after":

- Load before and after images from user-specified image directory and identify exact positions of the retroreflector patterns in either image separately. This is done using a pattern finding routine that requires the input of user-specified

numbers such as the number of rows and columns, “tile” widths and heights, and gaps between tiles (in pixels).

- Split each image into “tiles” and store as vector arrays. The number of tiles was 27 or 30 depending on the fabrication process. The contact printing process had one additional column of retroreflectors in each sensing region.
- Calculate relative offset of “tiles” between the before and after images, using a 2D registration algorithm, for accurate alignment.
- Subtract the after tiles from the before tiles to obtain a raw difference image.
- Use user-specified background threshold to normalize the difference images.
- Return “bead count” per tile as one of the following:
    - Total number of continuous regions above the background threshold (which does not account for aggregated beads)
    - Total number of maximas found in each continuous region above the background threshold (can distinguish aggregates)

Splitting each 1 sq. mm array of retroreflectors into tiles allowed for the robust alignment of image pairs in which the after image has undergone a slight lateral or angular displacement from the original position of the before image. The difference imaging program typically took less than 5 minutes to generate data from 147 sensing regions; this time could vary depending on the processing power of the computer used for analysis. The “bead counts” obtained by difference imaging were exported and visualized using statistical and graphing software such as Microsoft Excel or Origin. Figure 11 shows an example of difference imaging output.

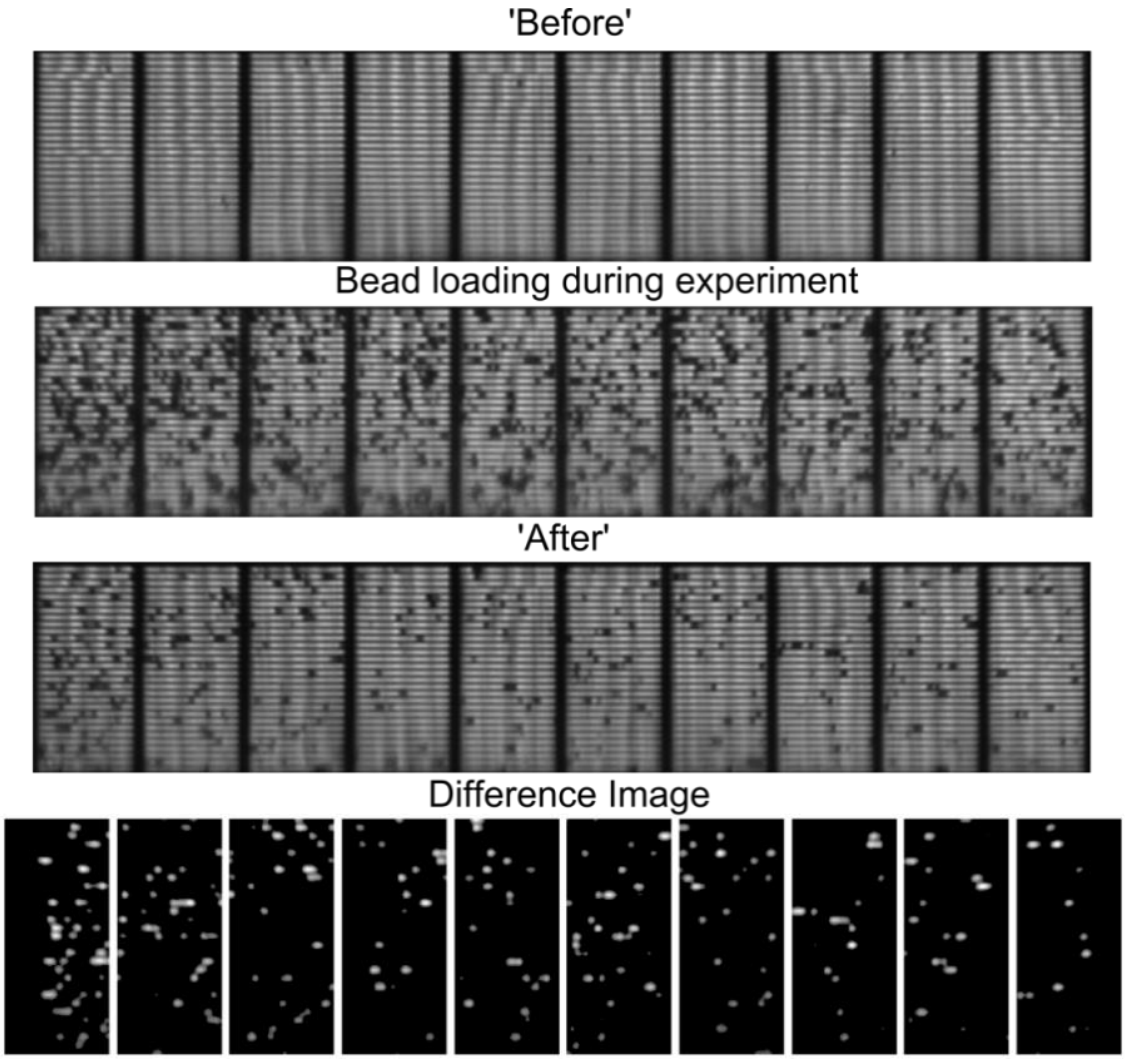

Figure 11. Representative example of difference imaging from an array of embedded microretroreflectors. Ten tiles are shown. Particle count per tile as calculated by the difference imaging algorithm: mean = 21, median = 19.

Results and Discussion

qNano characterization of *R. conorii* and beads

R. conorii (Rc) bacteria were quantified by real-time PCR in the Olano lab at UTMB after heat inactivation, and shipped to UH at a labeled concentration of 3.09 x 10^9 Rc/mL. Different aliquots of Rc were characterized using the qNano to verify their concentration and size distribution. Blockade magnitude distributions, an example of

which is shown in Figure 12, were obtained by measuring a dilution of Rc in PBS; they were useful in checking for aggregates or other structural anomalies. When the blockade magnitude measurements were calibrated using 960 nm polystyrene standards (Bangs Labs), Rc were found to have an equivalent spherical diameter of 678 nm (Figure 13). This value was in good agreement with the size of whole *R. conorii*, which are rod-like with a diameter between 0.3-0.5 µm and length between 0.8-2 µm. The concentration of Rc aliquots was measured by comparing their blockade frequency (slope of Rc line in Figure 14) to the blockade frequency of the 960 nm standards. The Izon-determined Rc concentration of 3.56 ± 0.15 x 10^9/mL was in good agreement with that determined by the Olano lab using PCR. Full width at half maximum (FWHM) duration distributions of 3 µm magnetic beads before and after surface functionalization with antibodies were used to qualitatively confirm successful modification, and to measure reproducible modification between different batches of functionalized beads (Figure 15).

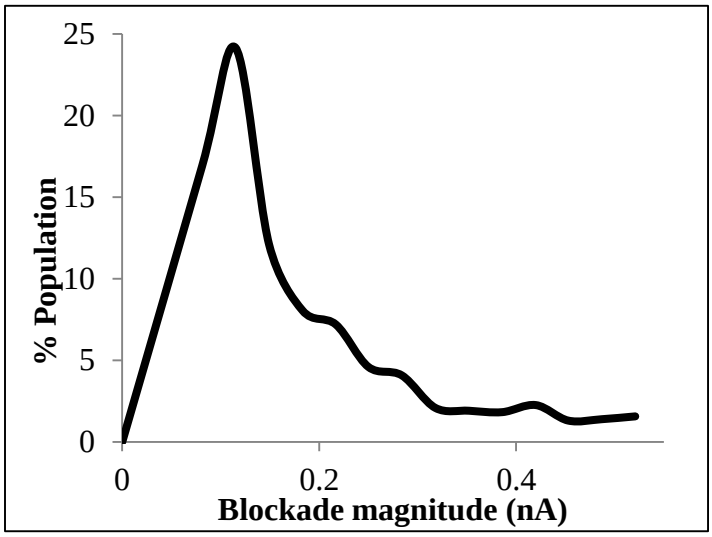

Figure 12. Plot connecting histogram midpoints and showing the distribution of *R. conorii* blockage magnitudes measured using Izon nanopore NP1000. 1,155 bacteria were measured. Mode = 0.12 nA; shoulders indicate aggregates. Measurement parameters: voltage = 0.22 V, average baseline current = 152.19 nA.

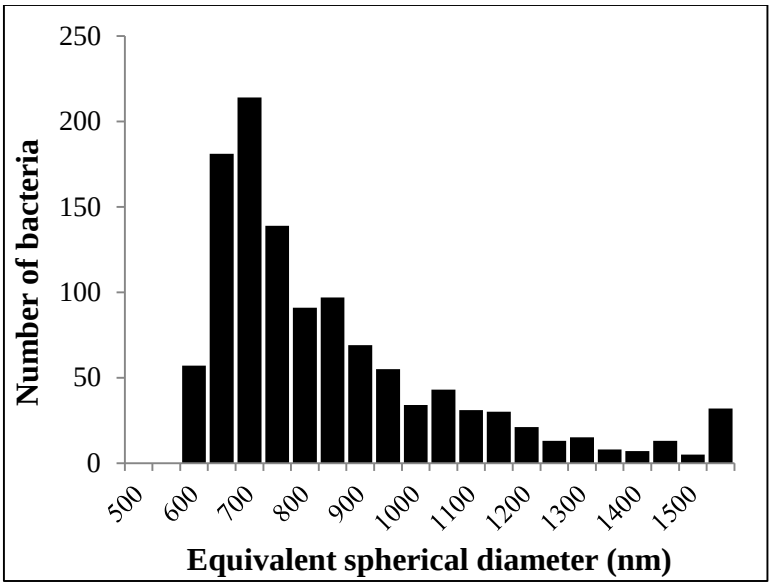

Figure 13. Equivalent spherical diameter distribution of *R. conorii* measured using the qNano. Distribution obtained by calibrating data from Figure 12. Mode = 678 nm.

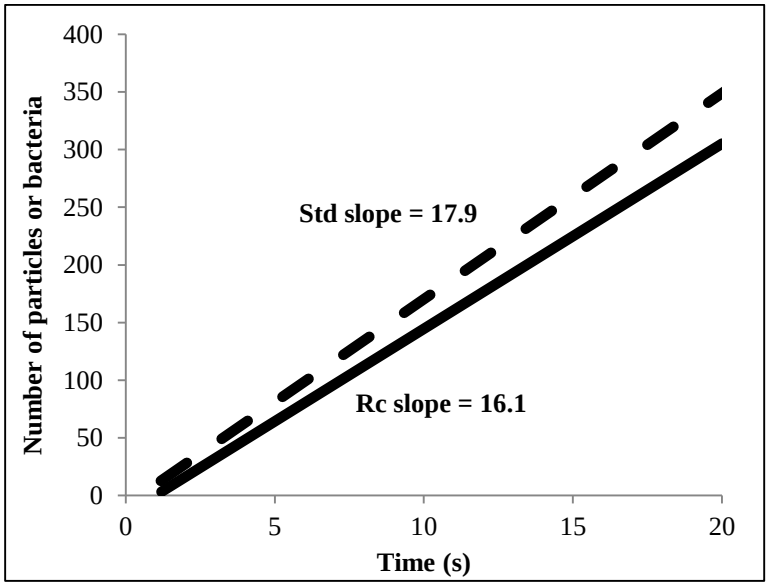

Figure 14. Plot representing blockade frequency of *R. conorii* measurement. (Rc, ~16 Rc per s) and 960 nm polystyrene standards (Std, ~18 particles per s). The ratio of slopes (17.9/16.1) was multiplied by the known concentration of Std's dilution to obtain the Rc sample's concentration.

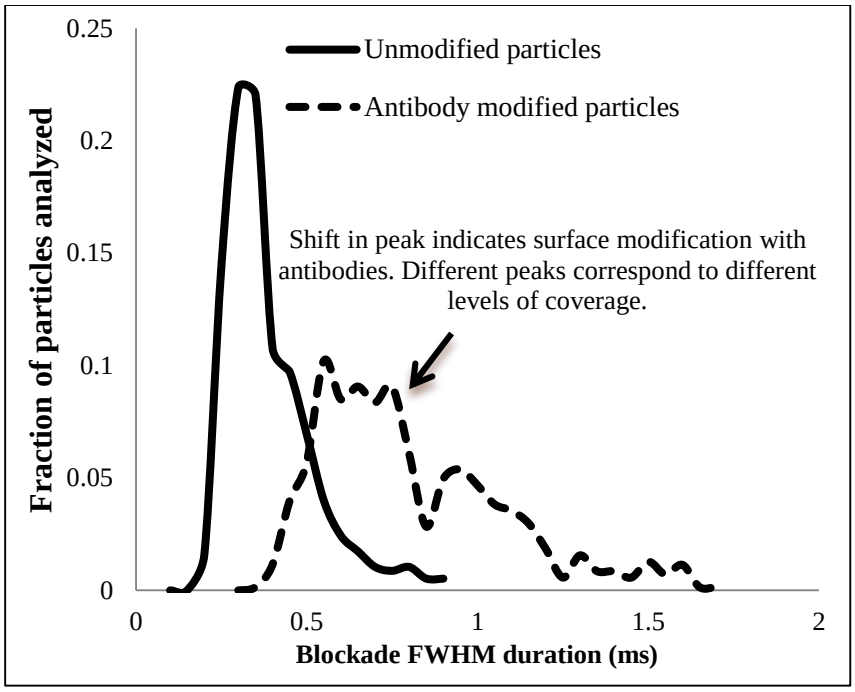

Figure 15. Change in FWHM distributions of beads with surface modification.

Antibody spotting concentration

The density of immobilized antibodies on the solid phase of an immunoassay is an important parameter that can influence assay sensitivity – a low density may reduce capture efficiency, while a high density could increase non-specific binding. To avoid oversaturation of embedded retroreflector surfaces with antibodies, different anti-Rc spotting concentrations were evaluated by using serial dilutions of Cy3-labeled anti-Rc antibodies to functionalize a gold-coated glass microscope slide by the protocol described in the Materials and Methods section. As shown in Figure 16, the surface was saturated at between 100 and 200 µg/mL spotted antibody concentrations.

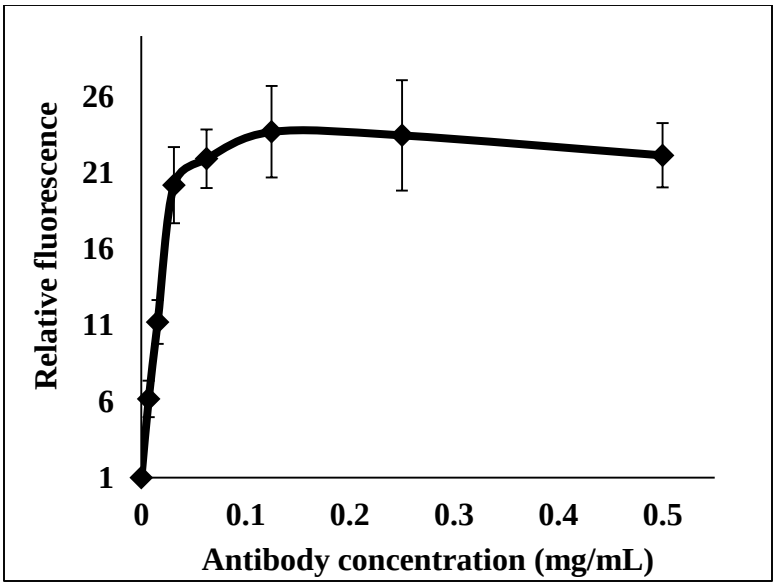

Figure 16. Experiment to determine maximum antibody spotting concentration for embedded retroreflector surfaces using fluorescently labeled antibodies.

Fluidic force discrimination – theory and application

Almost all solid-phase sandwich immunoassays include a washing or rinsing step to serve the purpose of reducing the "background" signal from labels that are unselectively or non-specifically bound to the surface. Non-specific binding or adsorption, which can result from electrostatic, hydrophobic or van der Waals interactions, is a major cause of low analytical sensitivity and specificity in immunoassays.

Atomic Force Microscopy (AFM) is usually used to measure bond strengths for specific and non-specific interactions. Although these measurements are highly dependent on AFM loading rate[77], they provide reasonable order of magnitude estimates; widely cited and accepted examples for specific interactions include the rupture forces of covalent bonds (ca. 2 nN) and sulfur-gold anchors (ca. 1.4 nN)[78], DNA duplexes (ca. 1 nN)[79], biotin-streptavidin interactions (ca. 1 nN)[80] and antibody-antigen interactions (ca. 250 pN)[81]. The strength of non-specific bonds in biological ligand-receptor systems has

been demonstrated to be at least an order of magnitude weaker than specific antibody-antigen bonds[79, 82], but hasn't been studied widely using AFM experiments. Based on related work in non-biological systems, including the measurement of hydrophobic bond strength (18 pN)[83] by Ray et al. and the calculation of van der Waals rupture forces by Lee et al. (12 pN)[80], non-specific interactions in biological systems are widely estimated as having rupture forces of 10 pN or less[54, 84]. The application of a force stronger than the strongest non-specific interaction, but weaker than the weakest specific interaction, can be expected to selectively rupture non-specific bonds and consequently increase assay sensitivity.

The application of controlled tangential laminar fluidic forces to surface-bound beads has been previously used to enhance the sensitivity of "surface coverage" assays[54, 57, 60]. In this work, controlled forces between 10-50 pN were applied to surface-bound magnetic beads for force discrimination. The calculation of volumetric flow rates that would result in the desired forces was done as follows.

The force on a stationary bead in bulk fluid flow is given by the Stokes drag

$$\mathbf{F_s = 6\pi\mu a v,} \tag{1}$$

where a is the bead radius, μ is the fluid viscosity, and v is the fluid velocity at the center of the bead.

Similarly, the torque in bulk fluid flow on a single bead is given by

$$\boldsymbol{\tau_s = 4\pi\mu a^2 v.} \tag{2}$$

Goldman et al. provided the exact laminar solutions[85] for the force and torque on a stationary bead at a wall in a semi-infinite fluid to be

$$\mathbf{F = 1.7005 * 6\pi\mu a v} \text{ and} \tag{3}$$

$$\boldsymbol{\tau = 0.94399 * 4\pi\mu a^2 v.} \tag{4}$$

The wall-modified force F and torque τ were used in the bead detachment model of Chang and Hammer[86], the geometry of which is shown in Figure 17. This model calculates the tension force on a molecular tether holding a bead to a surface as being much larger than the simple Stokes drag because of the offset between the bead-surface contact point and bead-tether point, which creates a mechanical lever.

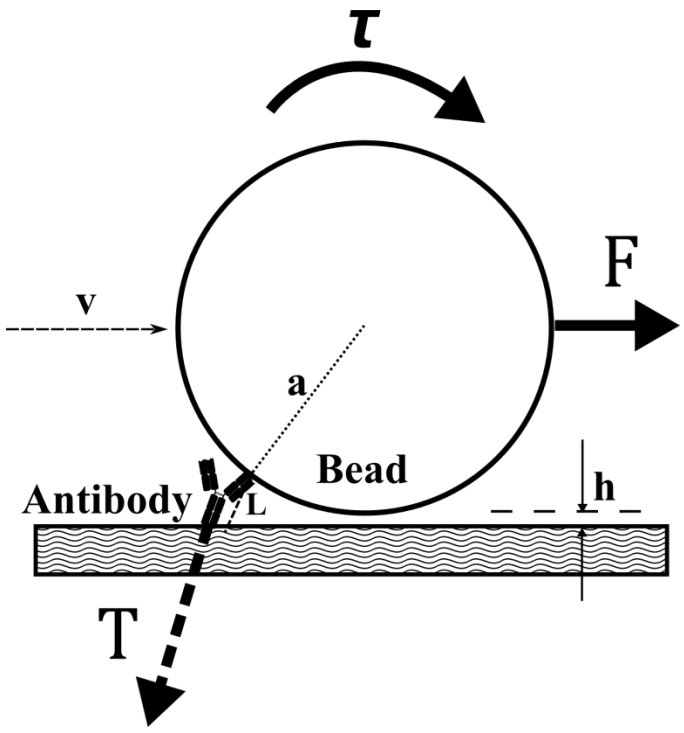

Figure 17. Geometry of the model used to estimate applied forces on the beads. a – radius of bead, h – separation distance between bead and embedded retroreflector surface, L – length of the tether binding the bead to the surface, T – tension on the tether, F – hydrodynamic force on the bead, τ – hydrodynamic torque.

According to this model, the tension on the bead-surface tether is

$$\mathbf{T \cong \left(F + \frac{\tau}{a}\right)\sqrt{\frac{a}{2(L-h)}}}. \quad (5)$$

A plot of tension T, as calculated using the above equation, against volumetric flow rate, for the microfluidic channel geometry used in this work, is shown in Figure 18 for 1µm beads and 3 µm beads. To generate this plot, the velocity at the center of the channel was calculated using the volumetric flow rate and channel cross-section, following which the velocity at the bead center was estimated by assuming a parabolic velocity profile. From the figure, it is immediately apparent that 3 µm beads can be readily force discriminated using more reasonable flow rates.

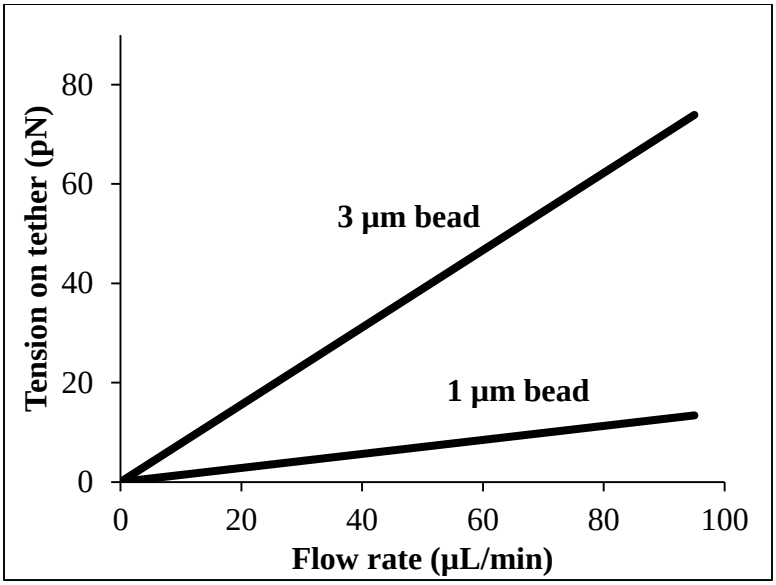

Figure 18. Tension on a single molecular tether holding beads to the surface, as calculated by the Chang and Hammer model. The tether was assumed to be 15 nm long. The parameter h, which indicates surface/bead roughness, was assumed to be negligible in comparison to L.

Assay development using 1 µm beads

During the development of the original ion beam lithography and reactive ion etching-based linear retroreflector process by the Ruchhoeft research group, immunoassay development was performed using 1 µm beads (purchased with COOH modification) as labels and SU-8 or Si coated with transparent 15 nm-thick gold as the sensing surfaces. This design was meant to exploit and optimize the well-developed surface chemistries available for the bio-functionalization of gold, and perform assays using microfluidic chips that simulated embedded microretroreflectors from a surface chemistry perspective.

In a bid to understand and avoid any potential mass transport issues, the magnitudes of Stokes drag and Brownian motion induced particle transport were calculated for different bead sizes. The Stokes settling velocity is derived from a force balance between Stokes drag, gravitational forces and buoyant forces acting on a particle with zero acceleration. The Stokes settling velocity, for or a particle of diameter x and density ρ_p in a fluid of viscosity µ and density ρ_f is given by

$$\mathbf{v_s} = \frac{(\boldsymbol{\rho_p} - \boldsymbol{\rho_f})\mathbf{g}\mathbf{x}^{\mathbf{2}}}{\mathbf{18}\mu}. \quad (6)$$

Einstein defined Brownian motion as a diffusion process occurring due to the disordered motion of the particles produced by thermal molecular motion. For the same case as above, a dynamic equilibrium between Brownian diffusion and Stokes drag gives the formula for the diffusion co-efficient of a sphere D (k is the Boltzmann constant and T is temperature in K) to be

$$\mathbf{D} = \frac{\mathbf{kT}}{\mathbf{3\pi\mu x}}\,. \tag{7}$$

An expression for the mean displacement (in one direction) due to the Brownian motion of a spherical particle suspended in a fluid can be obtained from the equation $\delta^2 = 2Dt$, using which

$$\boldsymbol{\delta} = \sqrt{\mathbf{t}}\sqrt{\frac{\mathbf{2kT}}{\mathbf{3\pi\mu x}}}\,. \tag{8}$$

Table 2. Comparison of Brownian motion and Stokes settling for different particles. All values computed for a temperature of 300K.

Particle	Brownian displacement in water in 1 s (μm)	Stokes settling velocity (in water), μm/s
3 μm ProMag beads	0.54	1.96
1 μm Sera-Mag Speedbeads	0.94	0.22
1 μm Sera-Mag bead bearing an *E. coli*	0.59	1.36
250 nm magnetic beads	1.87	0.014
40 nm gold	4.68	.016
2 nm gold	21	0.00004
***E. coli* (1.5 μm sphere)**	0.76	0.04

Table 2 lists the values of mean displacements calculated using the above equations and compares Stokes settling and Brownian motion in an attempt to set a lower limit for purely sedimentation-based capture in microfluidic channels. Though over-simplified, this analysis provided an insight into why additional forces might be needed to have analyte-bearing particles below a certain size interact with antibodies on the

bottom surface of the microchannel. The 1 μm beads under consideration, for instance, are significantly Brownian, and would require more than 10 minutes to sediment to the bottom of a 150 μm tall channel. The 3 μm beads are not strongly Brownian on their own, and settle to the bottom of a 150 μm channel in less than 90 s.

Magnetic force acting on a superparamagnetic bead

The superparamagnetic nature of the commercially purchased magnetic beads (indicated by the absence of hysteresis in Figure 19) used in this work aided sample pre-concentration and potentially contributed to better assay sensitivity. The magnetic nature of the beads potentially allows the manipulation of their transport in microfluidic channels in two ways – enhancing transport to the surface, and the removal of non-specifically bound beads. To explore these possibilities for the 1 μm magnetic beads, cylindrical permanent magnets (material: NdFeB), purchased from K&J Magnetics (Pipersville, PA), were evaluated computationally or experimentally using COMSOL Multiphysics and microfluidic experiments that incorporated an array of millimeter-sized permanent magnets directly under or above the channel (for pull-down or pull-off), respectively.

When a material is placed in a magnetic field of strength **H**, the individual atomic moments in the material combine to result in induction or flux density $\mathbf{B} = \mu_0(\mathbf{H} + \mathbf{M})$, where **M** is the magnetization of the material (magnetic moment per unit volume). The flux density **B** has units of Tesla (T), while the magnetization **M** and magnetic field strength **H** have units of A/m. The volumetric magnetic susceptibility χ (dimensionless) is the slope of the linear region of the M-H curve, which can be measured using a

magnetometer. Superparamagnetic beads have no remnant magnetization, and hence produce M-H curves similar to Figure 19.

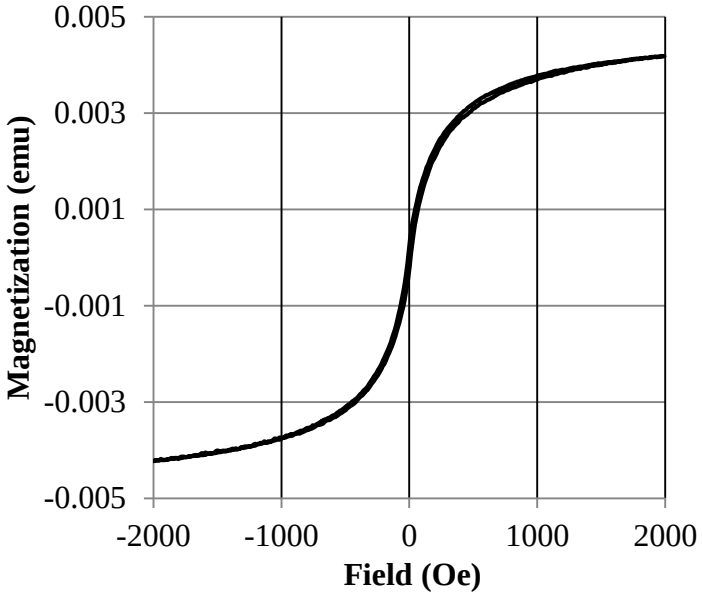

Figure 19. M-H curve of 1 µm superparamagnetic beads; data from Yi-Ju Wang.

If superparamagnetic beads are assumed to be point-like dipoles, the magnetic force acting on one bead ($\mathbf{F_m}$) can be written as a function of the gradient of the flux density **B**, the difference in volumetric susceptibility between the particle and the medium $\Delta\chi$ and volume of the particle V (μ_0 is the relative permeability of vacuum) as[87]

$$\mathbf{F_m} = \frac{\mathbf{V\Delta\chi}}{\mu_0}(\mathbf{B}.\boldsymbol{\nabla})\mathbf{B}\,. \tag{9}$$

The exact hydrodynamic drag (Stokes drag) acting on the particle is given by

$$\mathbf{F_d} = \mathbf{6\pi\eta r\Delta v f_d}, \tag{10}$$

where r is the radius of the particle, $\Delta\mathbf{v}$ is the velocity difference between the magnetic particle and liquid, and f_d is the drag co-efficient of the particle that is significant only

when the particle is close to the wall and thus ignored. The maximum particle velocity that can be generated by a magnetic force[87] can be obtained by equating (9) and (10), and is given by

$$\Delta \mathbf{v} = \frac{2\mathbf{r}^2 \Delta \boldsymbol{\chi} (\mathbf{B}.\nabla)\mathbf{B}}{9\mu_0 \boldsymbol{\eta} \mathbf{f_d}}. \qquad \textbf{(11)}$$

The magnetic fields generated by NdFeB permanent magnets were modeled using COMSOL, following which and the calculated magnetic flux densities and gradients were plugged into (11) to help model the behavior of 1 μm beads under magnetic fields. It should be noted that all the theory presented above was for the behavior of a single bead. Other forces, notably bead-bead interactions, come into play when analyzing more than one bead. An example model for the prediction of forces on a 1 μm superparamagnetic particle in a channel is shown in Figure 20.

The model consisted of an array of five 3 mm NdFeB magnets (that run the length of a microfluidic channel). Using the 2D magnetostatics module and post-processing in COMSOL 3.5a, the magnetic force on single particles at different vertical distances from the magnet array were calculated. As discussed earlier, force discrimination for specificity enhancement requires non-specifically bound labels to be subjected to at least 10 pN of force. The results of the COMSOL model predict this as being possible using an array of 3 mm NdFeB magnets placed 1 mm from the bead – if successful, this would enable magnetic "pull-off" to force discriminate specifically and non-specifically bound magnetic beads.

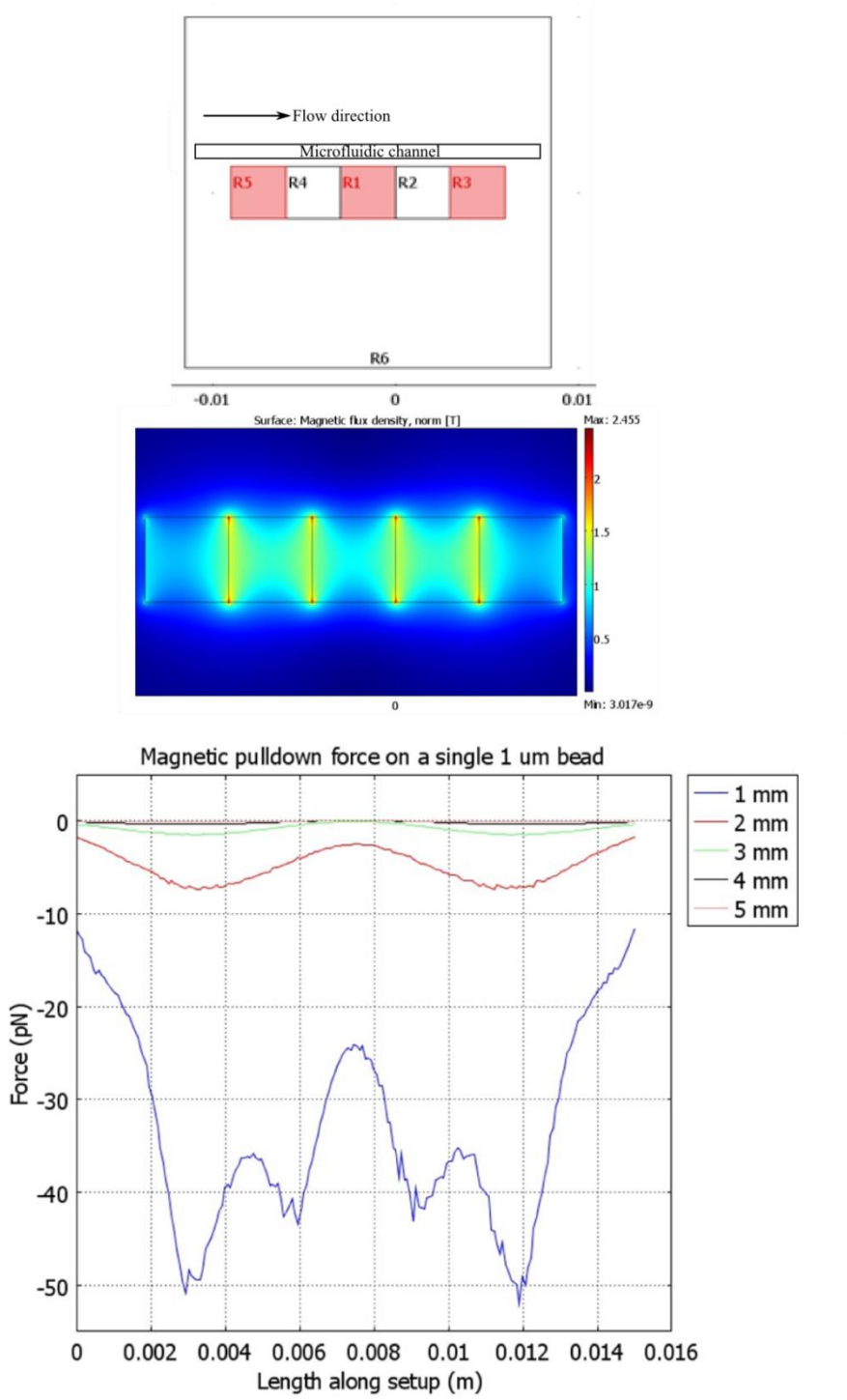

Figure 20. 2D COMSOL model for magnetic pull-down/pull-off. (top) 2D model showing array of five magnets; (middle) solution of model showing a surface plot of flux density; (bottom) a plot of the magnetic pull down force on a single 1 μm bead at different heights above the magnet array.

However, magnetic pull-off according to the model was deemed as being geometrically and spatially impractical to implement on routine basis. Moreover, the COMSOL model predicts a significant variation (between 10 and 50 pN) in the forces that would have been experienced by a bead along the length of the channel; this would not have boded well for intra-assay uniformity and inter-assay reproducibility. A review of the literature indicated that magnetic force discrimination assays implemented using permanent magnets and simple geometries have only been reported as generating forces on the order of 1 pN so far[56, 88]. It is therefore also possible that the model described here overestimated the magnetic forces that could be generated from simple permanent magnet arrangements. Experimentally, magnetic "pull-down" to enhance bead transport to the surface was unsuccessful – using the magnet array under a microfluidic channel during flow resulted in the beads irreversibly clumping together and aligning in the direction of the gradient as shown in Figure 21.

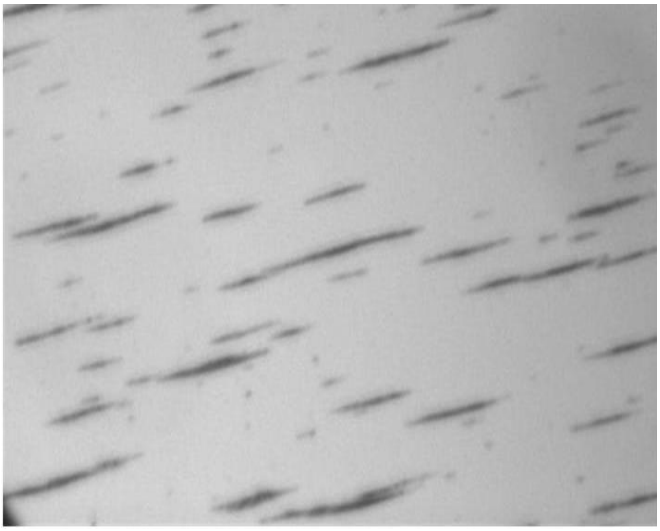

Figure 21. Aggregation and non-specific binding of 1 µm beads in a microfluidic channel placed over an array of NdFeB permanent magnets. A 0.057 mm^2 area of a gold-coated microfluidic surface is shown here.

R. conorii detection using 1 µm beads and top-down imaging

1 µm beads were used as labels in surface coverage assays for *R. conorii* detection, with direct optical imaging using a CCD camera linked to a 60x objective as the readout. Images acquired this way were analyzed using ImageJ software as follows – total grayscale values were calculated in pre-defined regions of interest inside the camera's field of view after applying a threshold to remove noise; these values were divided by the average pixel size of single beads to extract bead counts. These assays performed reasonably well for having being subjected to less than 10 pN of force in FFD. Overall, the combination of the low non-specifically binding PEGylation chemistry used on the gold-coated sensing surfaces, the faster gravitational settling of bead-bacteria complexes compared to beads alone during the period allowed for interaction with the channel surface, and moderate fluidic force discrimination resulted in an analytical limit of detection around 5×10^4 *R. conorii*/mL and 2×10^5 *R. conorii*/mL from buffer and serum, respectively (Figure 22).

R. conorii concentrations that resulted in bead counts at least three standard deviations above the background bead count were considered detectable. Interestingly, although the LOD in diluted human serum was around an order of magnitude worse than in buffer, the background bead counts were lower, lending credence to notion that serum proteins aid lower non-specific binding in immunoassays. The standard deviations in Figure 22 were computed from at least four independent measurements.

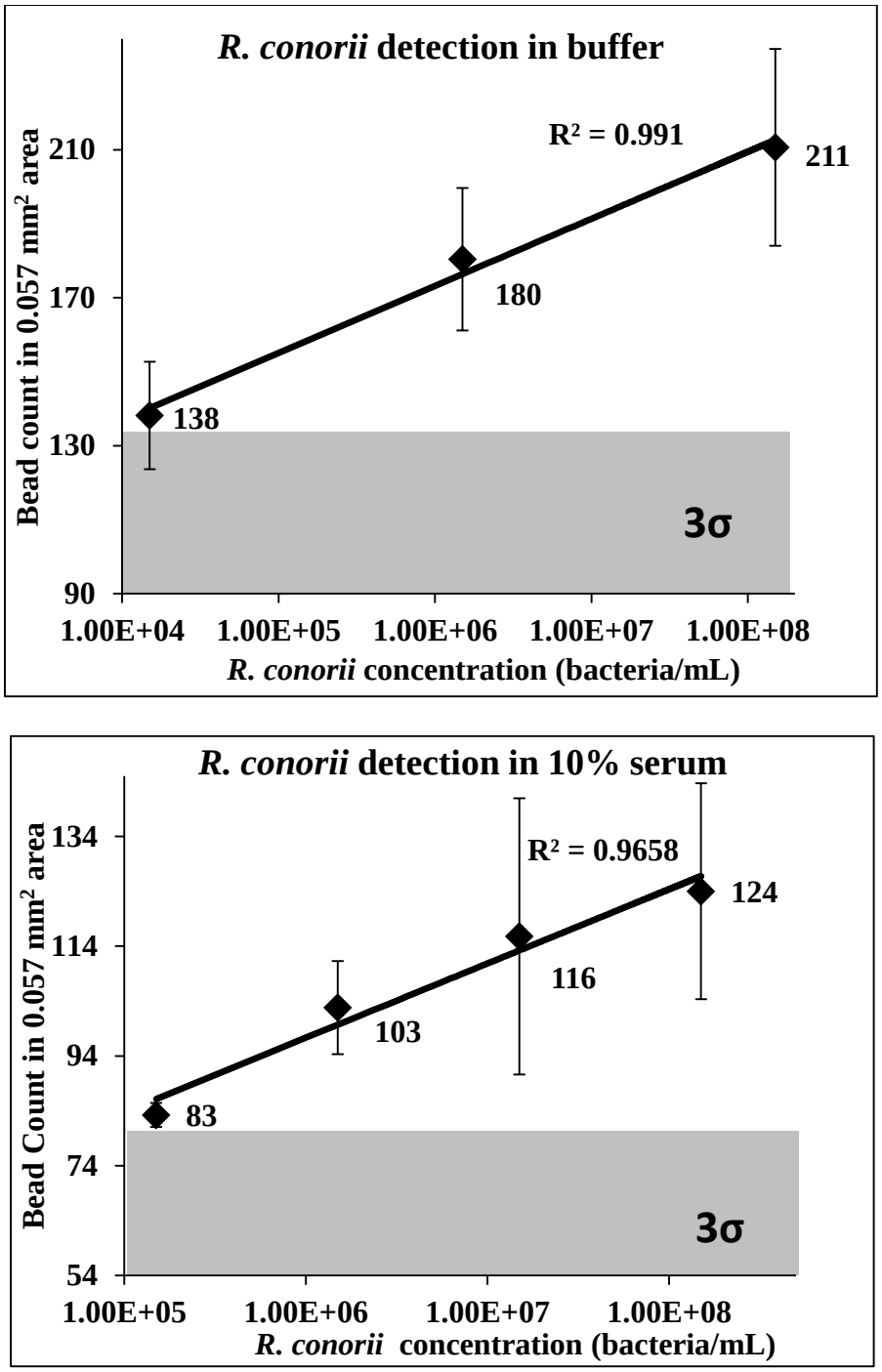

Figure 22. *Rickettsia* detection using 1 μm beads as labels. (top) Rc detection from PBS buffer. Background = 90; (bottom) Rc detection from 10% human serum. Background = 54. Shaded regions represent three standard deviations above background to help estimate LOD.

Switching to 3 μm beads as labels and antibody-coated PMMA as sensing surface

After initial assay development as described above, a switch from using 1 μm beads to 3 μm beads as labels was made for the following reasons:

- **Mass transport**. For the 150 μm channel used in this work the 1 μm beads require more than 10 minutes to sediment to the surface (assuming they start at the top). The 3 μm beads, on the other hand, require 75 seconds. This inadequacy of the smaller beads was partially overcome for this model analyte system by virtue of the captured bacteria increasing the size of the complex and therefore gravitational force acting on it. This is a luxury that might not present itself for, say, a protein analyte.
- **Fluidic force discrimination.** The tension on molecular tethers as calculated by the Chang and Hammer model scales as $a^{3/2}$, where a is the bead radius. The 3 μm beads therefore experience a much greater force than do the 1 μm beads at lower flow rates that are capable of being produced by more-portable pumping systems based upon electrokinetic or centrifugal flow.
- **Difference imaging.** The automated difference imaging algorithm, which uses larger field-of-view and lower numerical aperture optics than manual top-down imaging, was more accurate with 3 μm labels.

The surface chemistry stack used for immunosensing was switched at the same time as the size of the label, and went from the use of 15 nm thick, thermally evaporated (and transparent) thin gold films to spin-casted poly(methyl methacrylate) (PMMA) as the surface to be bio-functionalized with capture Anti-Rc antibodies. This change was made after repeatedly observing difficulties in reproducibly and completely covering SU-8

surfaces with thin gold films. Thermally evaporated thin films of gold are known to have discontinuous morphologies at low thicknesses, stemming from large values of residual tensile stress; this results from the formation of grain boundaries at the expense of strain energy[89]. Any attempts to prevent the formation of these gold "nanoislands" would have required precise control over the deposition rates and thickness, making it unattractive as a long term option. Additionally, gold is known to have adhesion issues with polymeric substrates[90], and a low bond strength with SU-8[91].

***R. conorii* detection using 3 µm beads and difference imaging**

Linear microretroreflectors were embedded in PMMA by spin-casting, and used directly for antibody immobilization by one of two strategies described in the Materials and Methods section: oxidation of the F_c region of Anti-Rc followed by directed immobilization, or primary amine-mediated immobilization after PEGylation of PMMA. The "bead count per tile", of which there were several hundred in each experiment, was used as the readout for retroreflective-imaging based experiments that used the automated difference imaging approach.

In the microfluidic approach described here, irregular bead counts were occasionally observed from a few tiles in certain channels. These outliers would skew a conventional averaging approach. They were caused by factors including, but not limited to the following:

- Local flow abnormalities from manual assembly of microfluidic chip
- Bubbles in the microchannels
- Irregularities in antibody densities within a microchannel from "coffee drop" effects

The adoption of an automated approach to imaging precludes the manual removal of extreme outliers in the data. Also, the fact that the assay is meant as a "yes/no" screening diagnostic obviates the need for quantitation or precise dose-response measurements; rather, a clear distinction between a "blank" sample and a sample containing a target analyte is sufficient. With these considerations in mind, bead counts per tile as calculated by the difference imaging algorithm for different *Rickettsia* concentrations were plotted and visualized as notched box plots.

A box plot is a non-parametric and convenient way of graphically depicting groups of numerical data through their quartiles. It displays the variation in samples of a statistical population without making any assumptions of the underlying statistical distribution. A variation thereof, a notched box plot, provides a rough guide to significance of difference of medians - notches on the box represent the equivalent of a confidence interval (for normal distributions) about the median value. In this work, the displayed notches extend to $\mathbf{1.58}\,(\mathbf{IQR})/\sqrt{\mathbf{n}}$ on either side of the median, where IQR is the interquartile range and n is the number of tiles from which bead counts are obtained. This value, based on the asymptotic normality of the median and roughly equal sample sizes for the two medians being compared, is insensitive to the underlying distributions of the samples. Non-overlapping notches, therefore, imply a significant difference in the medians of data represented by the relevant data sets with a 95% confidence level.[92-93]

Assay results for *R. conorii* detection, using directed F_c-mediated Anti-Rc immobilization on both beads and PMMA surfaces, are shown as notched box plots in Figure 23. 250 μL of PBS were used as samples for these experiments. The lowest detectable *R. conorii* concentration per sample, therefore, corresponded to an LOD of

4000 bacteria per mL. At least 100 tile counts were used to make the boxes corresponding to each sample. Lines at the intersection of notches indicate median bead counts (labeled on plot); for each box, lower and upper whiskers represent the 10th percentile and 90th percentile, respectively.

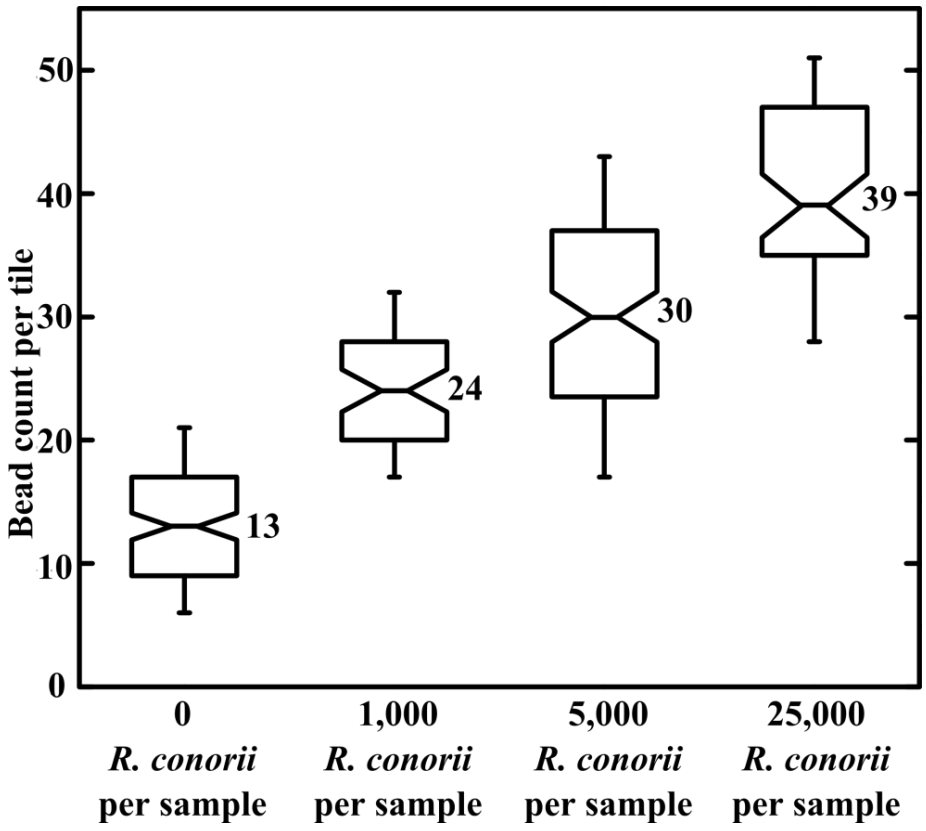

Figure 23. Detection of *R. conorii* in spiked buffer using directed antibody immobilization approach. Non-overlapping notches imply significantly differing median values with 95% confidence.

Assay results for *R. conorii* detection, using primary amine-mediated random Anti-Rc immobilization on PEGylated beads and PMMA surfaces, are shown as notched box plots in Figure 24, in which at least 150 tile counts were used to make the boxes corresponding to each sample. As in Figure 23, the lines at the intersection of notches

indicate median bead counts (labeled on plot); for each box, lower and upper whiskers represent the 10th percentile and 90th percentile, respectively.

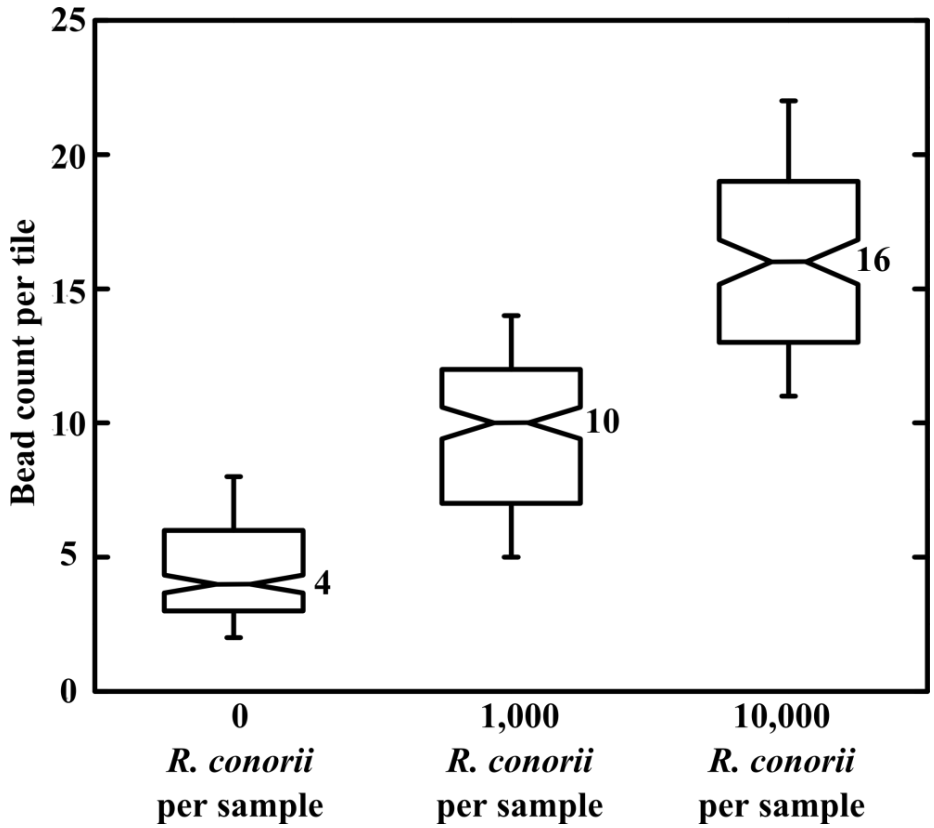

Figure 24. Detection of *R. conorii* in spiked buffer using PEGylation followed by random antibody immobilization. Non-overlapping notches imply significantly differing median values with 95% confidence.

The PEGylation approach to antibody immobilization was an attempt to lower the variability of the bead counts originally obtained for the "background" sample in the absence of analyte (first box to the left in Figure 23 with median bead count =10) and thereby enhance analytical sensitivity. As Figure 24 shows, the background bead count was substantially lowered by PEGylation (median bead count = 4). In addition, the "positive" samples had proportionately higher numbers in terms of the signal-to-noise ratio. However, the original analytical sensitivity was not improved upon, potentially indicating that the mass transport limit of affinity recognition during homogeneous

mixing and/or solid-phase capture for the current assay configuration may have been reached. The current analytical sensitivity of 4000 bacteria per mL is in the clinically relevant range for several pathogenic bacteria including *R. rickettsii E. chaffeensis, E. ewingii, P. aeruginosa,* and *N. meningitidis*[94].

Conclusions

In summary, a novel, amplification-independent optical immunoassay platform based on using embedded microfabricated linear retroreflectors as the sensing surface and micron-sized magnetic beads as light-blocking labels was developed and used for bacteria detection, with *R. conorii* serving as a model analyte. The platform was implemented in a semi-homogeneous microfluidic format – bacteria were captured by antibody-modified magnetic beads before introducing them into microchannels, the bases of which were formed by detector antibody-modified embedded retroreflectors. The microfluidic immunoassay, using analyte-loaded magnetic beads, was performed using a "stop and drop" method for loading, and fluidic force discrimination to remove non-specifically bound beads. An automated XYZ stage and image capture program were used for the automatic imaging of all sensing regions before the assay and after assay, and analyzed by a difference imaging algorithm to provide "bead counts", representing specifically-bound beads, as the readout. Assay development involved the use of different bead label sizes and surface chemistries, and the use of different materials to enable antibody-modification of embedded microretroreflectors. In its final form, the analytical sensitivity of the platform was determined to be 4000 *R. conorii* per mL in PBS. The analytical sensitivity of the platform developed in this work is in the range of clinical relevance for bacteria detection.

CHAPTER 3 – RECOMBINASE POLYMERASE AMPLIFICATION ASSAYS FOR DETECTION OF URINARY TRACT INFECTION PATHOGENS

Introduction

Urinary tract infections

Urinary tract infections (UTIs) are the most common bacterial infections in the United States[95] and the most common nosocomial infection affecting the elderly[96]. Besides accounting for as many as 35% of all nosocomial infections, they result in 7 million visits to outpatient clinics, 1 million visits to emergency rooms, and 100,000 hospitalizations annually[97]. The annual US healthcare costs directly related to community-acquired UTIs exceed $1.6 billion[98]. Bacteria routinely colonize the urinary tract, but are washed out during micturition in healthy individuals. Uncomplicated or lower UTIs occur when bacteria reach the bladder, multiply to significant numbers and colonize it – human anatomy allows for this to occur more frequently in women[97]. Bacterial colonization of the bladder resolves spontaneously in most people, but occasionally leads to symptoms such as frequency, urgency and dysuria[99]. The progress to symptomatic infection depends on the virulence characteristics of the bacterial pathogen, and host factors including sex, age, genetic predisposition, and sexual activity. If left untreated, complicated or upper UTIs such as acute pyelonephritis or kidney infection can result and possibly progress to septic shock[100], which can be life threatening. Enteric bacteria (*Escherichia coli* in particular) are the most common etiological agent of UTIs, but the distribution and frequency of causative agents vary

between patient populations, and depending on whether the infection is community- or hospital-acquired.

Diagnosis of UTIs

Following diagnosis using culture-based or culture-independent methods, most UTIs can usually be easily managed and resolved with antibiotics. However, the diagnosis of UTIs is not always straightforward – this is primarily due to the wide spectrum of urinary conditions ranging from asymptomatic bacteriuria (bacteria present in urine with no associated symptoms attributable to the genitourinary tract) to complicated UTIs and septic shock requiring hospitalization. In addition, there are different diagnostic criteria required for different patient populations (elderly, children). Nonculture methods for the laboratory diagnosis of UTIs include microscopy for the detection of bacteriuria or pyuria (the presence of leukocytes in urine) and rapid dipstick tests that non-specifically detect nitrite-producing bacteria or leukocyte esterase activity[101]. When used together, as they are in commercial automated L/N urinalysis systems, these tests generally have low sensitivities and positive predictive values, and high specificities and high negative predictive values[102-104]. This makes useful for ruling out UTIs (on the basis of a negative test result) in patient populations with a low pre-test probability of infection. Urine cultures, which are the only widely-used tests that provide information about pathogen identity and antibiotic susceptibility, are necessary for outpatients that have recurrent UTIs, treatment failures or complicated UTIs, and inpatients that develop UTIs. The imperfect nature of nonculture methods results in physicians ordering culture tests even when diagnoses seem straightforward. In many clinical laboratories, therefore, urine cultures are the most common type of culture[101].

Pathogen concentrations greater than 10,000 cfu/mL of urine is a common threshold used for UTI diagnosis[105-107]. This threshold may vary depending on the patient population – 100,000 cfu/mL is a threshold used for women with acute pyelonephritis[108], while 100 cfu/mL is use for catheterized patients where early detection is vital[109-110]. Culture results usually can be readily interpreted, and help guide physicians on the choice of antibiotics and the course of treatment. However, pathogen quantification and identification from culturing methods can take up to 48 hours. Also, some pathogens associated with UTIs are nonculturable[111].

Isothermal nucleic acid amplification techniques

Nucleic acid amplification techniques (NAATs) such as the Polymerase Chain Reaction (PCR), which are inherently faster than culture, are attractive as diagnostic tools replacing urine culture to establish pathogen identity and also identify genes that confer them with antibiotic resistance. Although platforms like the FilmArray system (discussed in Chapter 4) have taken PCR-based detection closer to routine use in near-patient settings, it is challenging to develop PCR technologies that are truly field portable and point-of-care, owing primarily to the need for thermal cycling. Isothermal NAATs, which offer comparable limits of detection to PCR in many cases and perform nucleic acid amplification at a constant reaction temperature, offer a cheaper alternative. Their isothermal nature translates into the need for less complex and expensive instrumentation and greater applicability in low-resource settings – reactions can be performed in a water bath or using simple resistive heaters, for example.

Various isothermal NAATs such as Loop-mediated Isothermal Amplification (LAMP), Cross-priming Amplification (CPA), Smart amplification (SMART-AMP),

Rolling Circle Amplification (RCA), Ramification amplification (RAM), Strand Displacement Amplification (SDA), Nicking Enzyme Amplification Reaction (NEAR), Isothermal Chain Amplification (ICA), Exponential Amplification Reaction (EXPAR), Transcription-mediated Amplification (TMA), Nucleic Acid Sequence-Based Amplification (NASBA), Signal-mediated amplification of RNA Technology (SMART), Helicase Dependent Amplification (HDA), and Recombinase Polymerase Amplification (RPA) that eliminate the need for thermal cycling have been developed in the last couple of decades and been reasonably successful[112-116]. They can be grouped based on the reaction principle – LAMP, CPA, SMART-AMP, RCA, and RAM are based on DNA polymerase-mediated strand displacement from linear or circular targets; SDA, NEAR, ICA, and EXPAR are based on polymerase extension and strand displacement following a single strand cutting event; NASBA, TMA, and SMART are primarily intended for RNA amplification, and use enzymatic RNA polymerization and reverse transcription-based amplification; HDA and RPA do not require an initial denaturation step, and are based on enzymatic duplex melting or primer annealing followed by polymerase extension.

Of the above methods, only TMA (Gen-Probe), NASBA (bioMérieux), and SDA (Beckton Dickinson) are well-established and commercially used, while LAMP (Eiken) and RPA (TwistDx) are slowly becoming mainstream. Of the DNA amplification techniques among these (SDA, LAMP, and RPA), RPA, which is relatively new, stands out by virtue of being the least complex to design and optimize, and the fastest-to-result. SDA and LAMP require the design of multiple sets of primers and probes for each target, and are 90-120 minute reactions, while RPA requires only one primer/probe set, and can

provide results in less than 20 minutes. Since its introduction in 2006[117], RPA has been validated in a variety of diagnostic applications and formats[118-122].

Recombinase polymerase amplification (RPA)

Recombinases are genetic recombination enzymes that catalyze the hybridization of short (30-40 nt) oligonucleotides to homologous regions of a double-stranded template, via strand exchange, in a directionally-sensitive manner. They are derived from bacteria or fungi, and are typically used in studies that manipulate the structure of genomes to activate or switch gene expression in a controlled manner, and to generate genetic diversity through the acquisition of advantageous genes or gene segments.[123-124] In recombinase polymerase amplification (RPA), recombinases are used along with target-specific forward and reverse primers to enable primer hybridization without the need for template melting (separation into single stranded DNA) as is required in PCR and other techniques.

A schematic of the general RPA cycle is shown in Figure 25. RPA begins when the phage T4 recombinase UvsX and its cofactor UvsY form a nucleoprotein complex with oligonucleotide primers (30-35 nt long) to scan for homologous sequences in a double-stranded DNA template. Homologous sequence recognition leads to strand invasion by the forward and reverse primer complexes. Following strand exchange, the displaced strand is bound and stabilized by single-stranded DNA binding proteins, thereby preventing ejection of the primers by branch migration. The recombinase molecules then disassemble from the primer, leaving the 3' end of the primers accessible to the strand-displacing Sau DNA polymerase (*Staphylococcus aureus*), which catalyzes primer extension. The cyclic repetition of this process, at a constant temperature (37-

42°C), yields dsDNA amplificates exponentially as in PCR. In “end-point RPA”, agarose gel electrophoresis is used to visualize amplified DNA after 20-30 minutes.

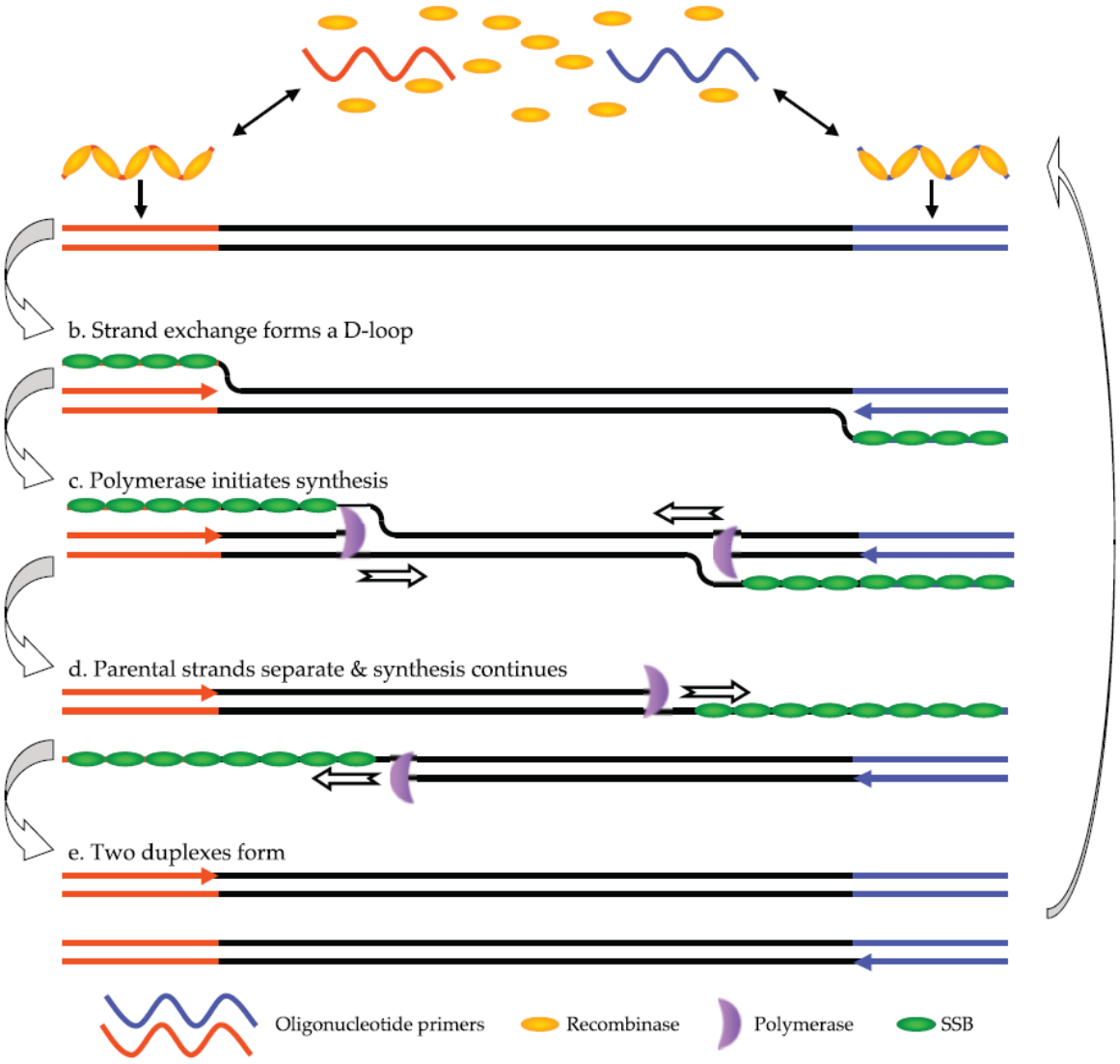

Figure 25. Schematic of an RPA cycle. Image from http://twistdx.co.uk.

Real-time RPA using TwistAmp exo probes

Real-time RPA can be performed using non-specific dsDNA intercalation dyes such as SYBR green to monitor the exponential amplification of DNA. However, the long primer lengths required in RPA make it extremely difficult to design highly non-

complementary primer sets and preclude the formation of primer dimers and other secondary structures that cause non-specific dyes to fluoresce. TwistAmp exo probes (TwistDX, Cambridge, UK), which are oligonucleotides with sequence homology to either the plus or minus strand of the target amplicon, can be used to monitor real-time amplification in RPA. They contain an abasic nucleotide analog (tetrahydrofuran or THF, sometimes called a 'dSpacer') located approximately 15 nucleotides (nt) upstream from the 3' end of the probe (45 to 55 nt) and flanked on either side by a fluorophore and corresponding quencher attached to thymines.

Exo probes are also blocked from polymerase extension at the 3' end by a suitable modification, such as a C3-spacer, a phosphate, or an amine. Any fluorescence from the fluorophore (typically fluorescein, or TAMRA which is rhodamine-derived) is quenched by the quencher (typically a suitable Black Hole Quencher, BHQ) located 2 to 4 bases 3' of the fluorophore. During a real-time RPA reaction, recombinase facilitates strand invasion and annealing of exo probes to the amplification product. This double stranded state triggers the cleavage of the dSpacer site, a substrate for the DNA repair enzyme exonuclease III (part of the TwistAmp exo kit), thereby releasing the probe section containing the quencher, and generating a fluorescent signal. Upon cleavage, the section of the probe originally 5' of the dSpacer is extended by the polymerase, creating additional amplification product. The development of fluorescence, therefore, is indicative of specific target amplification and also proportional to the degree of amplification. A schematic of a typical exo probe, along with typical fluorescence amplification curves, is shown in Figure 26. Because the THF residue is only cleaved

when the probe is specifically bound to the target, exo probes provide an additional layer of specificity checking besides enabling real-time monitoring of RPA reactions.

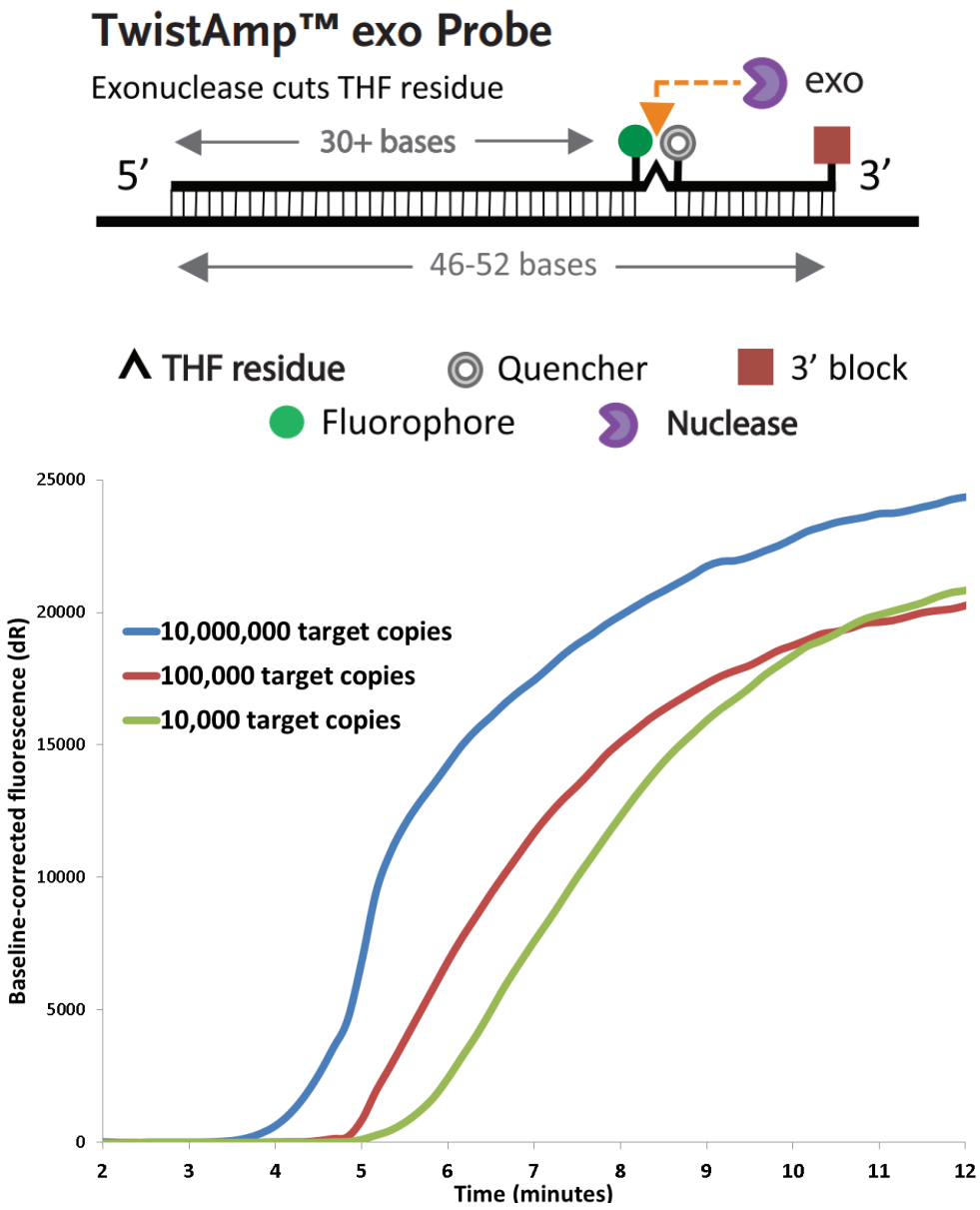

Figure 26. Real-time RPA using exo probes. (top) Schematic of an annealed TwistAmp exo probe (http://twistdx.co.uk); (bottom) Example of fluorescence (FAM fluorophore) amplification curves generated by real-time RPA using exo probes showing exponential amplification of DNA.

In the last five years, real-time RPA has emerged as a promising technology for POC applications owing to the commercial availability of lyophilized reagents pre-loaded into reaction tubes and the emerging widespread use of miniature handheld or benchtop fluorescence monitoring readers.

Outline of work

This chapter describes the development and small-scale clinical validation of a panel of real-time exo-probe based real-time RPA assays targeting six pathogens most commonly implicated as the etiologic agents of UTIs. These pathogens (*Escherichia coli*, *Proteus mirabilis*, *Klebsiella pneumoniae*, *Pseudomonas aeruginosa*, *Enterococcus faecalis* and *Enterococcus faecium*) were implicated in 84% and 85% of UTI samples that were part of the SENTRY Antimicrobial Surveillance Program in North America[125] and Europe[126], respectively; they could be more or less frequent for specific patient populations. A panel of readily POC RPA assays for these particular pathogens, if validated, would therefore offer clinical laboratories a cheaper and faster alternative to culture-based detection. In the following pages, the methods used in assay design and development are first described, following which analytical sensitivities and clinical sensitivities/specificities are determined using quantitative genomic DNA standards and a small cohort of well-characterized urine-extracted DNA samples, respectively.

Heather Goux, a PhD student in Biology and Biochemistry at the University of Houston and a rotation student in the Willson laboratory at the time, contributed to the work described in this chapter by assisting with primer and exo probe design. The clinical samples tested in this work, and their bacterial ID as determined by culture, were

provided by Medical Center Laboratories (Houston, Texas), a centralized laboratory that processes thousands of urine samples every year.

Materials and Methods

Quantitative genomic DNA standards

For analytical sensitivity determination, pure genomic DNA (gDNA) standards were generated by gDNA isolation and purification from colonies grown on culture plates. An UltraClean® Microbial DNA Isolation Kit (MO BIO Laboratories, Carlsbad, CA) was used, following the manufacturer's protocol, to isolate pure gDNA from sheep blood agar culture plates of each pathogen provided by Sri Rajagopalan (Scientific Director, Medical Center Laboratories). These plates had been streaked with reference strains of each pathogen purchased from American Type Culture Collection (Manassas, VA) and incubated overnight at 37°C. The absorbance of extracted gDNA samples at 260 nm (A260) was obtained using a Nanodrop 1000 instrument (NanoDrop Instruments, Wilmington, DE). Both A260/A280 and A260/A230 values were close to or greater than 2 for all samples, indicating negligible contamination by proteins or the organic solvents used in DNA extraction. In combination with the extinction coefficient of double stranded DNA (0.020 μg $mL^{-1}cm^{-1}$), average molar mass of double stranded DNA (650 Daltons/base pair) and genome size of each pathogen, the number of genomes per μL of the extracted pure gDNA was calculated (Table 3). Appropriate dilutions of these stocks were made, using deionized water, and stored at -20°C as quantitative genomic DNA standards in 5 μL aliquots containing 10^7, 10^6, 10^5, 10^4, 10^3, 10^2 or 10 genomes each.

Table 3. Pure gDNA stocks isolated from reference strain cultures and used for analytical sensitivity and specificity studies.

Organism and strain	Concentration (ng/µL)	Genome size (Mbp)	Genome mass (fg)	Genomes per µL (x 10^6)
E. coli ATCC 35218	33.6	4.64	5.01	6.70
P. aeruginosa ATCC 27853	36.2	6.30	6.80	5.32
K. pneumoniae ATCC 700603	31.4	5.30	5.72	5.49
E. faecalis ATCC 29212	15.2	3.34	3.60	4.20
P. mirabilis ATCC 25933	39.9	4.06	4.38	9.11

End-point RPA

End-point RPA was performed in a 50 µL volume using TwistAmp Basic kits (TwistDX, Cambridge, UK). Master mixes containing 480 nM RPA primers and TwistAmp rehydration buffer were prepared and distributed, in 42.5 µL volumes, into 0.2 mL reaction tubes, each containing a dried enzyme pellet. The enzyme pellet in each tube was rapidly solubilized by pipetting the master mix up and down upon addition. Subsequently, 5 µL of template DNA (purified genomic DNA or other template DNA), was added to the tubes. 2.5 µL of 14 mM magnesium acetate was pipetted into the tube lids, centrifuged into the tubes using a mini centrifuge, and immediately placed into a PCR thermal cycler programmed to operate at 42°C. End-point RPA reactions were typically performed for 30 minutes. A Qiagen PCR purification kit was used to remove the primers and other reagents from the reaction if the samples were to be sent for sequencing.

Real-time RPA

Real-time RPA was performed in a 50 μL volume using TwistAmp exo kits (TwistDX, Cambridge, UK). Master mixes containing 420 nM RPA primers, 120 nM RPA exo probes, and TwistAmp rehydration buffer were prepared and distributed, in 42.5 μL volumes, into reaction tubes supplied with dried enzyme pellets. 5 μL of template (quantitative gDNA standards or clinical sample) was then added to the tubes. To start the reaction, 2.5 μL of 14 mM magnesium acetate was added to each tube by pipetting into tube lids and centrifugation immediately before placing the tubes in an Agilent MxPro 3005 real-time PCR machine (Agilent Technologies, Santa Clara, CA). The real-time PCR machine was programmed to run for 30 minutes at 42°C and collect fluorescence data at 10 s intervals.

Culture-based identification of clinical samples

An automated culture-based bacterial identification and susceptibility testing system, VITEK 2 (bioMérieux, Hazelwood, MO), was used as the "gold standard" technique for the clinical evaluation of the RPA assay panel. The bacterial ID of 25 "true positive" urine samples and confirmation of "no growth" in 10 "true negative" urine samples as determined by VITEK 2, along with DNA extracted from all 35 samples, was provided by Medical Center Laboratories.

DNA extraction from clinical samples

A crude, high-throughput method[105] was used to extract DNA from urine. Briefly, 1 mL urine was pipetted into a 1.5 ml microcentrifuge tube and centrifuged at 12,000 x g for 5 min. The supernatant was discarded and 100 μL lysis buffer (1% Tween-20, 1% NP-40, 0.03% SDS, 5% Chelex 100 and 400 μg/mL proteinase K) was added to the pellet

and thoroughly mixed. The mixture was incubated at 56°C for 1 h, followed by 100°C for 10 min. The lysate was then centrifuged at 13,000 g for 5 min, and the supernatant, containing extracted DNA was transported in a patient de-identified form (50 μL of each sample) to the University of Houston for further testing.

Primers and probes

Complete genome sequences of the six targeted UTI pathogens are publicly available in the National Center for Biotechnology Information's (NCBI) GenBank database (http://www.ncbi.nlm.nih.gov/genbank). FASTA sequences of target genes, for each pathogen, were downloaded from GenBank and used for primer and probe design either as downloaded or following sequence alignment and consensus sequence generation using SeaView software[127]. When primer design was not performed manually, NCBI's Primer-BLAST website (http://www.ncbi.nlm.nih.gov/tools/primer-blast/) was used for initial primer design.

The specificity of all designed sequences (primers and probes) to their target was determined by performing a 'BLAST' search against all publicly available nucleotide sequences of a list of relevant species including the six UTI pathogens targeted in this work. So as to avoid the possibility of non-specifically amplifying human DNA often present in urine or unrelated UTI pathogens, this specificity-checking list included: *Homo sapiens, Escherichia coli*, *Proteus mirabilis*, *Klebsiella pneumoniae*, *Pseudomonas aeruginosa*, *Enterococcus faecalis*, *Enterococcus faecium*, *Citrobacter freundii*, *Enterobacter cloacae, Acinetobacter baumannii*, *Staphylcoccus aureus*, *Providencia rettgeri, Providencia stuartii*, *Morganella morganii*, and *Streptococcus agalactiae.* The

megablast and blastn algorithms on NCBI's nucleotide BLAST website were used using to perform specificity checking (http://blast.ncbi.nlm.nih.gov/Blast.cgi).

Secondary structure prediction and free energy calculations were performed using UNAfold software (Unified Nucleic Acid Folding and hybridization package, Rensselaer Polytechnic Institute). It is freely available through the "Oligo Analyzer" webpage (http://www.idtdna.com/analyzer/Applications/OligoAnalyzer) on the Integrated DNA Technologies (Coralville, IA) website. Primers were purchased from Integrated DNA Technologies, and TwistAmp exo probes were purchased from Biosearch Technologies (Petaluma, CA). They were reconstituted to the appropriate concentrations for RPA reactions using deionized Milli-Q water.

Determination of analytical sensitivity and specificity

The analytical sensitivities (limits of detection or LODs) of the panel of real-time RPA assays were estimated by performing real-time RPA on at least three and up to six replicates of different ten-fold serial dilutions of the quantitative gDNA standards, from 10^7 genome copies per reaction down to 10 genome copies per reaction. To check if the primers and probe designed for each UTI pathogen were specific to it (analytical specificity), they were used in real-time RPA reactions (run in triplicate) using at least 10^6 genome copies of non-specific gDNA (from the other pathogens on the panel) as the template.

Analysis of real-time RPA data

Fluorescence data (all probes used fluorescein-derived FAM as the fluorophore) was collected in 10 s intervals by the Agilent qPCR machine for each real-time RPA reaction. The reactions were typically run for between 20 and 30 minutes, resulting in the

collection of between 120 and 180 data points per experiment. This “raw” fluorescence data was not directly suitable for the comparison of experiments run using different fluorescent probes, and occasionally for the analysis of data from different reaction tubes using the same probe because of the following factors:

1. RPA reactions begin almost instantaneously upon the addition of magnesium acetate, which is why it was always added just before loading the reactions into the PCR machine or thermal cycler. This manual loading, however, could result in measurement variability.
2. Probes designed for different pathogens had different levels of background fluorescence in their quenched state – this stemmed from manufacturing variability and the inherent variability in their sequences (and therefore secondary structures), resulting in different levels of quenching.
3. Complex sample matrices sometimes have probe-independent background fluorescence that might vary from sample to sample.

To address the above issues, baseline functions and curve smoothing were implemented. Borrowing from how real-time PCR data is analyzed, and using MxPro software (Agilent Technologies), a baseline was calculated by fitting the raw fluorescence data obtained between manually specified times (between 120 s and up to 180 s from the beginning of the reaction; different time ranges were used for different exo probes) to a line using a linear least mean squares algorithm. This baseline function was subtracted from the raw fluorescence (R) function to obtain baseline-corrected fluorescence (dR).

The optimal time range for calculating the baseline function was empirically determined to be between the start of the reaction and 20 seconds before the raw fluorescence curve for the highest tested gDNA concentration (10^7 genomes per reaction) began to exponentially rise above the background. This baseline calculation method was individually determined for each exo probe (five in all) in the panel, and consistently used throughout this work, including for analyzing data from clinical samples. In addition, to reduce variation between replicates (though at the cost of losing some resolution), a 9-point moving average was applied to the smooth the amplification curve that plotted baseline-corrected fluorescence (dR) against time. Baseline subtraction and curve-smoothing help better visualize real-time RPA data obtained from different template dilutions and replicates.

For analytical sensitivity determination, threshold times were determined and compared for different serial dilutions of gDNA. The threshold time is a way of obtaining a single quantitative data point representative of each reaction. Slightly different background-based calculations – between 25 and 100 standard deviations above the average background fluorescence from the first 90 seconds to 4 minutes of the reaction – were developed for different exo probes and consistently used thereafter. The "threshold time" (analogous to threshold cycle in real-time PCR) represented the time, from the beginning of the reaction, at which the baseline-corrected fluorescence exceeded the threshold; higher target concentrations, therefore, were expected to result in shorter threshold times. The development of fluorescence towards the end of the exponential phase of amplification and beyond, however, was not proportional to starting template concentration, and was irrelevant to the analysis performed in this work.

Results and Discussion

A schematic of the overall assay development process is shown in Figure 27. There is no established way to design high sensitivity primer/probe combinations *a priori* for any NAAT, but established technologies like PCR have a well-defined set of rules that govern primer design and several commercially available software packages to automate the process. RPA, on the other hand, is relatively new, and does not afford this luxury. A systematic approach, which included bioinformatics-based primer and probe design, end-point RPA, Sanger sequencing, and primer screening using real-time RPA was used to guide and optimize real-time RPA assay development and optimization.

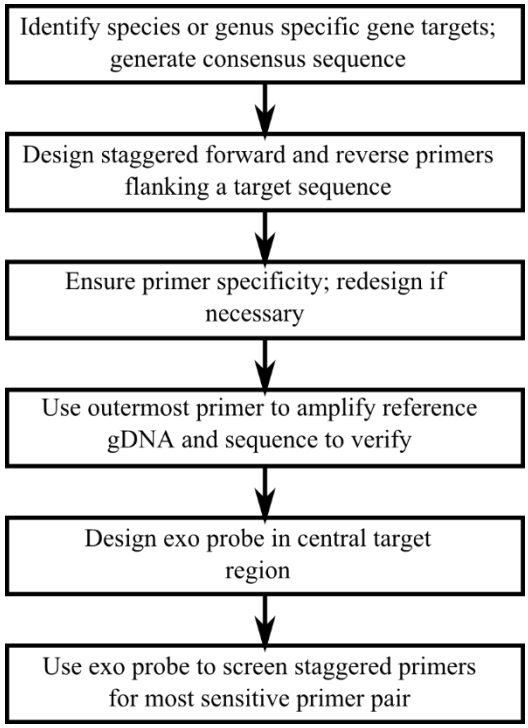

Figure 27. Flowchart of real-time RPA assay development process for UTI pathogen detection.

RPA primer design considerations

The following parameters were considered for RPA primer design:

1. **Primer length.** The primers were designed to be between 30 and 35 nt long, because the ability of recombinase proteins to enable strand invasion and priming decreases sharply below 30 nt lengths. The primers could have theoretically been longer than 35 nt, but excessively long primers were avoided due to the increased likelihood of secondary structures leading to primer noise.
2. **Sequence.** Although there are no fixed rules to predict the performance of a primer based on the order and composition of nucleotides, the following guidelines were followed based on empirical observations (manufacturer-recommended and otherwise):
    - Avoid long tracks of guanines (G) at the 5' end; preferably include cytidines (C) instead.
    - **G/C clamp:** The presence of Gs and/or Cs in the last three nucleotides at the 3' end of primers tends to improve performance by providing a more stable, 'clamped' target for the polymerase (Gs and Cs hybridize through three hydrogen bonds unlike As and Ts which hybridize through two hydrogen bonds).
    - Avoid long tracks of one particular nucleotide (example: AAAAA) or more than a few small repeats (example: ATATATAT).
    - Choose a GC content between 30 and 70%.

- Avoid sequence elements that are more likely to contribute to secondary structures (hairpins) and primer-primer interactions (this was done using UNAfold software).

3. **Amplification product length.** The TwistAmp kits, along with the reagent concentrations used, are optimized by the manufacturer to amplify targets shorter than 500 bp. In this work, therefore, all amplicons were designed to be between 100 and 250 bp long. Shorter products tended to result in an improved signal-to-noise ratio, and resulted in shorter assay times.

RPA probe design considerations

The following guidelines were followed for exo probe design based on TwistDx's recommendations:

1. Probe length - between 46 and 52 nt long (designed to target the plus or minus strands of the double-stranded template).
2. At least 30 nt 5' to the dSpacer (THF) residue, which replaces one base, and at least 15 nt 3' to it.
3. Avoid overlap of primers opposing the direction of the probe (this creates primer-probe dimers and amplification-independent fluorescence).

The internal fluorophore and quencher labels used in exo probes are currently only available commercially on thymines. This placed a restriction on finding probe sequences in the designed amplicon containing two thymines with fewer than 3 or 4 intervening nucleotides, in addition to satisfying the guidelines listed above, in order to maximize quenching efficiency. Because either strand of the target template could be used for probe

design, this restriction did not pose a major problem for the amplicons targeted in this work, and appropriate probe sequences were found.

RPA primer design strategy

A comprehensive review of the relevant literature was the starting point for amplicon, primer and probe design, in terms of picking the target regions of the pathogen's genome as highly species or genus-specific RPA targets. The final target genes: *chuA* for *E. coli*, *khe* for *K. pneumoniae*, *lasB* for *P. aeruginosa*, *ureR* for *P. mirabilis* and *rpoA* for *E. faecium* and *E. faecalis* have all been demonstrated as being appropriate for species-specific nucleic acid amplification in the literature (Table 4).

Table 4. Species or genus-specific genes used for real-time RPA amplicon design.

Pathogen	Target gene	Gene function	GenBank accession number or Gene ID(s) used for design
E. coli	*chuA*[128]	Codes for a 69-kDa outer membrane protein responsible for heme uptake[129]	AF280396
P. mirabilis	*ureR*[130]	Part of the urease operon; positive regulator of urease transcription in the presence of urea[131]	Z18752.1
K. pneumoniae	*khe*[132]	Codes for hemolysin, which lyses red blood cells (unique to *K. pneumoniae*[133])	AF293352.1
P. aeruginosa	*lasB*[134]	Codes for lasB elastase; elastases cleave elastin and contribute to invasion.[135]	JN118955.1
E. faecium and E. faecalis	*rpoA*[136]	Codes for the alpha-subunit of DNA-dependent RNA polymerase, which catalyzes transcription of DNA into RNA.	11956181, 16504448, 1199127, 12290933, 12998742, 12289363

These genes were used to design a set of five primer pairs and five exo probes targeting that constituted the final panel. The following sequence of general steps was followed for all five pathogens after having picked one or more target genes from the literature:

1. **Staggered primer design for screening.** Two or three primers were designed flanking a central target region, in the forward and reverse directions, in a staggered manner. Each of these primers were designed manually or using primer-BLAST, with a reasonable adherence to the guidelines described above.
2. **Specificity checking.** The designed primers were tested for sequence specificity to the desired target using a nucleotide BLAST search against all published sequences (available on NCBI GenBank) of a comprehensive list of UTI pathogens listed in the methods section. The parameters used for specificity checking was as follows: primers that had less than 6 overall mismatches to a non-specific target and/or less than 4 mismatches to a non-specific target in the last 6 nucleotides at the 3' end were rejected due to the possibility of non-specific priming and amplification. Steps 1 and 2 were iteratively performed until there were at least 2 or 3 specific candidate primers to each desired target sequence.
3. **End-point RPA and sequencing to validate amplicon design.** The outermost forward and reverse primers, designed for different genes of each pathogen, were used to amplify pure gDNA of that pathogen's ATCC reference strain using end-point RPA. The amplified DNA samples were run on 2% agarose gels to check for the right product size, following which they were Sanger sequenced in either direction, using as sequencing primers the same forward and reverse primers used

for amplification. The sequencing data was assembled and aligned against the reference sequence originally used for primer design to verify homology.

Exo probe design and secondary structure analysis

Exo probe design was performed manually, to be homologous to the positive- or negative-sense strands of the target regions flanked by staggered primers and validated by Sanger sequencing. Besides adhering to the general exo probe design considerations recommended by the manufacturer and described earlier, the secondary structures (hairpin folds) of a potential probe candidates were analyzed using IDT's Oligo Analyzer, which in this case used the mfold component of UNAfold software. The mfold algorithm was originally developed in 2003[137], and uses thermodynamic rules summarized by SantaLucia, Jr in 1998[138]. It predicts the minimum free energies (ΔG) of different foldings of single stranded DNA or RNA using an input comprising the sequence, oligo concentration, temperature, and monovalent and divalent ion concentration.

It is inevitable that an oligonucleotide the size of a typical exo probe (at least 46 nt in length) will fold on itself in some configuration – this usually does not pose a problem to the performance of real-time RPA because recombinase-binding unfolds such structures. A high background fluorescence can be expected, however, if a secondary structure of an exo probe is configured in a manner that makes it double-stranded in the vicinity of the dSpacer, resulting in exonuclease-induced cleavage before recombinase action. This was observed with the *K. pneumoniae* exo probe (Kp-exo), the first designed probe in this study for which hairpin structures were not analyzed. As shown in Figure 28, the predicted Kp-exo secondary structure with the most negative free energy creates a

double-stranded neighborhood around the eventual dSpacer site (2 bp on either side of the A at position 28).

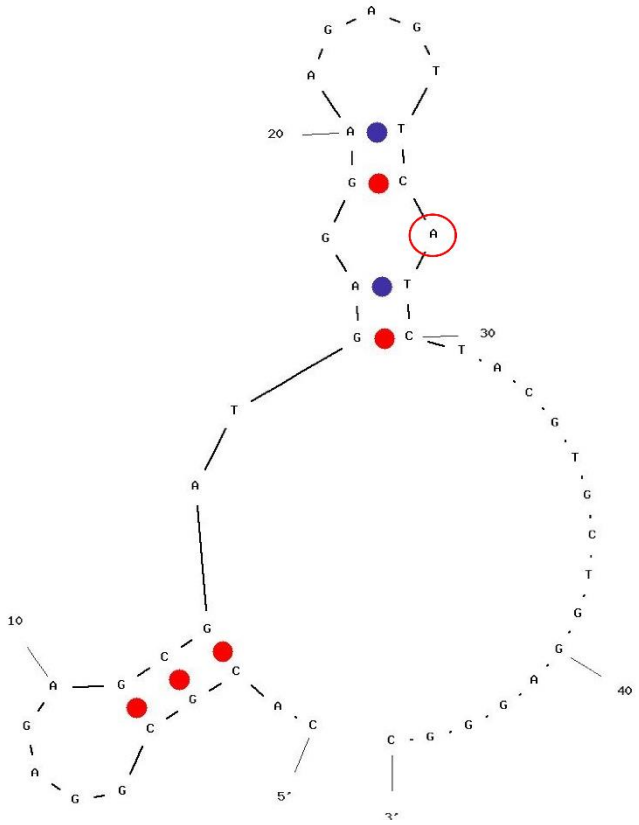

Figure 28. Most stable secondary structure of Kp-exo. ΔG = -3.52 kcal.mol^{-1}; the circle marks the nucleotide position replaced by a dSpacer. RPA salt conditions – 14 mM Mg^{2+}, 100 mM K^{+} - were used for predictions.

Consequently, Kp-exo had a consistently higher background fluorescence compared to the other probes, which resulted in a significantly higher background-based threshold being calculated for all experiments using the Kp-exo as the real-time RPA probe. In particular, the experiments involving clinical samples that used Kp-exo had widely variable and fluctuating background fluorescence values – this sometimes had the end result of negative dR values beyond the baseline for negative samples. Ultimately, Kp-exo performed well enough in terms of helping monitor exponential target

amplification in real time and being specific to *K. pneumoniae*, and was continued to be used. To avoid this situation with other exo probes, it was ensured that their three most stable (most negative ΔGs amongst predicted structures) foldings did not include the artefact observed with Kp-exo (most stable foldings shown in Figure 29).

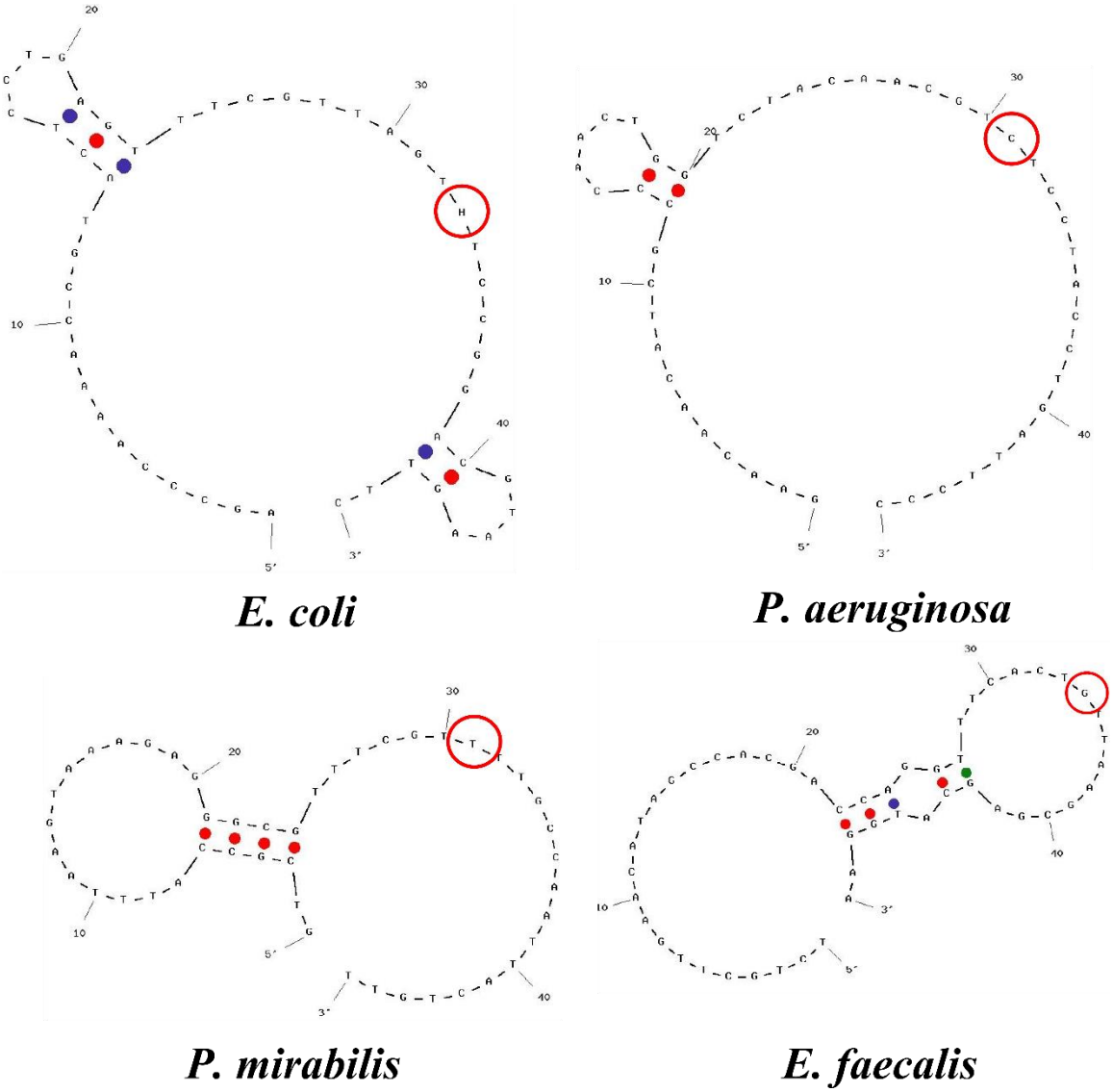

Figure 29. Most stable secondary structures of exo probes for *E. coli* (Ec-exo), *P. aeruginosa* (Pa-exo), *P. mirabilis* (Pm-exo) and *E. faecalis* (Ef-exo). Free energies as calculated by mfold: Ec-exo - ΔG = -1.63 kcal.mol^{-1}, Pa-exo - ΔG = 0.17 kcal.mol^{-1}, Pm-exo - ΔG = -2.56 kcal.mol^{-1} and Ef-exo - ΔG = -2.41 kcal.mol^{-1}. The circles mark the nucleotide positions replaced by dSpacers and eventually cleaved by exo III. RPA salt conditions – 14 mM Mg^{2+}, 100 mM K^{+} - were used for predictions.

***Enterococcus* primer and probe design – a special case**

The primers and probes for *K. pneumoniae*, *E. coli*, *P. aeruginosa*, and *P. mirabilis* were designed at a species-specific level. On the other hand, from a clinical decision-making perspective, it is only required that *Enterococcus* species be identified at the genus level. *E. faecium* and *E. faecalis* are the most common Enterococci that cause UTIs, with *E. faecalis* being much more frequent (>75% of *Enterococcus* infections). This led to the decision to design a primer set and exo probe that could be used to amplify both *E. faecalis* and *E. faecium*. To do this, for several different target genes, consensus sequences only containing bases homologous to both *Enterococcus* species were built using SeaView sequence alignment software, following which primer and probe design was carried out manually.

This proved to be somewhat challenging even though a review of the relevant literature provided several candidate genes as potential targets. These included *atpD*, *phoE*, *ddl*, *rpoB*, *tuf*, and *rpoA*, which are typically used for species-specific identification of *Enterococcus*. Only 16S and 23S DNA have been used thus far in the literature to generate genus-specific *Enterococcus* PCR primers. Using 16S or 23S *Enterococcus* DNA as targets were ruled out as options based on the fact that these genes are >90% homologous to their counterparts in *E. coli*, *K. pneumonia*, *P. aeruginosa*, and *P. mirabilis.* On the other hand, the amplicon-worthy sequences (no long strings of a single base, or short repeats) of *atpD*, *phoE*, *ddl*, *rpoB*, *tuf*, and *rpoA* did not allow the design of what would have been ideal – three regions (two 30-35 bp regions flanking a 46-52 bp region) 100% homologous between, and specific to, the published sequences of *E. faecalis* and *E. faecium*.

The following issues made this ideal design extremely difficult:

- The overall homologies of the candidate genes between *E. faecalis* and *E. faecium* were between 76-87%. The mismatches, however, were evenly spread along the entire length of the genes, making common primer and probe design difficult. When 100% consensus sequences were generated after having aligned six available *tuf* sequences from *E. faecalis* and *E. faecium*, for example, all primer- and probe-worthy stretches of bases had at least 20% mismatched bases.
- In two cases – *atpD* and *ddl* – the designed primers and/or probe were not specific to *Enterococcus*. For example, a >80% homology between the *atpD* genes of *E. faecalis* and *S. agalactiae* ruled it out as a possible gene target.

Ultimately, 3 sets of forward and reverse primers targeting the *rpoA* gene, with between 2 and 4 mismatches (implying at least 87% primer homology to template; mismatches were removed from the last 10 nt at the 3' end), and an exo probe with 4 mismatches (92% homology) were manually identified and used for further testing. These sequences were chosen to be homologous to the *E. faecalis* consensus sequence, but were expected to amplify *E. faecium* as well, with potentially lower sensitivity. Because reference gDNA of *E. faecium* was not readily available, the analytical evaluation of the *Enterococcus* primers and probe was only performed using *E. faecalis* gDNA. The final primers and probes used for analytical sensitivity and specificity testing, and ultimately, for clinical evaluation, are listed in Table 5.

Primer screening and selection

Different combinations of forward and reverse primers from amongst the designed and specificity-checked staggered primers were performance-screened in real-time RPA reactions using the exo probes to monitor amplification and mid-level concentrations (~10^4 genomes per reaction) of purified gDNA as the template. The primer pairs that resulted in the shortest threshold times and/or ideal exponential amplification curves were selected and used for all further testing. An illustration of a typical reason one primer pair was picked over others is shown in Figure 30. The figure shows the amplification curves for the same target concentration (10^4 genome copies per reaction) of primer pairs F1/R2, F1/R3 and F2/R3, which were designed to flank the same central region of a target (*ureR* gene of *P. mirabilis* in this case). For the other pathogens, at least three and up to six primer pairs were screened as shown in Figure 30.

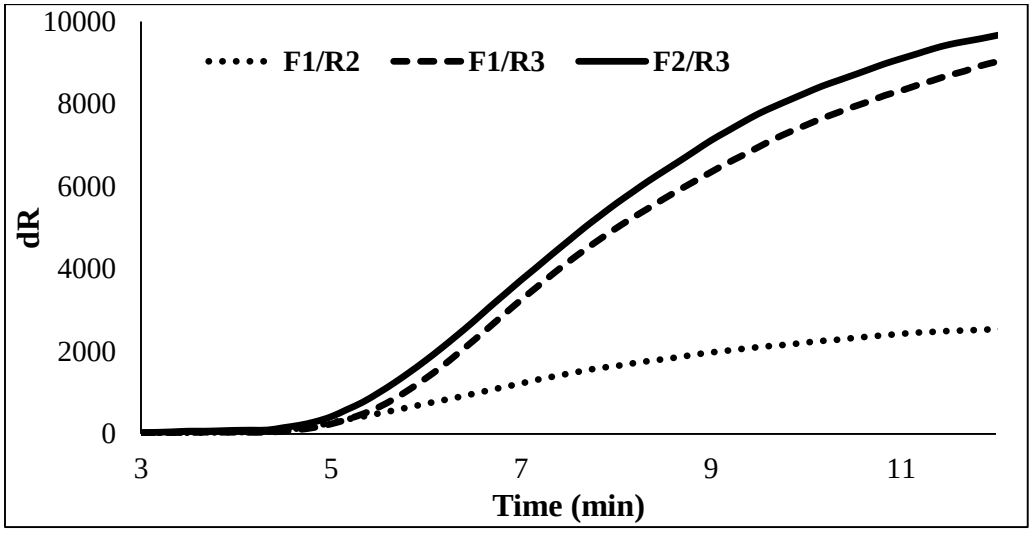

Figure 30. Representative example of testing different primer pairs using the same target concentration to determine the optimal pair. 10^4 genome copies of *P. mirabilis* gDNA amplified using Pm-exo and three different primer pairs – F1/R2, F1/R3, and F2/R3. F2/R3 was picked over the other two because of the earlier threshold time.

Table 5. Primer/probe sequences and amplicon lengths for the five UTI real time RPA assays. F, forward primer; R, reverse primer; P – exo probe; (FAM), Fluorescein coupled to a thymine; H, dSpacer; (BHQ), Black Hole Quencher-1 coupled to a thymine.

Organism	Accession number/GI	Target length	Sequence (5'-3')
E. coli	AF280396	178 bp	**F** - ATATGGCGGTGAGTATTATCGTCAGGAACAACATC
			R - GAGATGACCATTTGTCGGCATCAACATCTTTGTAG
			P - AGCCCAAAACCGTACTCCTGAGTTTCGTTAG**(FAM)H(BHQ)**CCGGACGTAAGTTC
K. pneumoniae	AF293352.1	202 bp	**F** - TTATCCCGACAGCCCGGAGCGTTTTTCGATTGG
			R - CAGCTTCCAGAGATAGCCGTTTATCCACACTTCCG
			P - CACGCGGAGAGCGATGAGGAAGAGT**(FAM)**C**H(BHQ)CT**ACGTGCTGGAGGGC
P. aeruginosa	JN118955.2	161 bp	**F** - GAGAATGACAAAGTGGAACTGGTGATCCGCCTG
			R - GCCAGGCCTTCCCACTGATCGAGCACTTCGCCG
			P - GAACAACATCGCCCAACTGGTCTACAACG**(FAM)H(BHQ)**CCTACCTGATTCCC
P. mirabilis	Z18752	163 bp	**F** - CAAAAACGCTCTATACTACACCATCAACATTAC
			R - GTTTAAATGCGTCACAAAAATAAGCATTACTAC
			P - GTCGCCATTTAAGTAAAGAGGGCGTTTCG**(FAM)H(BHQ)**TGCCAATTACTGTT
E. faecalis	1199127	166 bp	**F** - GGACCCGCTACCGTGACTGCCGGCGATATTATCG
			R - GAATCAACTGGAAGTACACCGATTGGCATATC
			P - TCTGCTTGAACATAGCCACGACCAGGTTTCAC**(FAM)H(BHQ)**TAAGCGAGCATGGAA

Analytical sensitivity and specificity of RPAs

The final panel of five primer/probe sets is summarized in Table 5. In the following text, "KP", "EC", "PA", "PM", and "EF" refer to the primer/probe sets of *K. pneumoniae, E. coli, P. aeruginosa, P. mirabilis*, and *E. faecalis*, respectively. The analytical sensitivity of molecular diagnostic assays is usually determined by testing several sample replicates containing lower and lower dilutions of a known molecular standard. The lower limit of detection (C_{95}) is typically defined as the concentration of the molecular standard that is identified as a "positive" (rises above a pre-defined threshold) in 95% of replicates for that concentration. C_{95} values of NAATs are commonly computed by probit regression analyses, a statistical technique to analyze studies that have binomial response variables ("positive" and "negative" in this case). Doing this was beyond the scope of this work, however, as probit analysis based studies need a large number of replicates (20 or more, usually) for narrow confidence intervals.

In this work, all primers and probes were tested in at least three, and up to six real-time RPA reaction replicates with different serial dilutions of the quantitative genomic DNA standards. The results are shown in Figures 31 to 35 as representative plots of background-subtracted fluorescence against time, and as semi-log plots of threshold time against concentration. To calculate the background-subtracted fluorescence (dR), baseline functions and background-based threshold calculation methods were determined for each probe individually, and consistently used thereafter. The baselines were calculated empirically, using raw fluorescence data from the beginning of the reaction to ten or twenty seconds before the time at which the raw fluorescence of the highest concentration of gDNA (10^7 copies, typically) began to

exponentially rise– this ranged from 120 s for *E. coli* to 180 seconds for *K. pneumoniae*. Threshold dR was different for each exo probe set as well, and was set to be between 25 and 100 standard deviations above the background fluorescence. This range of standard deviations resulted from empirically setting the threshold dR value to be in the exponential phase of amplification curve, as is the norm with quantitative PCR. With the data generated, the LODs of different assays on the panel were estimated to within an order of magnitude. The end of the linear range on a semi-log dose-response plot is widely accepted as being very close to the LOD for NAATs. The LODs for EC, PA, PM and EF are estimated to be between 10 and 100 genome copies per reaction from their respective semi-log regression lines (Figures 31 to 35). The KP assay comfortably detected 100 genome copies per reaction, but all 10 genome copies replicates returned a negative result. The assays were remarkably rapid, with the threshold times for the dilutions determined as lower limits of detection being only around ten minutes from the start of reaction.

The analytical specificities for EC, PA, PM, and EF were tested by running reactions using 10^6 genome copies per reaction of non-specific pathogen gDNA. dR curves for these non-specific reactions, also shown in Figures 31 to 35, never rose above threshold values except for two instances – PA and PM – in which two of the eight total non-specific reactions had a threshold time slightly shorter than those for the lowest dilution (10 genomes per reaction) of specific target.

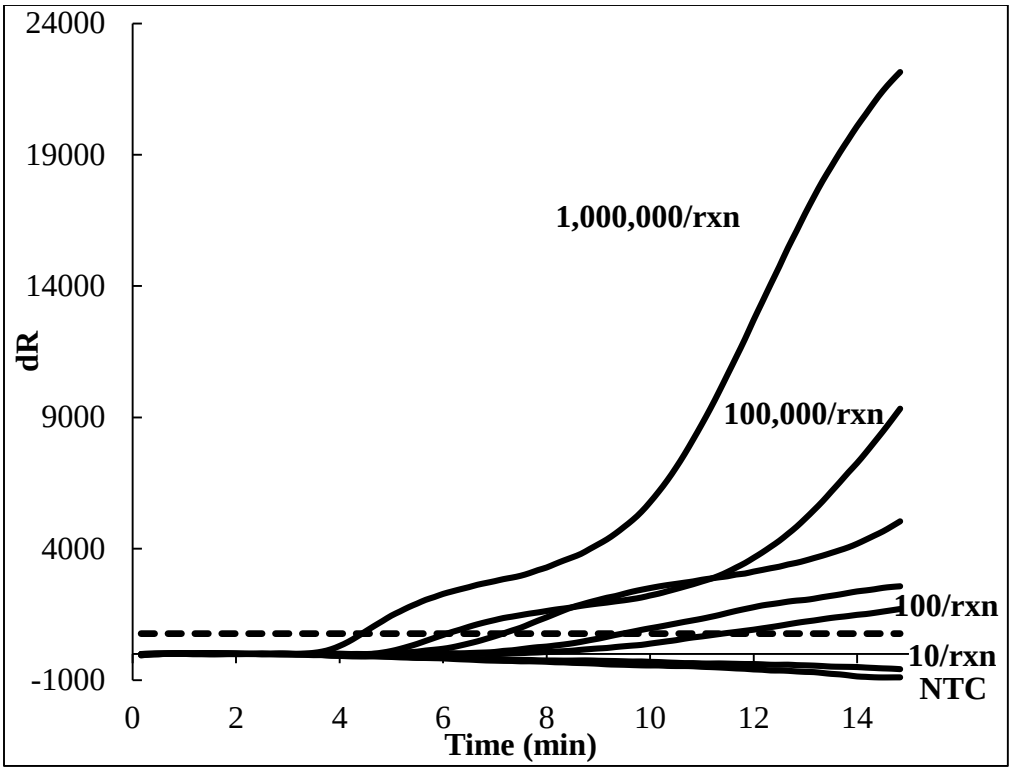

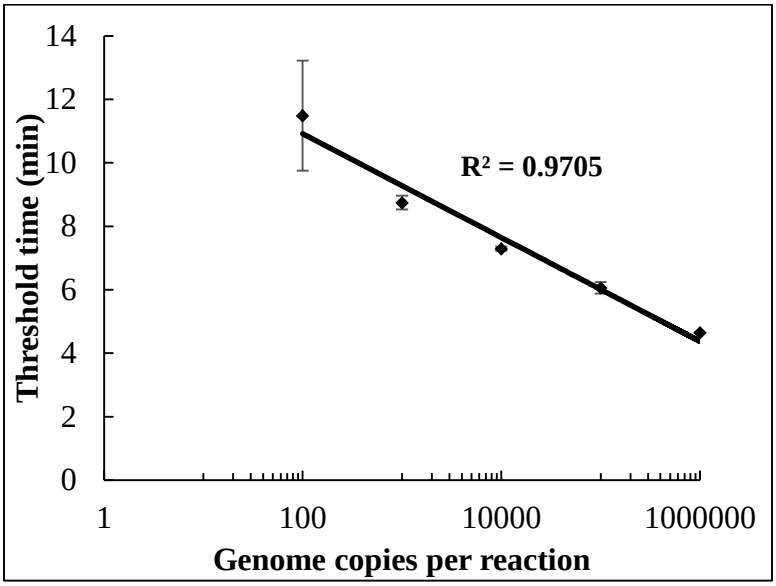

Figure 31. Analytical studies of *K. pneumoniae* primer/probe set. (top) Representative amplification curve, averaged from three replicates, of different dilutions of gDNA. Baseline calculated using fluorescence data from first three minutes. Dashed line - threshold; (bottom) Semi-log plot and regression line of threshold time against number of genome copies per reaction (10^6 to 10^2 per reaction). Threshold set to 50 standard deviations above background fluorescence from the first three minutes. NTC, no template control.

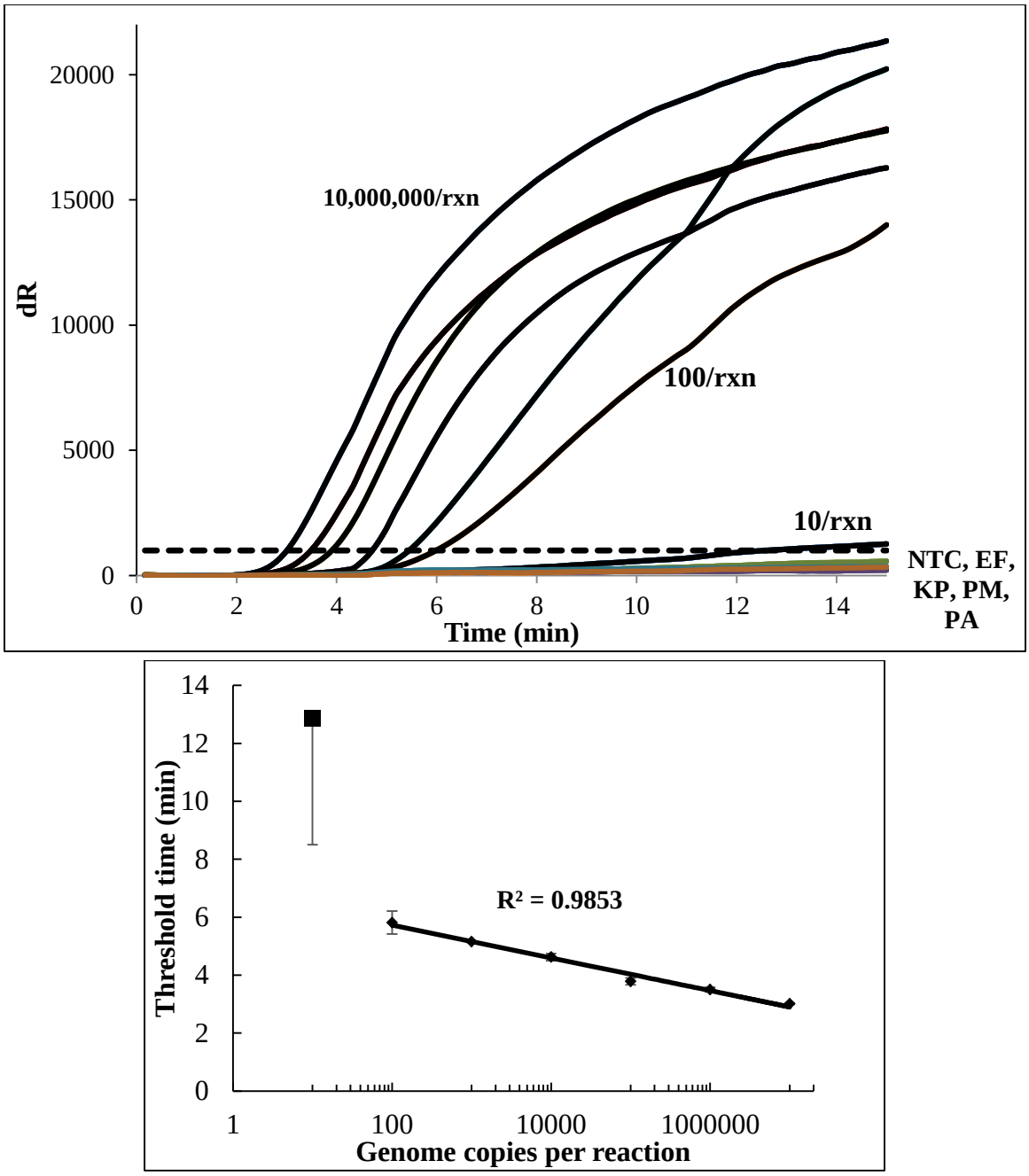

Figure 32. Analytical studies of *E. coli* primer/probe set. (top) Representative amplification curve, averaged from four replicates, of different dilutions of gDNA. Baseline calculated using fluorescence data from first two minutes. Dashed line - threshold; (bottom) Semi-log plot and regression line of threshold time against number of genome copies per reaction (10^7 to 10^2 per reaction). Square – data point for 10 genomes per reaction. Threshold set to 100 standard deviations above background fluorescence from the first 90 seconds. NTC, no template control. EF, 10^6 *E. faecalis* genomes. KP, 10^6 *K. pneumoniae* genomes. PM, 10^6 *P. mirabilis* genomes. PA, 10^6 *P. aeruginosa* genomes.

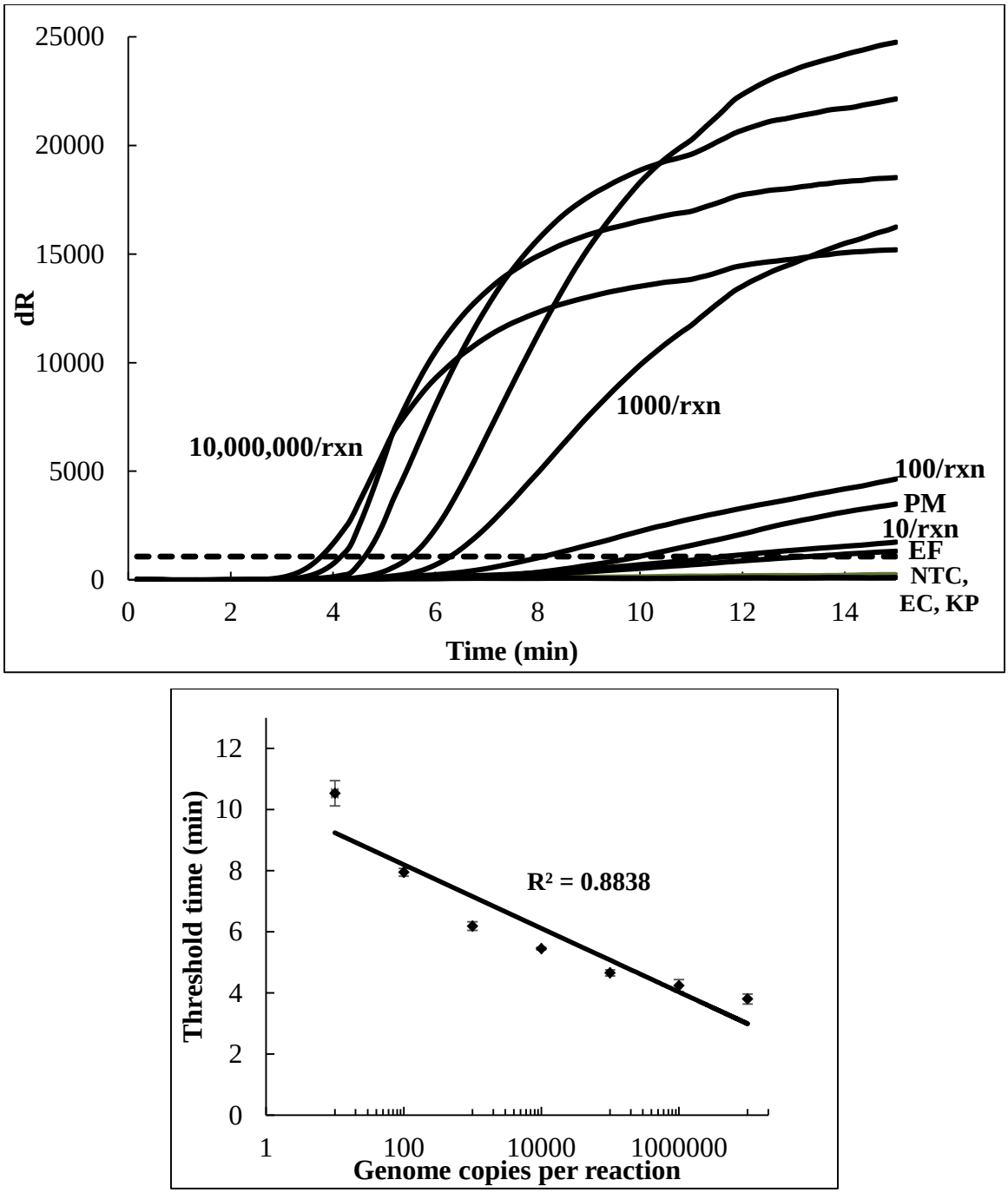

Figure 33. Analytical studies of *P. aeruginosa* primer/probe set. (top) Representative amplification curve, averaged from between three and five replicates, of different dilutions of *P. aeruginosa* gDNA. Baseline calculated using fluorescence data from first 160 seconds; (bottom) Semi-log plot and regression line of threshold time against number of genome copies per reaction (10^7 to 10^1 per reaction). Threshold set to 100 standard deviations above background fluorescence from the first 90 seconds. NTC, no template control. PM, 10^6 *P. mirabilis* genomes. EF, 10^6 *E. faecalis* genomes. KP, 10^6 *K. pneumoniae* genomes. EC, 10^6 *E. coli* genomes.

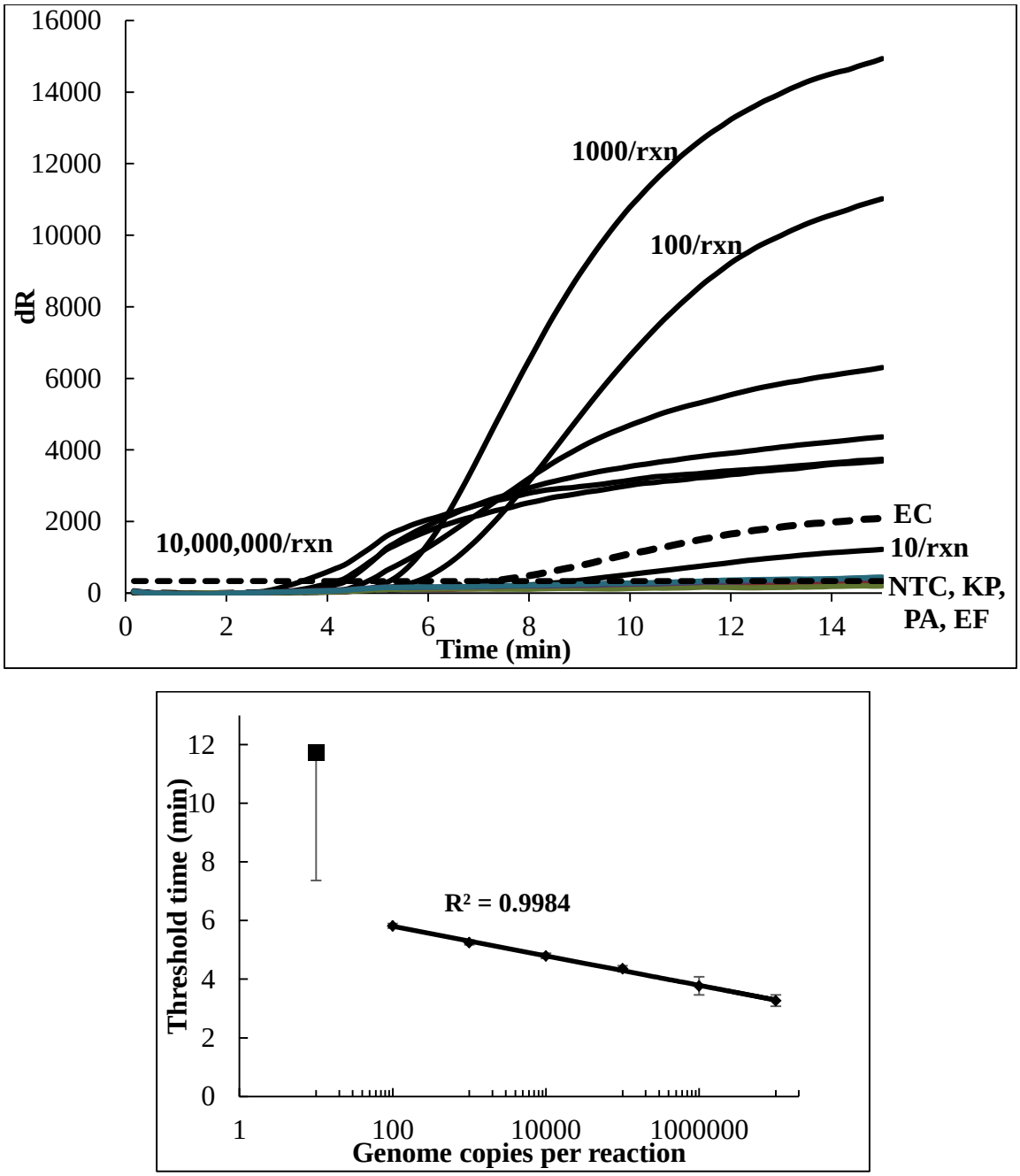

Figure 34. Analytical studies of *P. mirabilis* primer/probe set. (top) Representative amplification curve, averaged from between three and six replicates, of different dilutions of *P. mirabilis* gDNA. The baseline was calculated using fluorescence data from first 170 seconds; (bottom) Semi-log plot and regression line of threshold time against number of genome copies per reaction (10^7 to 10^2 per reaction). Square – 10 genomes per reaction. The threshold was set to 25 standard deviations above background fluorescence from the first 250 seconds. NTC, no template control. EC, 10^6 *E. coli* genomes. PA, 10^6 *P. aeruginosa* genomes. EF, 10^6 *E. faecalis* genomes. KP, 10^6 *K. pneumoniae* genomes.

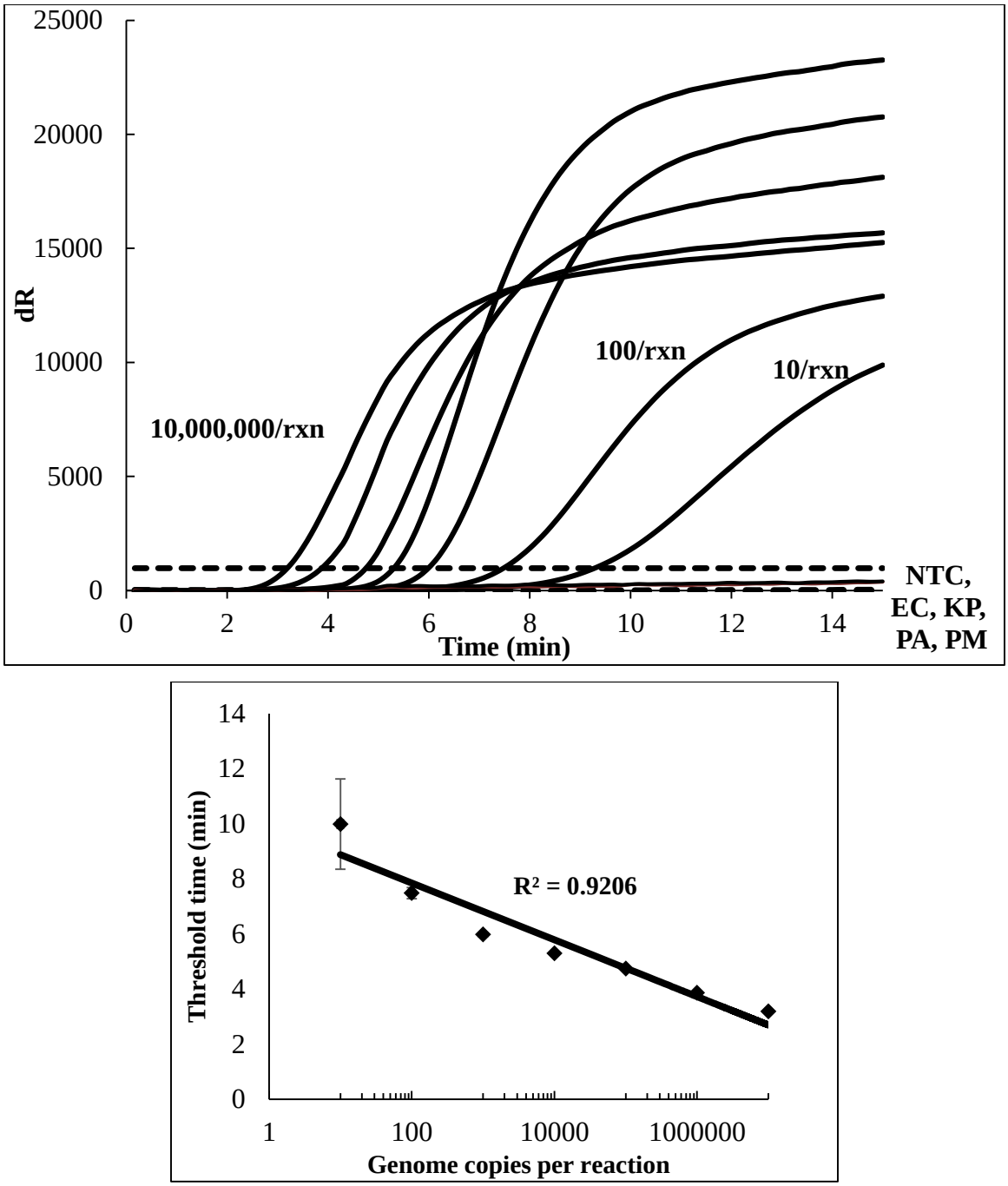

Figure 35. Analytical studies of *E. faecalis* primer/probe set. (top) Representative amplification curve, averaged from between three and five replicates, of different dilutions of *E. faecalis* gDNA. Baseline calculated using fluorescence data from first 150 seconds; (bottom) Semi-log plot and regression line of threshold time against number of genome copies per reaction (10^7 to 10^1 per reaction). Threshold set to 100 standard deviations above background fluorescence from the first 90 seconds. NTC, no template control. PM, 10^6 *P. mirabilis* genomes. PA, 10^6 *P. aeruginosa* genomes. KP, 10^6 *K. pneumoniae* genomes. EC, 10^6 *E. coli* genomes.

Clinical sensitivity and specificity evaluation

In the following text, figures and tables, running the "panel" refers to the running, in separate reaction tubes, of five real-time RPA assays using reagents (forward/reverse primers and exo probe listed in Table 5) targeting *K. pneumoniae, E. coli, P. aeruginosa, P. mirabilis,* and *E. faecalis/E. faecium*. Alternately, individual RPA assays are referred to by appending "KP", "EC", "PA", "PM", or "EF" to the sample ID. For example, the RPA reaction tube that tested patient sample 123456 using *E. coli* reagents is referred to as 123456-EC. "Positive" results by RPA indicate a threshold time of less than 10 minutes, and "negative" results by RPA indicate no amplification above the same threshold value within 10 minutes. To evaluate the **clinical specificity** of UTI RPA assays developed in this work, ten "true negative" samples (determined using the VITEK 2 system and listed in Table 6) were run against the panel using 5 μL of extracted DNA per reaction tube. As shown in Figures 36 to 40, none of these samples caused the baseline-subtracted fluorescence to rise above the threshold, resulting in 100% specificity. The **clinical sensitivity** of the panel was evaluated using 25 VITEK "true positive" samples that equally represented the five pathogens – sample details and amplification curves are shown in tables 7-11 and figures 41-45, respectively. Of the five true positives in each pathogen species, two were tested with the entire panel (five reaction tubes) to check for analytical specificity in a clinical sample matrix that could potentially include human DNA and the DNA of non-pathogenic bacteria. The other three true positive samples, for each pathogen, were tested using only the reagent set designed for that pathogen. The overall sensitivity of the panel, aggregated from the results of each pathogen, was determined to be 84% (21/24).

Table 6. "True negative" samples used for specificity studies and corresponding results.

Sample ID	Culture result	RT-RPA result	Specificity
536836	No Growth	EC, KP, PA, PM and EF negative	**100%**
530071	10,000-50,000 CFU/mL Skin Flora; <10,000 CFU/mL Gram Negative Rods		
341522	1,000-10,000 CFU/mL Skin Flora		
358596	>100,000 CFU/mL Skin Flora		
536876	No Growth		
506762	<10,000 CFU/mL Gram Negative Rods, Lactose Fermenters		
174133	10,000-50,000 CFU/mL Skin Flora; <10,000 CFU/mL Gram Negative Rods		
422230	No Growth		
536922	<10,000 CFU/mL Skin Flora		
509933	No Growth		

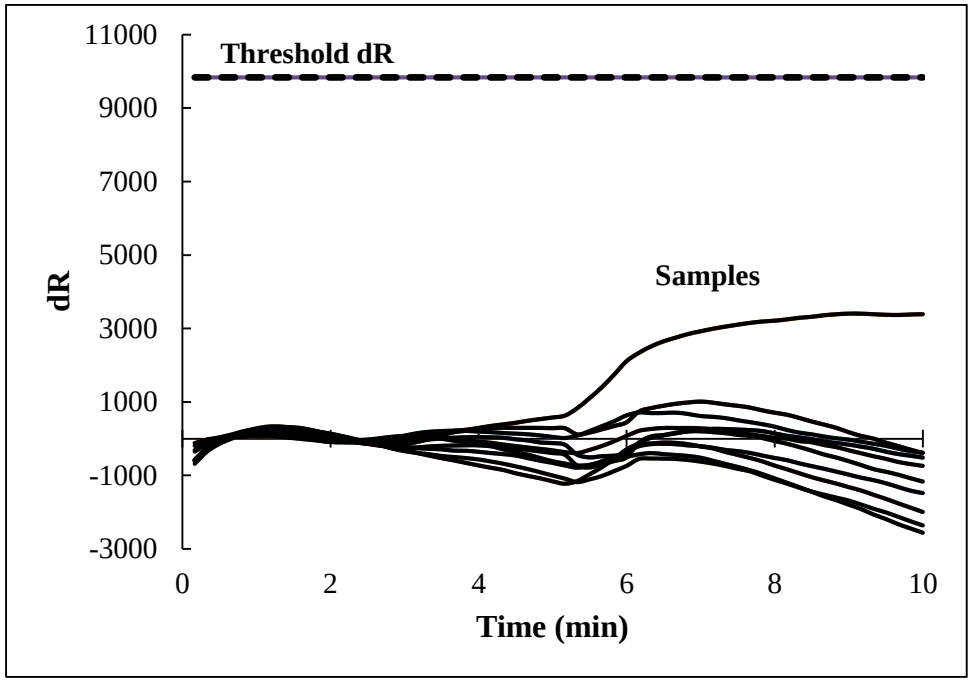

Figure 36. Amplification curves of "true negative" samples obtained using the *K. pneumoniae* primer/probe set. No amplification above the threshold, which was set to be the same as that used in KP analytical studies.

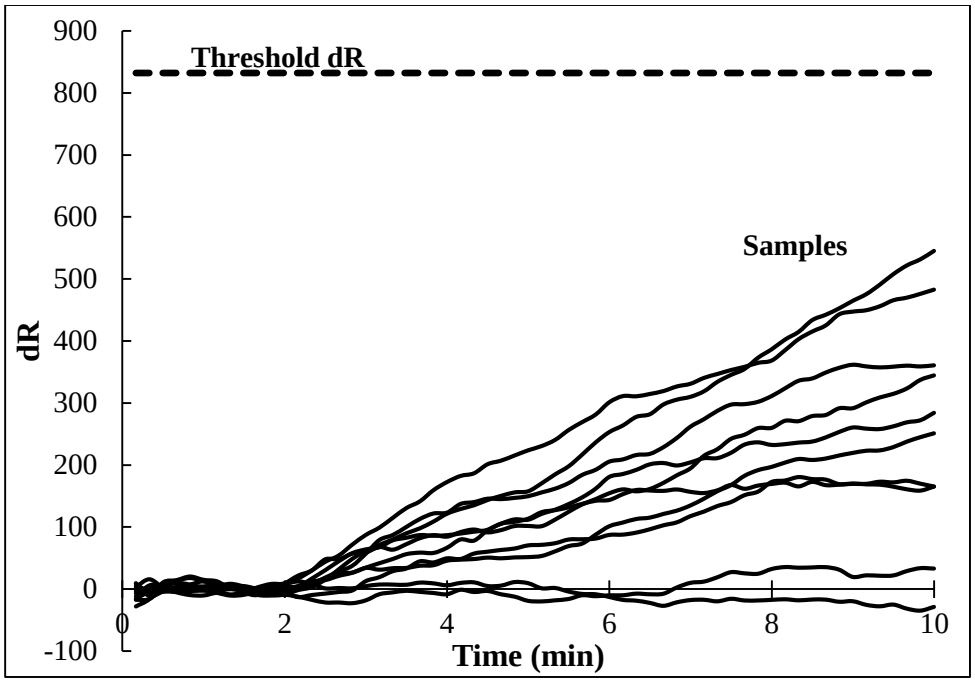

Figure 37. Amplification curves of "true negative" samples obtained using the *E. coli* primer/probe set. No amplification above the threshold, which was set to be the same as that used in EC analytical studies.

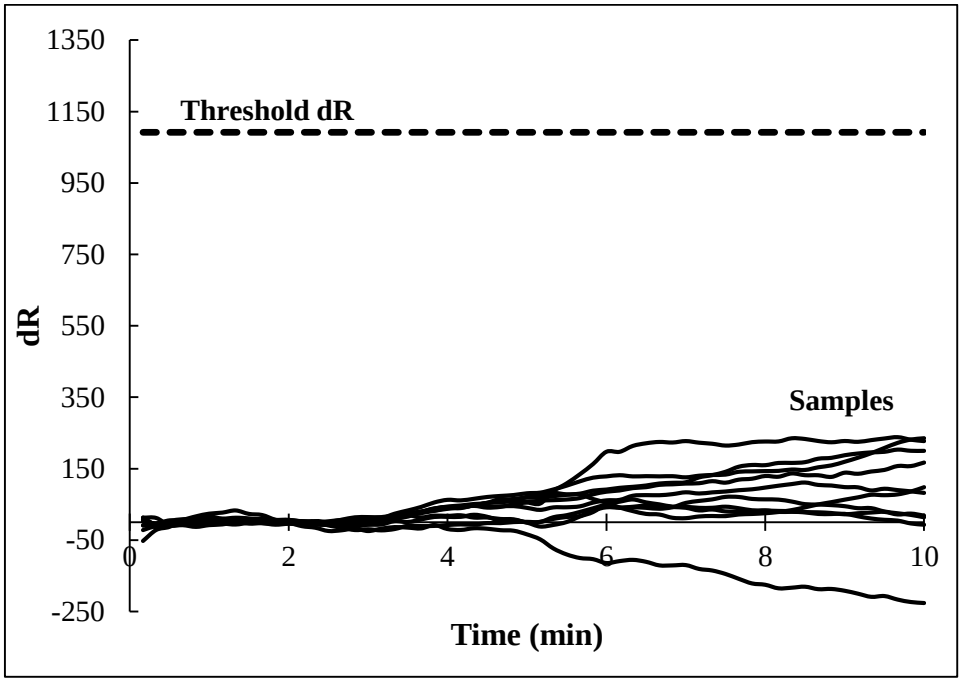

Figure 38. Amplification curves of "true negative" samples obtained using the *P. aeruginosa* primer/probe set. No amplification above the threshold, which was set to be the same as that used in PA analytical studies.

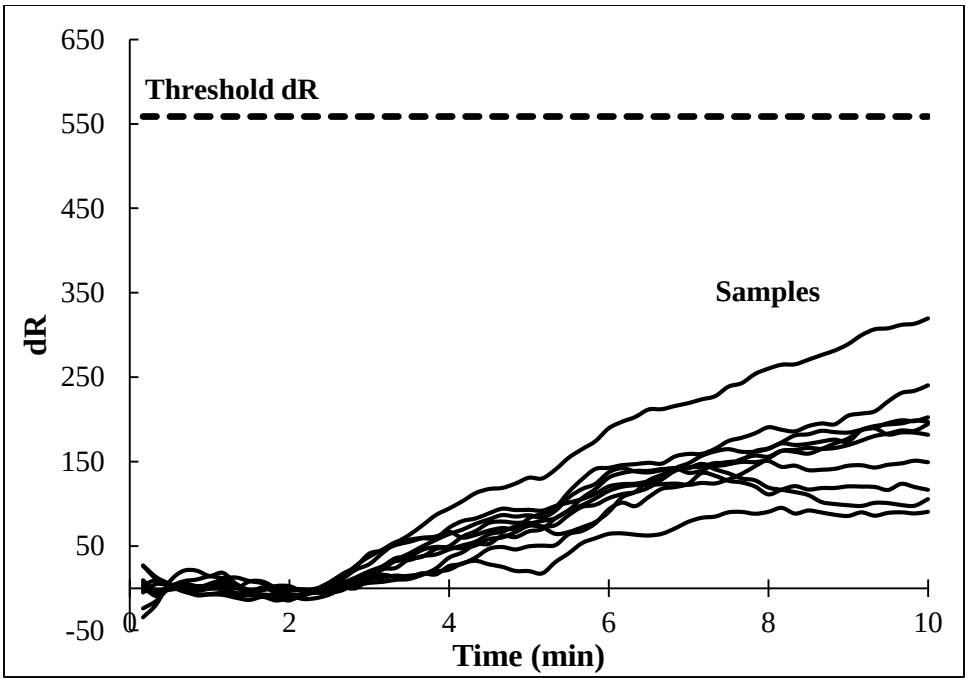

Figure 39. Amplification curves of "true negative" samples obtained using the *P. mirabilis* primer/probe set. No amplification above the threshold, which was set to be the same as used in PM analytical studies.

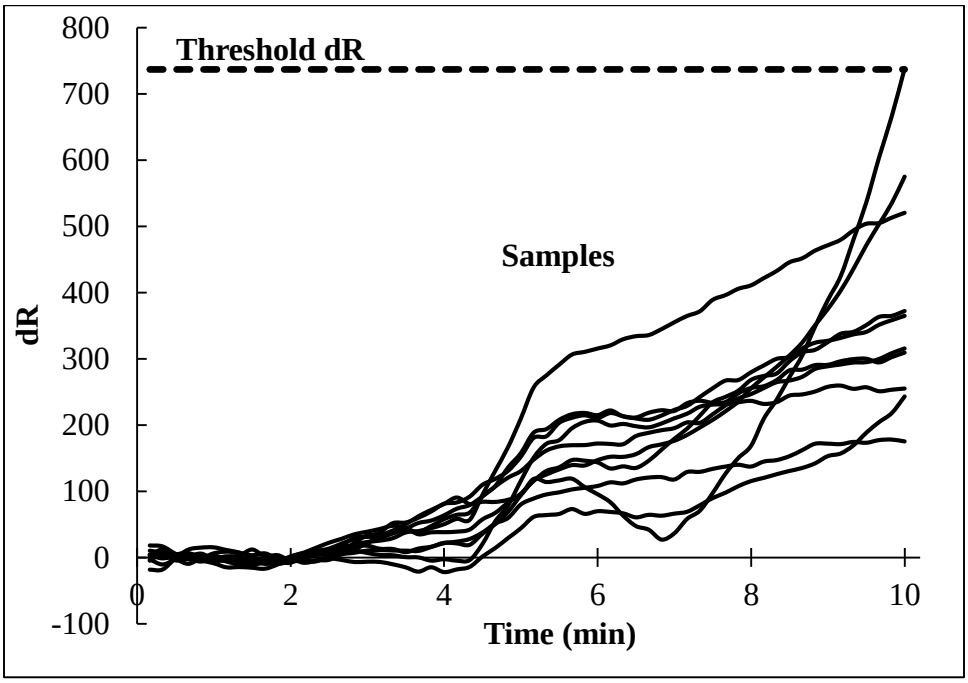

Figure 40. Amplification curves of "true negative" samples obtained using the *E. faecalis* primer/probe set. No amplification above the threshold, which was set to be the same as used in EF analytical studies.

Table 7. Culture-positive *K. pneumoniae* samples used for sensitivity studies, and corresponding RPA results.

Sample ID	Pathogen ID by culture	RT-RPA result	Sensitivity
453917	*K. pneumoniae*	KP negative; EC, PA, PM and EF negative	**80%**
197125	*K. pneumoniae*	KP positive; EC, PA, PM and EF negative	
166528	*K. pneumoniae*	KP positive	
426239	*K. pneumoniae*	KP positive	
329444	*K. pneumoniae*	KP positive	

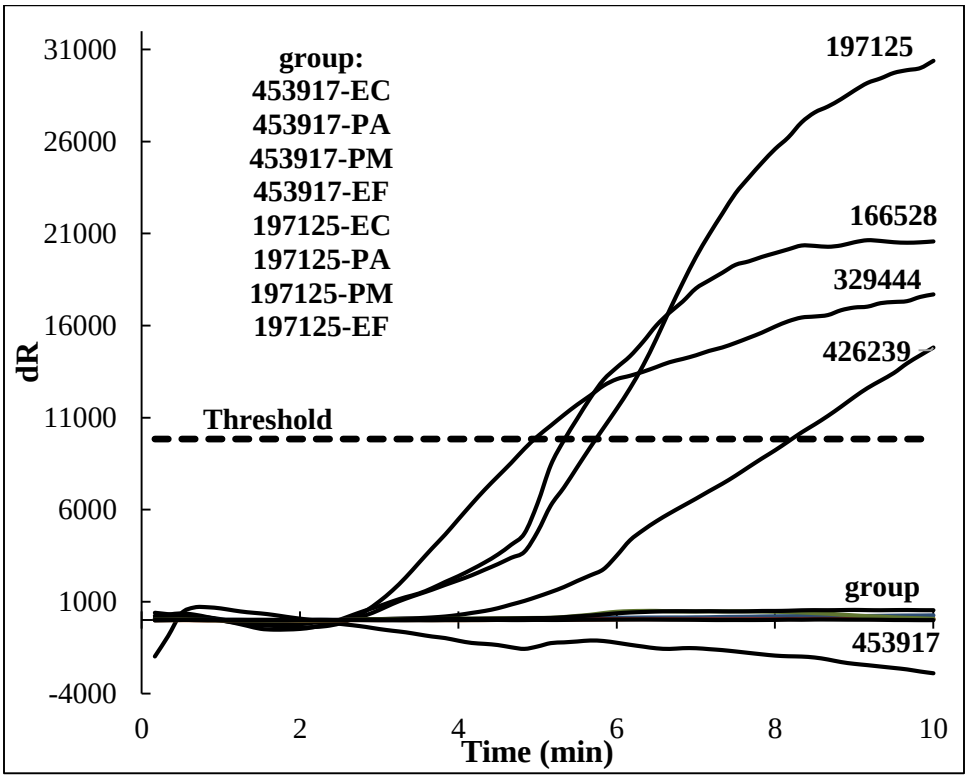

Figure 41. RPA amplification curves of culture-positive *K. pneumoniae* samples used for sensitivity studies.

Table 8. Culture-positive *E. coli* samples used for sensitivity studies, and corresponding RPA results.

Sample ID	Pathogen ID by culture	RT-RPA result	Sensitivity
247323	*E. coli*	EC positive; KP, PM, PA and EF negative	**80%**
532087	*E. coli*	EC positive; KP, PM, PA and EF negative	
240730	*E. coli*	EC negative	
462610	*E. coli ESBL*	EC positive	
119666	*E. coli*	EC positive	

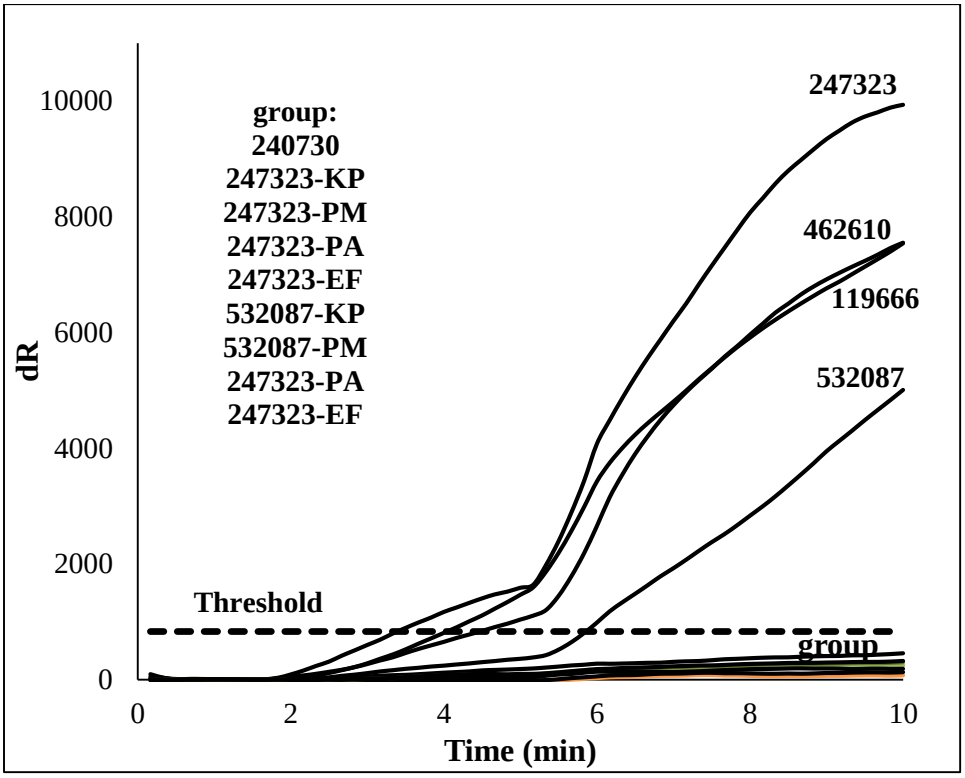

Figure 42. RPA amplification curves of culture-positive *E. coli* samples used for sensitivity studies.

Table 9. Culture-positive *P. aeruginosa* samples used for sensitivity studies, and corresponding RPA results.

Sample ID	Pathogen ID by culture	RT-RPA result	Sensitivity
358259	*P. aeruginosa*	PA positive; KP, EC, PM and EF negative	**80%**
487488	*P. aeruginosa*	PA positive; KP, EC, PM and EF negative	
476523	*P. aeruginosa*	PA positive	
424055	*P. aeruginosa*	PA positive	
277711	*P. aeruginosa*	PA negative	

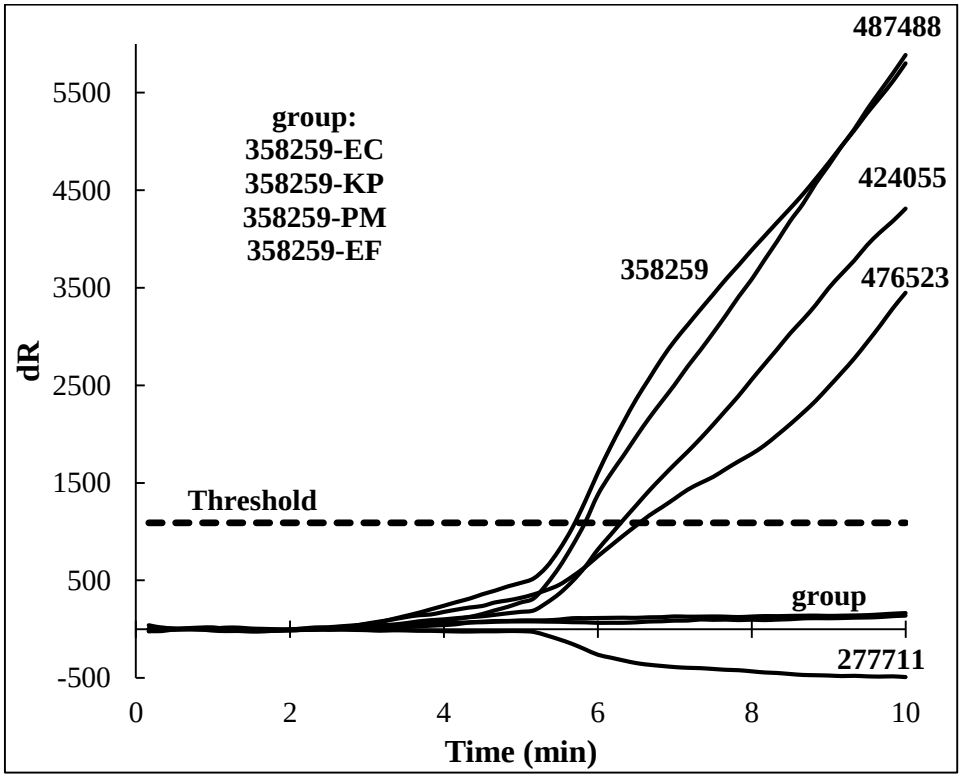

Figure 44. RPA amplification curves of culture-positive *P. aeruginosa* samples used for sensitivity studies.

Table 10. Culture-positive *P. mirabilis* samples used for sensitivity studies, and corresponding RPA results.

Sample ID	Pathogen ID by culture	RT-RPA result	Sensitivity
185727	*P. mirabilis*	PM positive; KP, EC, PA and EF negative	**100%**
423594	*P. mirabilis*	PM positive; KP, EC, PA and EF negative	
155469	*P. mirabilis*	PM positive	
511846	*P. mirabilis*	PM positive	
222825	*P. mirabilis*	PM positive	

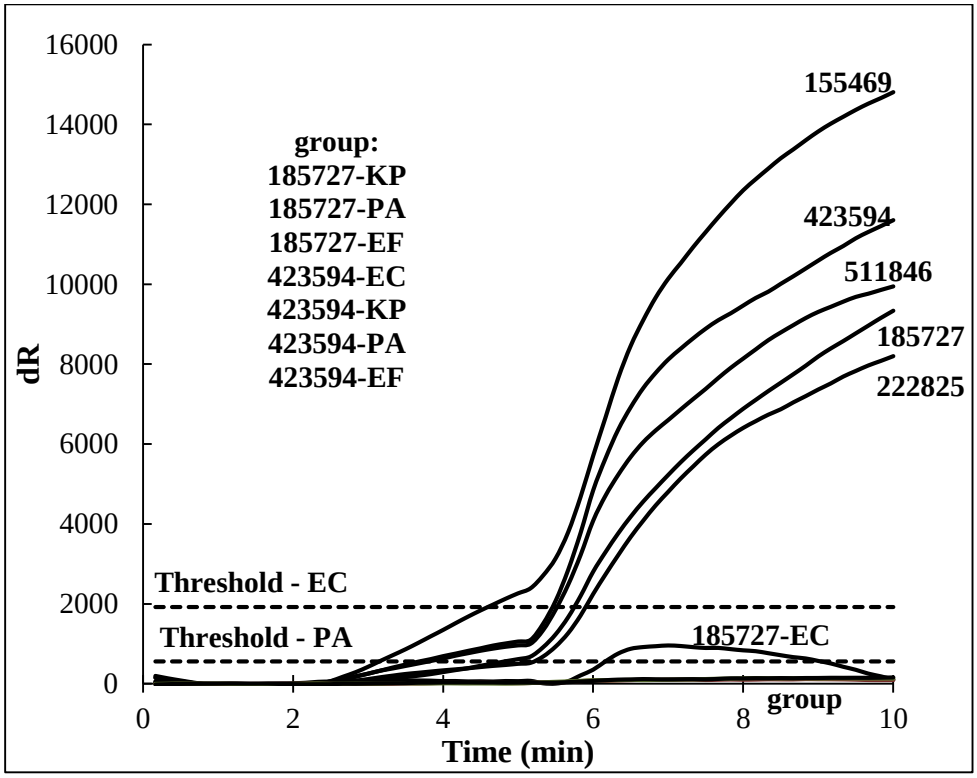

Figure 44. RPA amplification curves of culture-positive *P. mirabilis* samples used for sensitivity studies. The threshold for EC is included to illustrate that the curve for sample 185717-EC is well below the threshold calculated the method used for *E. coli* reagents.

Table 11. Culture-positive *Enterococcus* samples used for sensitivity studies, and corresponding RPA results.

Sample ID	Pathogen ID by culture	RT-RPA result	Sensitivity
503459	*Enterococcus species*	EF positive; EC, KP, PA, PM negative	**80%**
387656	*Enterococcus species*	EF positive; EC, KP, PA, PM negative	
523461	*Enterococcus species*	EF positive	
374507	*E. faecalis and skin flora*	EF negative	
473465	*Enterococcus species and skin flora*	EF positive	

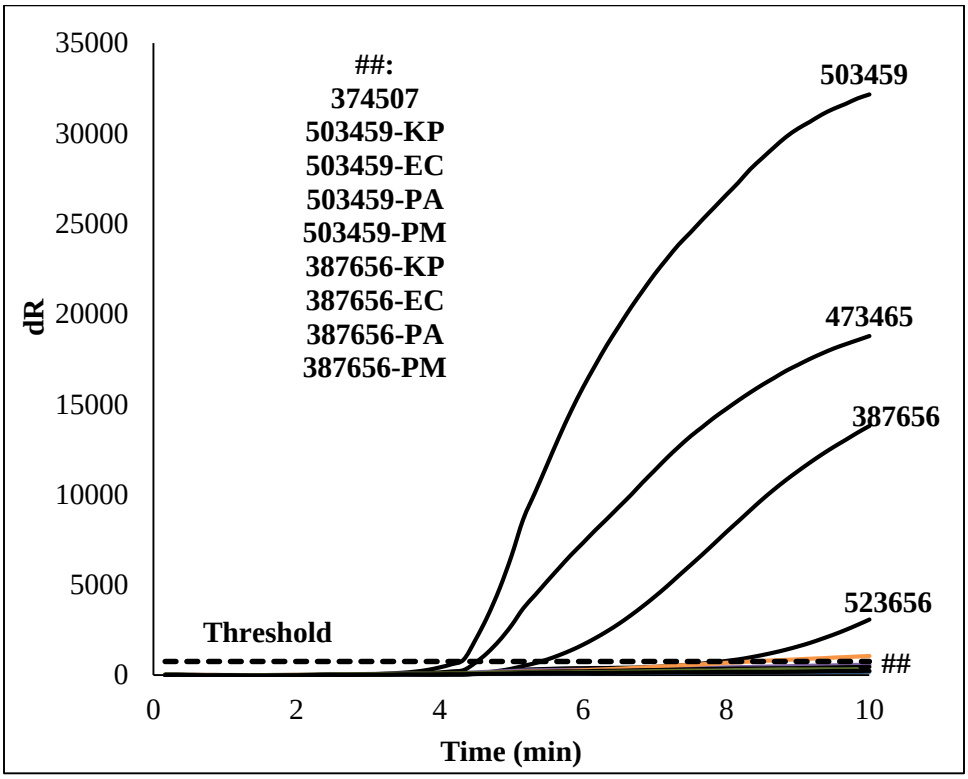

Figure 45. RPA amplification curves of culture-positive *Enterococcus* samples used for sensitivity studies.

Conclusions

A panel of very rapid and highly sensitive isothermal real-time RPA assays have been developed for the highly specific detection of five UTI pathogens. These assays showed good analytical sensitivity and specificity; all five assays detected target 100 genomes per reaction or less in around ten minutes, and showed no cross-reactivity with high concentrations of non-specific gDNA. The assay panel's overall clinical sensitivity, as determined from a 25-sample cohort of culture-positive urine samples, was 84%, and the clinical specificity, determined using a 10-sample cohort of culture-negative urine samples, was 100%.

It should be noted that the assay panel was not meant to be quantitative. The threshold times were determined for standard dilutions of genomes per reaction made in DI water; the semi-log regression lines generated as a result did not serve as standard curves to determine pathogen concentrations in complex and variable clinical samples. The relative ease (compared to other isothermal NAATs) of RPA design (three oligonucleotides), availability of dried reagents in stable pellet form, short time to result, and direct compatibility with low-footprint and relatively inexpensive (compared to real-time PCR machines) benchtop fluorescent readers such as the Qiagen ESEquant Tubescanner make this panel of assays (with more targets and validation) an attractive method for use in clinics or laboratories that seek rapid pathogen identification in specific populations of UTI-infected patients. RPA reactions that detect antibiotic resistance genes (*mecA*, *vanA/B* and KPC, for example) would add value, either by themselves or as a supporting panel to the pathogen ID panel, by helping clinicians prescribe the right antibiotic regimens.

CHAPTER 4 - EVALUATION OF THE FILMARRAY BLOOD CULTURE IDENTIFICATION PANEL AS A DIAGNOSTIC TOOL FOR URINARY TRACT INFECTIONS

Introduction

Point-of-care nucleic acid testing

The initial efforts towards moving away from culture-based pathogen detection were nucleic acid-based detection techniques that used DNA probe technology.[139-140] However, the limitations of probe-based detection rapidly became apparent – a large amount of starting target DNA was required for analysis, resulting in poor detection sensitivity. The invention of the Polymerase Chain Reaction (PCR) in 1983 almost immediately revolutionized several areas of molecular biology. In the more than three decades since, PCR-based nucleic acid testing (also called molecular testing) for infectious diseases, which relies on the specific amplification and detection of microbial DNA, has become commonplace and obtained FDA clearance for a variety of pathogens including *Chlamydia trachomatis*, Human Immunodeficiency Virus (HIV), *Mycobacterium tuberculosis* and Group B *Streptococcus*[141].

However, infectious disease testing using PCR and other Nucleic Acid Amplification Techniques (NAATs) has mostly been confined to large centralized labs that use high-end instrumentation costing hundreds of thousands of dollars and employ skilled personnel. Because NAATs are readily capable of achieving the limits of detection often required of pathogen testing (at or less than 100 organisms/mL), there are

enormous economic and public health benefits in making them available in formats suitable for use in point-of-care (POC) settings such as primary care clinics, community healthcare locations and hospital emergency rooms. They would need to have rapid turnaround times, be affordable, and only require minimally trained personnel.

The technologies aiming to do this seek to combine the three main parts of an NAAT – sample preparation, amplification and detection – into a fully integrated, POC friendly system[112]. Under the United States Clinical Laboratory Improvement Amendments (CLIA) act of 1988, diagnostic tests are classified as "waived", "moderately complex", or "highly complex"[142-143]. Technology that enables a CLIA-waived NAAT is a holy grail of molecular diagnostics. POC settings like homes or pharmacies are only allowed the use of "waived" tests that are "so simple and accurate as to render the likelihood of erroneous results by the user negligible." "Moderately complex" NAAT-based infectious disease diagnostic tests are still a significant improvement over traditional PCR-based systems, where the "high complexity" results from the bottleneck of sample preparation from clinical specimens, which is typically manual, and the need for highly controlled and contamination-free environments to minimize false positives[144-146].

Isothermal NAAT-based platforms, including TwistDX based on RPA (described in Chapter 3), Eiken's LA-200 based on Loop-mediated isothermal amplification (LAMP), and Diagnostics for the Real World's SAMBA, can provide rapid results with inexpensive instrumentation, but do not include sample preparation[112]. The more expensive and currently most POC applicable real-time PCR based, benchtop NAAT-based platforms that combine sample preparation, amplification, and detection in fully-

integrated systems, with times-to-result of between 60 and 120 minutes, include Cepheid's GeneXpert[147], IQuum's Liat Analyzer[148], Biocartis' MDx, Enigma's EL/ML, and Biofire Diagnostics' FilmArray.

The FilmArray platform

The FilmArray system (Biofire Diagnostics, Salt Lake City, Utah) is a closed end-to-end molecular detection platform (Figure 46) that combines automated sample preparation, nucleic acid extraction, and the multiplexed detection of several target pathogens from a single unprocessed sample in around one hour. It performs nested and multiplexed PCR in a two-stage assay, which when combined with amplicon melt curve analysis enables it to distinguish between multiple pathogens simultaneously[149]. It is a benchtop instrument that weighs less than 20 lb, has a longest dimension of 39 cm, and only requires two minutes of hands-on time that involves adding an unprocessed clinical specimen and rehydration buffer to an enclosed 'pouch' containing lyophilized reagents. It is marketed as being intended for use by minimally trained personnel, and is FDA-cleared for two panels: the Blood Culture Identification (BCID) Panel that can identify 24 pathogens and 3 antibiotic resistance genes associated with bloodstream infections, and the Respiratory Panel (RP) that identifies 20 respiratory viruses and bacteria.

The FilmArray BCID panel (Table 12) covers ten bacteria commonly implicated in UTIs, and also detects *mecA*, *vanA/B* and KPC resistance genes, thereby making it an attractive diagnostic option for UTIs. It has been validated as being highly sensitive and specific for the identification of pathogens from blood cultures in several studies[150-154].

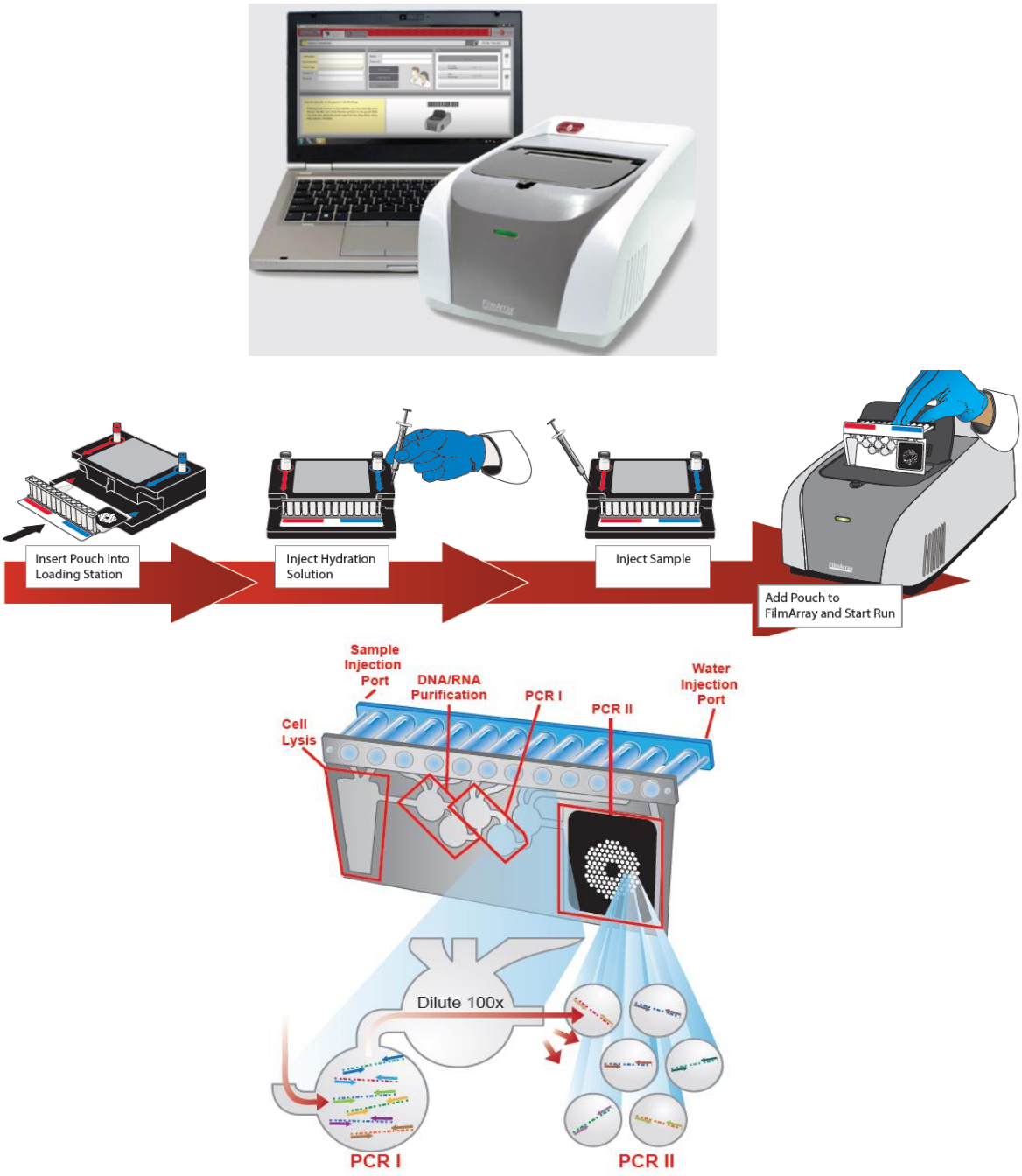

Figure 46. The FilmArray system. (top) a picture of the instrument; (middle) user steps performed in running the instrument; (bottom) a representation of the FilmArray "pouch" showing its various chambers. Images from www.biofiredx.com.

Table 12. Pathogens identified by the FilmArray Blood Culture Identification (BCID) panel

Gram negative bacteria	Gram positive bacteria	Fungi	Antibiotic resistance
Klebsiella oxytoca	***Staphylococcus* spp.**	*Candida albicans*	*mecA* - methicillin resistance
Klebsiella pneumoniae	*Staphylococcus aureus*	*Candida glabrata*	*vanA/B* - vancomycin resistance
Serratia spp.	***Streptococcus* spp.**	*Candida krusei*	KPC - carbapenem resistance
Proteus spp.	*Streptococcus agalactiae*	*Candida parapsilosis*	
Acinetobacter baumannii	*Streptococcus pyogenes*	*Candida tropicalis*	
Hemophilius influenzae	*Streptococcus pneumoniae*		
Neisseria meningitidis	*Enterococcus* spp.		
Psuedomonas aeruginosa	*Listeria monocytogenes*		
Enterobacteriaceae			
Escherichia coli			
Enterobacter cloacae			

Outline of work

Laboratory-developed tests (LDTs) are *in vitro* diagnostic (IVD) tests that are designed, manufactured and used in a single laboratory. They are typically not considered IVDs by the Food and Drug Administration (FDA) for regulatory purposes as they are not sold on the open market. Medical Center Laboratories (MCL; Houston, TX), a CLIA-certified reference laboratory that serves the Greater Houston area, typically returns bacterial identification information to healthcare providers at least 24 hours and up to 72 hours from when samples are received; an initial overnight urine culture is followed by bacterial identification using automated systems that require at least 12 more hours. Due to the potential economic and clinical benefits of having a faster turnaround time, MCL attempted to clinically validate the FilmArray system's BCID panel, which includes several Gram-positive and Gram-negative bacteria associated with UTIs, as a viable tool for UTI pathogen detection, following which they could offer it as an LDT. Culture-based detection was used as the "gold standard", and reported the identity of the top two pathogen isolates from each sample. This clinical evaluation resulted in several discordant and partially concordant results between FilmArray and culture unique to a study of this kind. For example, both FilmArray and culture might have identified a urine sample to be a "positive", but returned different pathogen identities.

In this work, a combination of universal PCR using 16S rDNA primers and Sanger sequencing was first evaluated, albeit unsuccessfully, as a method of establishing true pathogen identity in a small subset of such discordant samples. Following this, for a separate cohort of samples, RPA-based methods were successfully used to establish pathogen identity. The results obtained from these methods, which included using the

real-time RPA panel described in Chapter 3, and end-point RPA in combination with Sanger sequencing, gave rise to interesting conjectures that need to be further investigated, besides pointing to the inadequacies of using culture-based determination of pathogen identity as a reference standard.

Materials and methods

Clinical study

The study was performed using a total of 109 randomly selected clinical samples from those collected by MCL between January 24 and February 12, 2014. The list of 109 samples, along with their pathogen identities as determined by FilmArray and culture-base detection, is provided in Appendix I. MCL routinely receives urine specimens from patients suspected of having UTIs; it serves several hospitals and nursing homes in its region, and processes thousands of samples each year. All samples analyzed in this study were midstream-catch urine specimens collected at the hospitals or nursing homes and transferred to the laboratory. The FilmArray experiments were performed internally at MCL facilities. A total of 20 samples – 15 from this 109 sample study, and 5 from an earlier study by MCL – were identified as being representative of all possible types of discordancy and partial concordance. Total DNA extracted from these 20 samples was transferred to the University of Houston for further study. The University of Houston's Committee for the Protection of Human Subjects (CPHS) approved an application to exempt this study from requiring Institutional Review Board (IRB) approval due to the de-identified nature of the samples.

FilmArray experiments using BCID panel

Urine samples were processed using the FilmArray instrument according to the manufacturer's specifications. Each BCID "pouch", a cartridge containing all reagents necessary for processing a single sample in lyophilized form, was first rehydrated by loading 1 mL Hydration Solution through a syringe. 0.1 mL of a urine sample was then mixed in a Sample Buffer vial using a transfer pipette, following which 0.3 mL of the Sample Mix was loaded into the sample port of the pouch. The pouch was then run by following the instructions on the software screen, and results were obtained in 65 minutes.

Pathogen identification from culture

A culture-based testing system, the MicroScan WalkAway (Siemens, Sacramento, CA), was used as the "gold standard" to establish "true" pathogen identity in the culture-positive samples under study. The WalkAway instrument is a high-throughput automated bacterial identification and susceptibility system based on photometric identification[155]. The manufacturer's specifications were followed – briefly, individual colonies from urine culture plates were inoculated into 96-well microtiter bacterial identification and antibiotic susceptibility testing panels and loaded into the instrument. MicroScan's LabPro software automatically interpreted biochemical results after overnight incubation, with an option to remove panels and verify manually if necessary.

DNA extraction from discordant samples

A protocol described elsewhere[105] was used to extract DNA from urine samples. Briefly, 1 mL urine was pipetted into a 1.5 mL microcentrifuge tube and centrifuged at 12,000 g for 5 min. The supernatant was discarded and 100 μL lysis buffer (1% Tween-

20, 1% NP-40, 0.03% SDS, 5% Chelex 100 and 400 μg/mL proteinase K) was added to the pellet and thoroughly mixed. The mixture was incubated at 56 °C for 1 hour, followed by 100°C for 10 min. The lysate was then centrifuged at 13,000 g for 5 min; the supernatant was stored at -20°C and used as template for further studies. All identifiers connecting the samples to their respective patients were removed before transportation to University of Houston for testing. *E. coli*, *S. agalactiae*, and *K. pneumoniae* gDNA were extracted from culture plates using the same protocol to serve as positive controls for 16S PCR.

PCR using 16S universal primers and sequencing

The pioneering work of Woese and Fox[156] established the use of 16S rDNA sequencing for phylogenetic studies. The presence of both highly conserved regions, enabling the creation of "universal" primers, and genus or species-specific regions makes the 16S rDNA gene an attractive target for use in diagnostic PCR, especially when sequencing PCR products is an option[157]. Universal 16S primers (Table 13) containing deoxyinosine (I) modifications that made them dual priming (DP) were ordered from Integrated DNA Technologies (Coralville, Iowa). The primer pair is meant to amplify roughly the first 500 bases of the 16S gene of almost all bacteria[158-159]. DP oligos are expected to ensure target-specific extension by virtue of containing two functional segments, connected by five consecutive deoxyinosine bases, with distinct annealing properties. The low tolerance for mismatches is due to the short 3′ segment (6 to 12 bp) only binding if there is already stable annealing of the 5′ end.

Table 13. Universal 16S dual-priming PCR primers. I – deoxyinosine modification.

Primer name	Primer sequence
U-16S-FWD	AGAGTTTGATCCTGGTCAIIIIIAACGCT
U-16S-REV	CGCGGCTGCTGGCAIIIAITTAGC

PCRs were performed in 25 μL reaction tubes on an Mx3005 machine (Agilent Technologies). The PCR mixture consisted of 12.5 μL of Brilliant III SYBR Master Mix (Agilent Technologies), forward and reverse primers at 0.4 μM each, 10 μL of PCR-grade water, and 2 μL of urine-extracted DNA or bacterial gDNA as the template. The PCR thermal profile included an initial denaturation step of 3 minutes at 95°C, followed by 45 cycles of 10 s at 95°C (melt), 15 s at 62°C (annealing), and 20 s at 72°C (extension). PCR products were purified using the QIAquick kit (Qiagen) and shipped to SeqWright (Houston, TX) for Sanger sequencing using the same FWD primer as used for PCR. Agarose gel electrophoresis was performed, using a 2% agarose gel and ~100 ng DNA per well, to visualize product sizes after running for 30 minutes at 100 V.

End-point RPA and sequencing

The real-time RPA panel described in Chapter 3 does not cover six pathogen species that were identified by either FilmArray or WalkAway in the discordant and partially concordant samples. End-point RPA, followed by Sanger sequencing using the same forward primers as used for RPA, was used to establish pathogen identity in these cases. The RPA primers designed to target these pathogens in a species-specific manner, using the methods validated in Chapter 3, are listed in Table 14.

End-point RPA was performed in a 50 μL volume using TwistAmp Basic kits (TwistDX, Cambridge, UK). Master mixes containing 480 nM RPA primers and TwistAmp rehydration buffer were prepared and distributed, in 42.5 μL volumes, into 0.2 mL reaction tubes, each containing a lyophilized enzyme pellet. The enzyme pellet in each tube was rapidly solubilized by pipetting the master mix up and down upon addition. Subsequently, 5 μL of clinical sample-extracted DNA was added to the tubes. 2.5 μL of 14 mM magnesium acetate was pipetted into the tube lids, centrifuged into the reaction tubes, and immediately placed into a thermal cycler programmed to operate at 42°C. End-point RPA reactions were typically performed for 30 minutes. A QiaQuick PCR purification kit was used to remove the primers and other reagents from the reaction for the samples to be sent for sequencing.

Real-time RPA

Real-time RPA was performed, using the relevant primer/probe set (developed in Chapter 3) targeting the pathogen being tested for, in a 50 μL volume using TwistAmp exo kits (TwistDX, Cambridge, UK). Master mixes containing 420 nM RPA primers, 120 nm RPA exo probes, and Twist Amp rehydration buffer were prepared and distributed, in 42.5 μL volumes, into reaction tubes supplied with dried enzyme pellets. To start the reaction, 5 μL of clinical sample-extracted DNA and 2.5 μL of 14 mM magnesium acetate was added to each tube by pipetting into tube lids and centrifugation immediately before placing the tubes in an Agilent MxPro 3005 real-time PCR machine (Agilent Technologies, Santa Clara, CA). The real-time PCR machine was programmed to run for 30 minutes at 42°C and collect fluorescence data at 10 s intervals. As in Chapter 3, the criteria for designating a "positive" result was a threshold time of less than 10 minutes.

Table 14. RPA primers designed to target pathogens not covered by real-time RPA panel developed in Chapter 3. F, forward primer; R, reverse primer.

Organism	Target gene	Accession number	Amplicon length (bp)	Primer/probe sequences (5'-3')
Staphylococcus aureus	*nuc*[160]	DQ399678	95	**F**-TAACTTTAGTTGTAGTTTCAAGTCTAAGTAGC
				R-TACTGTTGGATCTTCAGAACCACTTCTATTTAC
Streptococcus agalactiae	*cpn60*[161]	GQ251502.1	291	**F**-CTGTTTCAGCAGCAGTTGAAGAGCTAAAAGA
				R-GGATATACGGATTCTCAAGTTCAGAGACCA
Providencia stuartii	*phoN*[162]	X64820.1	141	**F**-TATCATCACCTAACTCTTGAGCAAAAACCATTC
				R-CAAGGTGATCAGTTATTGATGTTTTATTTAGAC
Acinetobacter lwoffii	$bla_{\text{OXA-235}}$[163]	KF460532	188	**F**-ACTCAAGCCATTGCCCAATTATTTGATCAGGCG
				R-TCATTGGTTGTGGCTTTGCCATGTTGCAGGC
Enterobacter cloacae	*oriC*[164]	DQ227470.1	154	**F**-GTTAGAAAGGATCGTTTGCTGTGAATGATCG
				R-ATGTGGATAACTCTGGTTAAAAGCTCGTATT

Statistical analysis

The sequencing data obtained in the study (16S PCR and end-point RPA) was compared to all publicly available nucleotide sequences (nr/nt database) on GenBank using the blastn and megablast algorithms of NCBI's BLAST website (http://blast.ncbi.nlm.nih.gov/Blast.cgi). Sequence data that had a Phred quality score below 20, implying a base call accuracy of less than 99%, was not used in BLAST searches. A BLAST searched that returned at least 98% sequence alignment, for at least 50 continuous bases, with nucleotide sequences of the pathogen species being tested for was used as the criteria for designating a "positive" result by this method.

Results and Discussion

PCR using 16S universal primers for discordant sample resolution

The initial set of five discordant samples that were subjected to universal PCR is summarized in Table 15.

Table 15. Discordant clinical samples tested using universal PCR primers

	Sample	FilmArray Pathogen ID	Culture Pathogen ID
1	198629	None Detected	*S. agalactiae, E. coli, Enterococcus*
2	281799	*Enterococcus, K. pneumoniae*	*Enterococcus*
3	422572	*S. aureus, C. albicans*	*S. aureus, Enterococcus*
4	192963	None Detected	*Enterococcus*
5	97801	*Enterococcus, E. coli*	*E. coli*

As shown in Figure 47, the PCR products of all samples showed a band around 500 bp as expected. The sequencing results, however, were inconclusive for bacterial pathogen identity when compared to GenBank sequences using BLAST. Sanger sequencing, for

samples 1-4, either produced sequences of human origin or mixed chromatograms that had very a low number of high quality (Phred score 20 and above) bases. Sample 5 produced a portion of the 16S gene of *Staphylococcus epidermidis*, with a 99% identity match of 461 Phred20-quality bases when BLASTed. *S. epidermidis* is a known, ubiquitous colonizer of human skin[165] and was most likely a contaminant in the sample provided by MCL. The sequencing results of the positive controls, on the other hand, produced 16S bacterial sequences that were a >98% match to their corresponding GenBank reference sequences (lanes Ec, Kp and Sa in Figure 47).

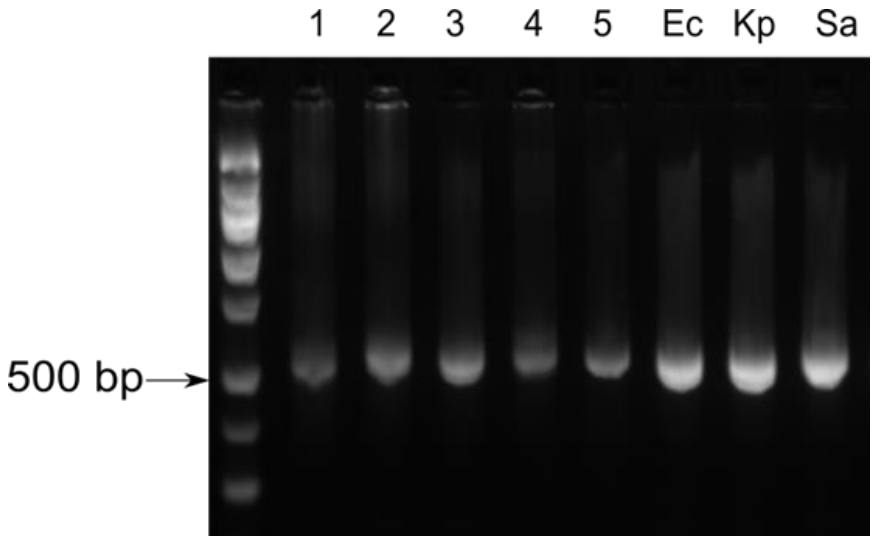

Figure 47. Agarose gel showing products of PCR, obtained using universal 16S primers, for the samples summarized in Table 15.

DNA was extracted from the positive control samples using the same method as that used for urine samples. This ruled out interference, from the surfactants or enzymes used in that process, as a possible reason for the failure to specifically amplify any bacterial DNA. The results summarized in Figure 47, therefore, pointed to the significant non-specific amplification of human DNA from urine-extracted DNA samples. MCL serves a population of mostly elderly patients. Pyuria, the presence of neutrophils in

urine, is commonly associated with UTIs[101] and is known to be significantly higher in older patients at levels up to 500,000 WBCs per mL of urine.[110] There was, therefore, a high background of human DNA and potentially very low copy numbers of bacterial 16S genes that enabled non-specific priming and amplification to dominate. The clinical samples tested using the universal PCR were exhausted in doing so, and could not be tested using either RPA method.

RPA methods for discordant sample resolution

The nature of the concordance or discordance between FilmArray and culture-based detection in this study is summarized in Table 16. In all, 15 partially concordant (designation C3) or fully discordant samples (designations D1, D2 and D3) from the 109 sample study were analyzed using RPA methods.

Fully discordant samples. In traditional clinical evaluations, samples are tested by two methods and designated by each as simply being "positive" or "negative" for disease. A method comparison analysis of the new method with the designated reference or gold standard yields a result that fits in one of three categories – equivalent, commutable, or incompatible. Complete equivalency (100% concordance) is rare; therefore, commutability is the criterion often used. The tolerable commutability that justifies replacement of the reference standard with the new assay varies with the medically tolerated error for the disease under consideration. In an evaluation of the traditional kind, all D2 type samples (Table 16) would be considered false positives and contribute to a lower calculated specificity for the FilmArray. Similarly, samples of type D1 (Table 16) would be considered false negatives, lowering the calculated sensitivity.

Table 16. Summary of initial results from the evaluation of FilmArray BCID panel for UTI pathogen detection. "Culture" refers to pathogen ID (top two pathogens) provided by the MicroScan system for **POSITIVE** samples, and to no overnight growth on sheep blood agar plates for **NEGATIVE** samples.

Designation	Sample type	Number of samples	% of total number		Number of samples analyzed in this work
C1	**NEGATIVE** by both FilmArray and culture	23	21.1	**82.6% concordance**	0
C2	**POSITIVE** by both FilmArray and culture, same species detected by both methods	37	33.9		0
C3	**POSITIVE** by both FilmArray and culture, at least one common pathogen identified or "multiple organisms"	30	27.5		8
D1	**NEGATIVE** by FilmArray but **POSITIVE** by culture	8	7.3	**17.4% discordance**	2
D2	**POSITIVE** by FilmArray and **NEGATIVE** by culture	8	7.3		2
D3	**POSITIVE** by both FilmArray and culture, but no common pathogen identification	3	2.8		3
	TOTAL	**109**			**15**

Reference standards including culture are rarely 100% sensitive and 100% specific. Therefore, the use of a third method, besides the reference standard and method under evaluation, to corroborate or contradict results from the other two methods is a reasonable approach. In this work, RPA was used as the third method. The two D1 type samples evaluated in this work (Table 17 - samples 135100 and 385312) confirmed the culture based result. It was interesting that both samples involved *Enterococcus* species, potentially implying that FilmArray is not as sensitive for *Enterococcus* as it is for other species.

In the analyzed type D2 samples, real-time RPA confirmed the presence of *E. coli* only, or *E. coli* and *K. pneumoniae,* in samples 213965 and 426239, respectively, and therefore verified FilmArray results. The use of a three-method approach for evaluating the FilmArray, rather than just using one gold standard, therefore, could potentially improve the calculated specificity of the system. In this study, for example, the clinical specificity of the FilmArray is 74.2% using a two method approach (23 FilmArray negatives compared to 31 "true" negatives). Upon incorporating the discordancy resolution reported above, the specificity immediately jumps up to 86.2% (23 FilmArray negatives compared to 29 "true" negatives). Speculatively, this number could have been higher, had all D2 type samples been analyzed by RPA. Similar arguments can be made about the clinical sensitivity.

Table 17. Discordant sample resolution by RPA methods

Designation	Sample ID	FilmArray pathogen ID	Culture pathogen ID	RPA pathogen ID
C3	468179	*E. coli, P. aeruginosa*	*E. coli*	*P. aeruginosa*
C3	473268	*E. coli, S. agalactiae*	*E. coli*	*E. coli, S. agalactiae*
C3	174118	*S. agalactiae, E. cloacae, K. pneumoniae*	Multiple organisms	*E. cloacae, K. pneumoniae*
C3	173335	*E. coli, P. aeruginosa*	*E. coli*	*E. coli, P. aeruginosa*
C3	329444	*E. coli, K. oxytoca*	*E. coli*	*E. coli, K. pneumoniae*
C3	467973	*P. aeruginosa, E. coli*	*E. coli*	*P. aeruginosa, E. coli*
C3	204290	*E. coli, Proteus*	*E. coli*	*E. coli, P. mirabilis*
C3	113931	*S. agalactiae, Proteus*	*P. mirabilis*	*S. agalactiae, Proteus*
D1	135100	None detected	*E. coli, Enterococcus*	*Enterococcus*
D1	385312	None detected	*Enterococcus*	*Enterococcus*
D2	213965	*E. coli*	No pathogens	*E. coli*
D2	426239	*E. coli, K. pneumoniae*	No pathogens	*E. coli, K. pneumoniae*
D3	138875	*Enterococcus, E. coli, Proteus*	*Providencia stuartii*	*Enterococcus, E. coli, P. mirabilis, Providencia stuartii*
D3	475387	*P. aeruginosa*	*Acinetobacter lwoffii*	*P. aeruginosa*
D3	477616	*Staphylococcus*	*Enterococcus*	*Enterococcus*

The designation D3 was given to samples that were identified as being positive by both FilmArray and culture, but with completely different pathogen identities being reported. The RPA results obtained from the three D3 type samples analyzed couldn't be used to draw any major conclusions. For example, in the sample identified as containing three pathogens by FilmArray (138875) and a completely different pathogen by culture, RPA identified all four pathogens. The two other D3 type samples had opposite resolutions: 475387's FilmArray result was confirmed, and 477616's culture result was confirmed.

Partially concordant samples. In addition to fully discordant sample results, the right resolution of which could significantly impact the calculated clinical sensitivity and specificity, partially concordant samples (designated C3 in Table 17) were tested by RPA. One of these samples, 174118, had three pathogens identified by FilmArray and a "multiple organisms" designation by culture. This was because the laboratory that provided culture identification reports a WalkAway result of three or more pathogens as "multiple organisms". Two of the three pathogens identified by FilmArray were confirmed as being present by RPA methods, and the third, *S. agalactiae*, was a negative.

Seven other samples of the C3 type were tested to evaluate whether the seeming ability of FilmArray to pick up two pathogens where culture only picked up one could be confirmed. In one of these samples, 468179, only one of two pathogens identified by FilmArray could be confirmed. In the remaining 6 samples, a "positive" result was obtained by RPA for both pathogens identified as being present by FilmArray. Molecular detection methods, such as FilmArray or RPA, do not require that the organisms being detected be viable, unlike culture. For all C3 and D2 type samples, this could potentially

have been why culture failed to identify the pathogens confirmed by both FilmArray and RPA.

Conclusions

Biofire Diagnostics' FilmArray is a closed bench-top instrument for molecular detection, with a sample-to-result time of around one hour, and a promising POC-friendly, NAAT-based platform. Discordant and partially concordant sample results, generated during the clinical evaluation of FilmArray's BCID panel for UTI pathogen detection, were analyzed by universal 16S PCR or end-point RPA followed by sequencing, or the real-time RPA panel developed in Chapter 3.

16S PCR non-specifically and preferentially amplified human DNA, which was potentially present as a vast excess to bacterial DNA in urine-extracted total DNA samples. This occurred despite the primers used being deoxyinosine-modified, and therefore dual priming and supposedly more specific to bacterial DNA. 16S PCR was therefore unsuccessful in establishing the true pathogen identity of an initial set of discordant samples.

In another set of 15 discordant samples, RPA-based methods were successful in fully or partially corroborating or contradicting the original pathogen IDs obtained by FilmArray and culture-based detection in all samples. This set of samples likely had similar levels of human DNA as in the samples analyzed by PCR, but no non-specific amplification was observed by real-time RPA, and the amplification was specific enough to enable the generation of sequencing data when end-point RPA was used. Moreover, in the samples analyzed by real-time RPA, results were obtained in less than ten minutes from the start of reactions.

Through the RPA results, the FilmArray system was shown to be successful in identifying multiple pathogens (up to three simultaneously in the samples studied) in cases where culture could only identify one. In two cases that were originally FilmArray positive but culture-negative, and therefore counted as false positives, RPA identified the same pathogen(s) as FilmArray, pointing to the inadequacy of culture as a reference standard, and the need to use a three-method approach for future clinical evaluations.

CHAPTER 5 – CONCLUSIONS AND SUGGESTIONS FOR FUTURE WORK

Microfluidic Retroreflector Diagnostics

The work presented in this dissertation has described the development and analytical evaluation of a novel embedded microretroreflector-based automated optical biosensing platform for immunoassays. The analytical sensitivity of the system was determined to be 4000 *R. conorii* per mL from buffer. The key features of this platform include the use of magnetic beads as both sample capture substrates and detection labels, thereby enabling 10-100 fold concentration of analyte before detection, and the automated image capture and difference imaging approach. For this platform to translate into a product that has a public impact, the following suggestions are provided:

- **Replace syringe pump.** The syringe pump is the least portable component of the microfluidic setup in its current form. An alternative approach involving centrifugal microfluidics is being developed by Carmen Pascente to address this issue. A second promising alternative approach is the use of low voltage electrokinetic pumps that could potentially be operated on small and inexpensive batteries.
- **Disposable manifolds.** The reusable microfluidic manifold will need to be replaced by a disposable microfluidic cartridge that can interface with fluidics.
- **Integrate sample preparation into microfluidics.** For true POC applicability, the system will need to be of a "plug and measure" nature. This calls for automated sample preparation approaches that will allow a user to add a small

quantity (ideally a finger prick, potentially more) of an unprocessed patient sample such as whole blood to the device and get a result in under one hour. This will require the sample preparation device or cartridge to be able to lyse blood cells (for intracellular pathogens like *R. conorii*), manipulate magnetic beads for sample capture, concentration and purification, and deliver the processed sample to the embedded microretroreflector chip for detection.

Recombinase Polymerase Amplification based diagnostics

RPA is a promising isothermal NAAT, and has grown to be used in a widespread manner by research laboratories around the world to develop diagnostic panels like the one described in this work. It is easier to develop than other isothermal NAATs by virtue of only needing the design of three oligonucleotides. Also, it is amenable to a range of detection formats, including real-time fluorescence-based real-time detection and lateral flow. In the work presented in this dissertation, recombinase polymerase amplification (RPA) was used for the rapid, sensitive and specific identification of UTI pathogens through the development of a real-time RPA panel that targeted the six most frequently occurring UTI pathogens. The panel demonstrated excellent analytical sensitivities and specificities. All five primer/probe sets detected 100 genomes per reaction or less in around ten minutes, and did not amplify high amounts of non-specific pathogen DNA. Clinical studies on a larger scale are required to further evaluate the applicability of the developed RPA panel for routine UTI pathogen detection. Sample preparation, involving DNA extraction from urine samples, is still a bottleneck in the way of the panel being truly point-of-care. The direct use of boiled urine samples as a template for RPA is a possibility that should be explored.

REFERENCES

1. M. S. Frazier; J. Drzymkowski, *Essentials of Human Diseases and Conditions*. 5th ed.; Saunders: 2013.
2. N. P. Pai; C. Vadnais; C. Denkinger; N. Engel; M. Pai, "Point-of-Care Testing for Infectious Diseases: Diversity, Complexity, and Barriers in Low- and Middle-Income Countries". *PLoS Med* **2012,** *9* (9), e1001306.
3. The Lewin Group *Laboratory Medicine: A National Status Report (Centers for Disease Control and Prevention)*; 2008; pp 25-31.
4. The Lewin Group *The Value of Diagnostics Innovation, Adoption and Diffusion into Health Care (Advanced Medical Technology Association)*; Washington, DC, 2005; pp 30-40.
5. V. Gubala; L. F. Harris; A. J. Ricco; M. X. Tan; D. E. Williams, "Point of Care Diagnostics: Status and Future". *Anal Chem* **2012,** *84* (2), 487-515.
6. N. Papadopoulos; K. W. Kinzler; B. Vogelstein, "The Role of Companion Diagnostics in the Development and Use of Mutation-Targeted Cancer Therapies". *Nat Biotechnol* **2006,** *24* (8), 985-95.
7. D. M. Morens; G. K. Folkers; A. S. Fauci, "The Challenge of Emerging and Re-Emerging Infectious Diseases". *Nature* **2004,** *430* (6996), 242-9.
8. W. F. Wright, *Essentials of Clinical Infectious Diseases*. Demos Medical Publishing: 2013.
9. E. Keeler; M. D. Perkins; P. Small; C. Hanson; S. Reed; J. Cunningham; J. E. Aledort; L. Hillborne; M. E. Rafael; F. Girosi; C. Dye, "Reducing the Global

Burden of Tuberculosis: The Contribution of Improved Diagnostics". *Nature* **2006,** *444 Suppl 1*, 49-57.

10. Y. W. Lim; M. Steinhoff; F. Girosi; D. Holtzman; H. Campbell; R. Boer; R. Black; K. Mulholland, "Reducing the Global Burden of Acute Lower Respiratory Infections in Children: The Contribution of New Diagnostics". *Nature* **2006,** *444 Suppl 1*, 9-18.
11. RAND Corporation. Estimating the Global Health Impact of Improved Diagnostic Tools for the Developing World 2007. http://www.rand.org/content/dam/rand/pubs/research_briefs/2007/RAND_RB9293.pdf (accessed September 20, 2014).
12. L. C. Clark, Jr.; C. Lyons, "Electrode Systems for Continuous Monitoring in Cardiovascular Surgery". *Ann N Y Acad Sci* **1962,** *102*, 29-45.
13. National Institutes of Health A Timeline of Pregnancy Testing. http://history.nih.gov/exhibits/thinblueline/timeline.html (accessed September 20, 2014).
14. J. H. Nichols, "Point of Care Testing". *Clin Lab Med* **2007,** *27* (4), 893-908, viii.
15. M. Schito; T. F. Peter; S. Cavanaugh; A. S. Piatek; G. J. Young; H. Alexander; W. Coggin; G. J. Domingo; D. Ellenberger; E. Ermantraut; I. V. Jani; A. Katamba; K. M. Palamountain; S. Essajee; D. W. Dowdy, "Opportunities and Challenges for Cost-Efficient Implementation of New Point-of-Care Diagnostics for Hiv and Tuberculosis". *J Infect Dis* **2012,** *205 Suppl 2*, S169-80.
16. C. P. Price; A. St John, Point-of-Care Testing in Primary Care. In *Point-of-Care Testing*, 2nd ed.; AACC Press: Washington DC, 2004; pp 3-9.

17. R. W. Peeling; K. K. Holmes; D. Mabey; A. Ronald, "Rapid Tests for Sexually Transmitted Infections (Stis): The Way Forward". *Sex Transm Infect* **2006,** *82 Suppl 5*, v1-6.

18. A. J. Saah; D. R. Hoover, ""Sensitivity" and "Specificity" Reconsidered: The Meaning of These Terms in Analytical and Diagnostic Settings". *Ann Intern Med* **1997,** *126* (1), 91-4.

19. A. De Rossi; A. E. Ades; F. Mammano; A. Del Mistro; A. Amadori; C. Giaquinto; L. Chieco-Bianchi, "Antigen Detection, Virus Culture, Polymerase Chain Reaction, and in Vitro Antibody Production in the Diagnosis of Vertically Transmitted Hiv-1 Infection". *Aids* **1991,** *5* (1), 15-20.

20. A. M. Vandamme, "Polymerase Chain Reaction (Pcr) as a Diagnostic Tool in Hiv Infection". *Verh K Acad Geneeskd Belg* **1994,** *56* (3), 231-65.

21. R. S. Yalow; S. A. Berson, "Immunoassay of Endogenous Plasma Insulin in Man". *J Clin Invest* **1960,** *39*, 1157-75.

22. Y. H. Tan; M. Liu; B. Nolting; J. G. Go; J. Gervay-Hague; G. Y. Liu, "A Nanoengineering Approach for Investigation and Regulation of Protein Immobilization". *ACS Nano* **2008,** *2* (11), 2374-84.

23. G. M. Whitesides, "The Origins and the Future of Microfluidics". *Nature* **2006,** *442* (7101), 368-73.

24. D. Mark; S. Haeberle; G. Roth; F. von Stetten; R. Zengerle, "Microfluidic Lab-on-a-Chip Platforms: Requirements, Characteristics and Applications". *Chem Soc Rev* **2010,** *39* (3), 1153-82.

25. T. Uno; H. Tabata; T. Kawai, "Peptide-Nucleic Acid-Modified Ion-Sensitive Field-Effect Transistor-Based Biosensor for Direct Detection of DNA Hybridization". *Anal Chem* **2007,** *79* (1), 52-9.

26. H. J. Park; S. K. Kim; K. Park; H. K. Lyu; C. S. Lee; S. J. Chung; W. S. Yun; M. Kim; B. H. Chung, "An Isfet Biosensor for the Monitoring of Maltose-Induced Conformational Changes in Mbp". *FEBS Lett* **2009,** *583* (1), 157-62.

27. R. McKendry; J. Zhang; Y. Arntz; T. Strunz; M. Hegner; H. P. Lang; M. K. Baller; U. Certa; E. Meyer; H. J. Guntherodt; C. Gerber, "Multiple Label-Free Biodetection and Quantitative DNA-Binding Assays on a Nanomechanical Cantilever Array". *Proc Natl Acad Sci U S A* **2002,** *99* (15), 9783-8.

28. J. Voros; J. J. Ramsden; G. Csucs; I. Szendro; S. M. De Paul; M. Textor; N. D. Spencer, "Optical Grating Coupler Biosensors". *Biomaterials* **2002,** *23* (17), 3699-710.

29. Z. Lai; Y. Wang; N. Allbritton; G. P. Li; M. Bachman, "Label-Free Biosensor by Protein Grating Coupler on Planar Optical Waveguides". *Opt Lett* **2008,** *33* (15), 1735-7.

30. X. D. Hoa; A. G. Kirk; M. Tabrizian, "Towards Integrated and Sensitive Surface Plasmon Resonance Biosensors: A Review of Recent Progress". *Biosens Bioelectron* **2007,** *23* (2), 151-60.

31. K. Lange; B. E. Rapp; M. Rapp, "Surface Acoustic Wave Biosensors: A Review". *Anal Bioanal Chem* **2008,** *391* (5), 1509-19.

32. A. Bernard; B. Michel; E. Delamarche, "Micromosaic Immunoassays". *Anal Chem* **2001,** *73* (1), 8-12.

33. S. Cesaro-Tadic; G. Dernick; D. Juncker; G. Buurman; H. Kropshofer; B. Michel; C. Fattinger; E. Delamarche, "High-Sensitivity Miniaturized Immunoassays for Tumor Necrosis Factor Alpha Using Microfluidic Systems". *Lab Chip* **2004,** *4* (6), 563-9.

34. M. L. Chabinyc; D. T. Chiu; J. C. McDonald; A. D. Stroock; J. F. Christian; A. M. Karger; G. M. Whitesides, "An Integrated Fluorescence Detection System in Poly(Dimethylsiloxane) for Microfluidic Applications". *Anal Chem* **2001,** *73* (18), 4491-8.

35. L. Gervais; E. Delamarche, "Toward One-Step Point-of-Care Immunodiagnostics Using Capillary-Driven Microfluidics and Pdms Substrates". *Lab Chip* **2009,** *9* (23), 3330-7.

36. J. Yakovleva; R. Davidsson; A. Lobanova; M. Bengtsson; S. Eremin; T. Laurell; J. Emneus, "Microfluidic Enzyme Immunoassay Using Silicon Microchip with Immobilized Antibodies and Chemiluminescence Detection". *Anal Chem* **2002,** *74* (13), 2994-3004.

37. S. A. Lange; G. Roth; S. Wittemann; T. Lacoste; A. Vetter; J. Grassle; S. Kopta; M. Kolleck; B. Breitinger; M. Wick; J. K. Horber; S. Dubel; A. Bernard, "Measuring Biomolecular Binding Events with a Compact Disc Player Device". *Angew Chem Int Ed Engl* **2005,** *45* (2), 270-3.

38. D. M. Bruls; T. H. Evers; J. A. Kahlman; P. J. van Lankvelt; M. Ovsyanko; E. G. Pelssers; J. J. Schleipen; F. K. de Theije; C. A. Verschuren; T. van der Wijk; J. B. van Zon; W. U. Dittmer; A. H. Immink; J. H. Nieuwenhuis; M. W. Prins, "Rapid

Integrated Biosensor for Multiplexed Immunoassays Based on Actuated Magnetic Nanoparticles". *Lab Chip* **2009,** *9* (24), 3504-10.

39. C. Li; L. A. Shutter; P. M. Wu; C. H. Ahn; R. K. Narayan, "Potential of a Simple Lab-on-a-Tube for Point-of-Care Measurements of Multiple Analytes". *Lab Chip* **2010,** *10* (11), 1476-9.

40. C. Pohlmann; M. Sprinzl, "Electrochemical Detection of Micrornas Via Gap Hybridization Assay". *Anal Chem* **2010,** *82* (11), 4434-40.

41. G. Proczek; A. L. Gassner; J. M. Busnel; H. H. Girault, "Total Serum Ige Quantification by Microfluidic Elisa Using Magnetic Beads". *Anal Bioanal Chem* **2012,** *402* (8), 2645-53.

42. Z. Fu; G. Shao; J. Wang; D. Lu; W. Wang; Y. Lin, "Microfabricated Renewable Beads-Trapping/Releasing Flow Cell for Rapid Antigen-Antibody Reaction in Chemiluminescent Immunoassay". *Anal Chem* **2011,** *83* (7), 2685-90.

43. Y. Zhang; S. Ge; S. Wang; M. Yan; J. Yu; X. Song; W. Liu, "Magnetic Beads-Based Electrochemiluminescence Immunosensor for Determination of Cancer Markers Using Quantum Dot Functionalized Ptru Alloys as Labels". *Analyst* **2012,** *137* (9), 2176-82.

44. H. Neubert; J. Gale; D. Muirhead, "Online High-Flow Peptide Immunoaffinity Enrichment and Nanoflow Lc-Ms/Ms: Assay Development for Total Salivary Pepsin/Pepsinogen". *Clin Chem* **2010,** *56* (9), 1413-23.

45. E. Temur; A. Zengin; I. H. Boyaci; F. C. Dudak; H. Torul; U. Tamer, "Attomole Sensitivity of Staphylococcal Enterotoxin B Detection Using an Aptamer-

Modified Surface-Enhanced Raman Scattering Probe". *Anal Chem* **2012,** *84* (24), 10600-6.

46. H. Chon; C. Lim; S. M. Ha; Y. Ahn; E. K. Lee; S. I. Chang; G. H. Seong; J. Choo, "On-Chip Immunoassay Using Surface-Enhanced Raman Scattering of Hollow Gold Nanospheres". *Anal Chem* **2010,** *82* (12), 5290-5.

47. L. Sasso; I. Johnston; M. Zheng; R. Gupte; A. Ündar; J. Zahn, "Automated Microfluidic Processing Platform for Multiplexed Magnetic Bead Immunoassays". *Microfluidics and Nanofluidics* **2012,** *13* (4), 603-612.

48. B. Teste; A. Ali-Cherif; J. L. Viovy; L. Malaquin, "A Low Cost and High Throughput Magnetic Bead-Based Immuno-Agglutination Assay in Confined Droplets". *Lab Chip* **2013,** *13* (12), 2344-9.

49. V. Mani; D. P. Wasalathanthri; A. A. Joshi; C. V. Kumar; J. F. Rusling, "Highly Efficient Binding of Paramagnetic Beads Bioconjugated with 100,000 or More Antibodies to Protein-Coated Surfaces". *Anal Chem* **2012,** *84* (23), 10485-91.

50. S. Krishnan; V. Mani; D. Wasalathanthri; C. V. Kumar; J. F. Rusling, "Attomolar Detection of a Cancer Biomarker Protein in Serum by Surface Plasmon Resonance Using Superparamagnetic Particle Labels". *Angew Chem Int Ed Engl* **2011,** *50* (5), 1175-8.

51. B. S. Munge; A. L. Coffey; J. M. Doucette; B. K. Somba; R. Malhotra; V. Patel; J. S. Gutkind; J. F. Rusling, "Nanostructured Immunosensor for Attomolar Detection of Cancer Biomarker Interleukin-8 Using Massively Labeled Superparamagnetic Particles". *Angew Chem Int Ed Engl* **2011,** *50* (34), 7915-8.

52. V. N. Morozov; Y. M. Shlyapnikov; J. Kidd; T. Y. Morozova; E. A. Shlyapnikova, "Conic Electrophoretic Concentrator for Charged Macromolecules". *Anal Chem* **2011,** *83* (14), 5548-55.

53. H. C. Tekin; M. Cornaglia; M. A. Gijs, "Attomolar Protein Detection Using a Magnetic Bead Surface Coverage Assay". *Lab Chip* **2013,** *13* (6), 1053-9.

54. S. P. Mulvaney; C. L. Cole; M. D. Kniller; M. Malito; C. R. Tamanaha; J. C. Rife; M. W. Stanton; L. J. Whitman, "Rapid, Femtomolar Bioassays in Complex Matrices Combining Microfluidics and Magnetoelectronics". *Biosens Bioelectron* **2007,** *23* (2), 191-200.

55. Y. Wang; J. Dostalek; W. Knoll, "Magnetic Nanoparticle-Enhanced Biosensor Based on Grating-Coupled Surface Plasmon Resonance". *Anal Chem* **2011,** *83* (16), 6202-7.

56. R. L. Edelstein; C. R. Tamanaha; P. E. Sheehan; M. M. Miller; D. R. Baselt; L. J. Whitman; R. J. Colton, "The Barc Biosensor Applied to the Detection of Biological Warfare Agents". *Biosens Bioelectron* **2000,** *14* (10-11), 805-13.

57. S. P. Mulvaney; C. N. Ibe; C. R. Tamanaha; L. J. Whitman, "Direct Detection of Genomic DNA with Fluidic Force Discrimination Assays". *Anal Biochem* **2009,** *392* (2), 139-44.

58. P. S. Waggoner; M. Varshney; H. G. Craighead, "Detection of Prostate Specific Antigen with Nanomechanical Resonators". *Lab Chip* **2009,** *9* (21), 3095-9.

59. H. Lee; T. J. Yoon; R. Weissleder, "Ultrasensitive Detection of Bacteria Using Core-Shell Nanoparticles and an Nmr-Filter System". *Angew Chem Int Ed Engl* **2009,** *48* (31), 5657-60.

60. S. P. Mulvaney; K. M. Myers; P. E. Sheehan; L. J. Whitman, "Attomolar Protein Detection in Complex Sample Matrices with Semi-Homogeneous Fluidic Force Discrimination Assays". *Biosens Bioelectron* **2009,** *24* (5), 1109-15.

61. J. Luoma; J. Schumann; E. C. Traube, "Effects of Retroreflector Positioning on Nighttime Recognition of Pedestrians". *Accid Anal Prev* **1996,** *28* (3), 377-83.

62. P. Schultz; B. Cumby; J. Heikenfeld, "Investigation of Five Types of Switchable Retroreflector Films for Enhanced Visible and Infrared Conspicuity Applications". *Appl Opt* **2012,** *51* (17), 3744-54.

63. M. Switkes; B. L. Ervin; R. P. Kingsborough; M. Rothschild; M. Sworin, "Retroreflectors for Remote Readout of Colorimetric Sensors". *Sensors and Actuators B: Chemical* **2011,** *160* (1), 1244-1249.

64. P. L. Bender; D. G. Currie; S. K. Poultney; C. O. Alley; R. H. Dicke; D. T. Wilkinson; D. H. Eckhardt; J. E. Faller; W. M. Kaula; J. D. Mulholland; H. H. Plotkin; E. C. Silverberg; J. G. Williams, "The Lunar Laser Ranging Experiment: Accurate Ranges Have Given a Large Improvement in the Lunar Orbit and New Selenophysical Information". *Science* **1973,** *182* (4109), 229-38.

65. M. Bohling; T. Seiler; B. Wdowiak; J. Jahns; J. Mohr; M. Borner, "Highly Precise Micro-Retroreflector Array Fabricated by the Liga Process and Its Application as Tapped Delay Line Filter". *Appl Opt* **2012,** *51* (25), 5989-95.

66. W. Nyka, "Rickettsiae in the Blood of Mice and Rats Infected Experimentally with Typhus". *J Infect Dis* **1950,** *86* (1), 81-7, illust.

67. A. F. Azad, "Pathogenic Rickettsiae as Bioterrorism Agents". *Clin Infect Dis* **2007,** *45 Suppl 1*, S52-5.

68. E. Astrup; T. Lekva; G. Davi; K. Otterdal; F. Santilli; E. Oie; B. Halvorsen; J. K. Damas; D. Raoult; G. Vitale; J. P. Olano; T. Ueland; P. Aukrust, "A Complex Interaction between Rickettsia Conorii and Dickkopf-1--Potential Role in Immune Evasion Mechanisms in Endothelial Cells". *PLoS One* **2012,** *7* (9), e43638.

69. G. R. Willmott; R. Vogel; S. S. Yu; L. G. Groenewegen; G. S. Roberts; D. Kozak; W. Anderson; M. Trau, "Use of Tunable Nanopore Blockade Rates to Investigate Colloidal Dispersions". *J Phys Condens Matter* **2010,** *22* (45), 454116.

70. R. Vogel; G. Willmott; D. Kozak; G. S. Roberts; W. Anderson; L. Groenewegen; B. Glossop; A. Barnett; A. Turner; M. Trau, "Quantitative Sizing of Nano/Microparticles with a Tunable Elastomeric Pore Sensor". *Anal Chem* **2011,** *83* (9), 3499-506.

71. R. Vogel; W. Anderson; J. Eldridge; B. Glossop; G. Willmott, "A Variable Pressure Method for Characterizing Nanoparticle Surface Charge Using Pore Sensors". *Anal Chem* **2012,** *84* (7), 3125-31.

72. D. Kozak; W. Anderson; R. Vogel; S. Chen; F. Antaw; M. Trau, "Simultaneous Size and Zeta-Potential Measurements of Individual Nanoparticles in Dispersion Using Size-Tunable Pore Sensors". *ACS Nano* **2012,** *6* (8), 6990-7.

73. A. Nasrullah; D. Smith; T. Sherlock; P. Ruchhoeft; D. Litvinov, "Near Neighbor Averaging: A Technique for Improving Image Uniformity in Aperture Array Lithography". *Journal of Vacuum Science & Technology B* **2009,** *27* (6), 2674-2678.

74. E. Girardi; M. D. Holdom; A. M. Davies; B. J. Sutton; A. J. Beavil, "The Crystal Structure of Rabbit Igg-Fc". *Biochem J* **2009,** *417* (1), 77-83.

75. S. Puertas; M. Moros; R. Fernández-Pacheco; M. R. Ibarra; V. Grazú; J. M. d. l. Fuente, "Designing Novel Nano-Immunoassays: Antibody Orientation Versus Sensitivity". *Journal of Physics D: Applied Physics* **2010,** *43* (47), 474012.

76. F. Fixe; M. Dufva; P. Telleman; C. B. Christensen, "Functionalization of Poly(Methyl Methacrylate) (Pmma) as a Substrate for DNA Microarrays". *Nucleic Acids Res* **2004,** *32* (1), e9.

77. R. Merkel; P. Nassoy; A. Leung; K. Ritchie; E. Evans, "Energy Landscapes of Receptor-Ligand Bonds Explored with Dynamic Force Spectroscopy". *Nature* **1999,** *397* (6714), 50-3.

78. M. Grandbois; M. Beyer; M. Rief; H. Clausen-Schaumann; H. E. Gaub, "How Strong Is a Covalent Bond?". *Science* **1999,** *283* (5408), 1727-30.

79. G. U. Lee; L. A. Chrisey; R. J. Colton, "Direct Measurement of the Forces between Complementary Strands of DNA". *Science* **1994,** *266* (5186), 771-3.

80. G. U. Lee; D. A. Kidwell; R. J. Colton, "Sensing Discrete Streptavidin-Biotin Interactions with Atomic Force Microscopy". *Langmuir* **1994,** *10* (2), 354-357.

81. P. Hinterdorfer; W. Baumgartner; H. J. Gruber; K. Schilcher; H. Schindler, "Detection and Localization of Individual Antibody-Antigen Recognition Events by Atomic Force Microscopy". *Proc Natl Acad Sci U S A* **1996,** *93* (8), 3477-81.

82. S. W. Metzger; M. Natesan; C. Yanavich; J. Schneider; G. U. Lee, "Development and Characterization of Surface Chemistries for Microfabricated Biosensors". *Journal of Vacuum Science & Technology A* **1999,** *17* (5), 2623-2628.

83. C. Ray; J. R. Brown; B. B. Akhremitchev, "Single-Molecule Force Spectroscopy Measurements of "Hydrophobic Bond" between Tethered Hexadecane Molecules". *J Phys Chem B* **2006,** *110* (35), 17578-83.

84. J. Rife; L. Whitman, Fluidic Force Discrimination. Google Patents: 2003.

85. A. J. Goldman; R. G. Cox; H. Brenner, "Slow Viscous Motion of a Sphere Parallel to a Plane Wall—Ii Couette Flow". *Chemical Engineering Science* **1967,** *22* (4), 653-660.

86. K.-C. Chang; D. A. Hammer, "Influence of Direction and Type of Applied Force on the Detachment of Macromolecularly-Bound Particles from Surfaces". *Langmuir* **1996,** *12* (9), 2271-2282.

87. M. A. Gijs; F. Lacharme; U. Lehmann, "Microfluidic Applications of Magnetic Particles for Biological Analysis and Catalysis". *Chem Rev* **2010,** *110* (3), 1518-63.

88. G. U. Lee; S. Metzger; M. Natesan; C. Yanavich; Y. F. Dufrene, "Implementation of Force Differentiation in the Immunoassay". *Anal Biochem* **2000,** *287* (2), 261-71.

89. J. Mertens; M. Calleja; D. Ramos; A. Tarýn; J. Tamayo, "Role of the Gold Film Nanostructure on the Nanomechanical Response of Microcantilever Sensors". *Journal of Applied Physics* **2007,** *101* (3), 034904.

90. B. Moazzez; S. M. O'Brien; S. E. Merschrod, "Improved Adhesion of Gold Thin Films Evaporated on Polymer Resin: Applications for Sensing Surfaces and Mems". *Sensors (Basel)* **2013,** *13* (6), 7021-32.

91. M. Nordström; A. Johansson; E. S. Noguerón; B. Clausen; M. Calleja; A. Boisen, "Investigation of the Bond Strength between the Photo-Sensitive Polymer Su-8 and Gold". *Microelectronic Engineering* **2005,** *78–79* (0), 152-157.

92. J. M. Chambers; W. S. Cleveland; B. Kleiner; P. A. Tukey, *Graphical Methods for Data Analysis*. Wadsworth & Brooks/Cole: 1983.

93. R. McGill; J. W. Tukey; W. A. Larsen, "Variations of Box Plots". *The American Statistician* **1978,** *32* (1), 12-16.

94. M. W. Eshoo; C. D. Crowder; H. Li; H. E. Matthews; S. Meng; S. E. Sefers; R. Sampath; C. W. Stratton; L. B. Blyn; D. J. Ecker; Y. W. Tang, "Detection and Identification of Ehrlichia Species in Blood by Use of Pcr and Electrospray Ionization Mass Spectrometry". *J Clin Microbiol* **2010,** *48* (2), 472-8.

95. J. D. Sammon; P. Sharma; H. Rahbar; F. Roghmann; K. R. Ghani; S. Sukumar; P. I. Karakiewicz; J. O. Peabody; J. S. Elder; M. Menon; M. Sun; Q. D. Trinh, "Predictors of Admission in Patients Presenting to the Emergency Department with Urinary Tract Infection". *World J Urol* **2014,** *32* (3), 813-9.

96. T. G. Emori; S. N. Banerjee; D. H. Culver; R. P. Gaynes; T. C. Horan; J. R. Edwards; W. R. Jarvis; J. S. Tolson; T. S. Henderson; W. J. Martone; et al., "Nosocomial Infections in Elderly Patients in the United States, 1986-1990. National Nosocomial Infections Surveillance System". *Am J Med* **1991,** *91* (3b), 289s-293s.

97. B. Foxman, "The Epidemiology of Urinary Tract Infection". *Nat Rev Urol* **2010,** *7* (12), 653-60.

98. B. Foxman; R. Barlow; H. D'Arcy; B. Gillespie; J. D. Sobel, "Urinary Tract Infection: Self-Reported Incidence and Associated Costs". *Ann Epidemiol* **2000,** *10* (8), 509-15.

99. G. R. Nielubowicz; H. L. Mobley, "Host-Pathogen Interactions in Urinary Tract Infection". *Nat Rev Urol* **2010,** *7* (8), 430-41.

100. L. E. Nicolle, "Complicated Urinary Tract Infection in Adults". *Can J Infect Dis Med Microbiol* **2005,** *16* (6), 349-60.

101. M. L. Wilson; L. Gaido, "Laboratory Diagnosis of Urinary Tract Infections in Adult Patients". *Clin Infect Dis* **2004,** *38* (8), 1150-8.

102. H. Semeniuk; D. Church, "Evaluation of the Leukocyte Esterase and Nitrite Urine Dipstick Screening Tests for Detection of Bacteriuria in Women with Suspected Uncomplicated Urinary Tract Infections". *J Clin Microbiol* **1999,** *37* (9), 3051-2.

103. R. Oneson; D. H. Groschel, "Leukocyte Esterase Activity and Nitrite Test as a Rapid Screen for Significant Bacteriuria". *Am J Clin Pathol* **1985,** *83* (1), 84-7.

104. M. T. Pezzlo; M. A. Wetkowski; E. M. Peterson; L. M. de la Maza, "Detection of Bacteriuria and Pyuria within Two Minutes". *J Clin Microbiol* **1985,** *21* (4), 578-81.

105. J. Lu; R. Yu; Y. Yan; J. Zhang; X. Ren, "Use of Pyromark Q96 Id Pyrosequencing System in Identifying Bacterial Pathogen Directly with Urine Specimens for Diagnosis of Urinary Tract Infections". *J Microbiol Methods* **2011,** *86* (1), 78-81.

106. J. W. Warren; E. Abrutyn; J. R. Hebel; J. R. Johnson; A. J. Schaeffer; W. E. Stamm, "Guidelines for Antimicrobial Treatment of Uncomplicated Acute

Bacterial Cystitis and Acute Pyelonephritis in Women. Infectious Diseases Society of America (Idsa)". *Clin Infect Dis* **1999,** *29* (4), 745-58.

107. R. H. Rubin; E. D. Shapiro; V. T. Andriole; R. J. Davis; W. E. Stamm, "Evaluation of New Anti-Infective Drugs for the Treatment of Urinary Tract Infection. Infectious Diseases Society of America and the Food and Drug Administration". *Clin Infect Dis* **1992,** *15 Suppl 1*, S216-27.

108. G. W. Smith; W. Brumfitt; J. Hamilton-Miller, "Diagnosis of Coliform Infection in Acutely Dysuric Women". *N Engl J Med* **1983,** *309* (22), 1393-4.

109. R. P. Stark; D. G. Maki, "Bacteriuria in the Catheterized Patient. What Quantitative Level of Bacteriuria Is Relevant?". *N Engl J Med* **1984,** *311* (9), 560-4.

110. P. A. Tambyah; D. G. Maki, "The Relationship between Pyuria and Infection in Patients with Indwelling Urinary Catheters: A Prospective Study of 761 Patients". *Arch Intern Med* **2000,** *160* (5), 673-7.

111. M. Anderson; D. Bollinger; A. Hagler; H. Hartwell; B. Rivers; K. Ward; T. R. Steck, "Viable but Nonculturable Bacteria Are Present in Mouse and Human Urine Specimens". *J Clin Microbiol* **2004,** *42* (2), 753-8.

112. A. Niemz; T. M. Ferguson; D. S. Boyle, "Point-of-Care Nucleic Acid Testing for Infectious Diseases". *Trends Biotechnol* **2011,** *29* (5), 240-50.

113. J. Kim; C. J. Easley, "Isothermal DNA Amplification in Bioanalysis: Strategies and Applications". *Bioanalysis* **2011,** *3* (2), 227-39.

114. P. Craw; W. Balachandran, "Isothermal Nucleic Acid Amplification Technologies for Point-of-Care Diagnostics: A Critical Review". *Lab Chip* **2012,** *12* (14), 2469-86.

115. P. J. Asiello; A. J. Baeumner, "Miniaturized Isothermal Nucleic Acid Amplification, a Review". *Lab Chip* **2011,** *11* (8), 1420-30.

116. P. Gill; A. Ghaemi, "Nucleic Acid Isothermal Amplification Technologies: A Review". *Nucleosides Nucleotides Nucleic Acids* **2008,** *27* (3), 224-43.

117. O. Piepenburg; C. H. Williams; D. L. Stemple; N. A. Armes, "DNA Detection Using Recombination Proteins". *PLoS Biol* **2006,** *4* (7), e204.

118. M. Euler; Y. Wang; D. Heidenreich; P. Patel; O. Strohmeier; S. Hakenberg; M. Niedrig; F. T. Hufert; M. Weidmann, "Development of a Panel of Recombinase Polymerase Amplification Assays for Detection of Biothreat Agents". *J Clin Microbiol* **2013,** *51* (4), 1110-7.

119. F. Shen; E. K. Davydova; W. Du; J. E. Kreutz; O. Piepenburg; R. F. Ismagilov, "Digital Isothermal Quantification of Nucleic Acids Via Simultaneous Chemical Initiation of Recombinase Polymerase Amplification Reactions on Slipchip". *Anal Chem* **2011,** *83* (9), 3533-40.

120. S. Lutz; P. Weber; M. Focke; B. Faltin; J. Hoffmann; C. Muller; D. Mark; G. Roth; P. Munday; N. Armes; O. Piepenburg; R. Zengerle; F. von Stetten, "Microfluidic Lab-on-a-Foil for Nucleic Acid Analysis Based on Isothermal Recombinase Polymerase Amplification (Rpa)". *Lab Chip* **2010,** *10* (7), 887-93.

121. B. A. Rohrman; R. R. Richards-Kortum, "A Paper and Plastic Device for Performing Recombinase Polymerase Amplification of Hiv DNA". *Lab Chip* **2012,** *12* (17), 3082-8.

122. M. Euler; Y. Wang; P. Otto; H. Tomaso; R. Escudero; P. Anda; F. T. Hufert; M. Weidmann, "Recombinase Polymerase Amplification Assay for Rapid Detection of Francisella Tularensis". *J Clin Microbiol* **2012,** *50* (7), 2234-8.

123. N. D. Grindley; K. L. Whiteson; P. A. Rice, "Mechanisms of Site-Specific Recombination". *Annu Rev Biochem* **2006,** *75*, 567-605.

124. A. Nern; B. D. Pfeiffer; K. Svoboda; G. M. Rubin, "Multiple New Site-Specific Recombinases for Use in Manipulating Animal Genomes". *Proc Natl Acad Sci U S A* **2011,** *108* (34), 14198-203.

125. R. N. Jones; K. C. Kugler; M. A. Pfaller; P. L. Winokur, "Characteristics of Pathogens Causing Urinary Tract Infections in Hospitals in North America: Results from the Sentry Antimicrobial Surveillance Program, 1997". *Diagn Microbiol Infect Dis* **1999,** *35* (1), 55-63.

126. A. C. Fluit; M. E. Jones; F. J. Schmitz; J. Acar; R. Gupta; J. Verhoef, "Antimicrobial Resistance among Urinary Tract Infection (Uti) Isolates in Europe: Results from the Sentry Antimicrobial Surveillance Program 1997". *Antonie Van Leeuwenhoek* **2000,** *77* (2), 147-52.

127. M. Gouy; S. Guindon; O. Gascuel, "Seaview Version 4: A Multiplatform Graphical User Interface for Sequence Alignment and Phylogenetic Tree Building". *Mol Biol Evol* **2010,** *27* (2), 221-4.

128. O. Clermont; S. Bonacorsi; E. Bingen, "Rapid and Simple Determination of the Escherichia Coli Phylogenetic Group". *Appl Environ Microbiol* **2000,** *66* (10), 4555-8.

129. A. G. Torres; S. M. Payne, "Haem Iron-Transport System in Enterohaemorrhagic Escherichia Coli O157:H7". *Mol Microbiol* **1997,** *23* (4), 825-33.

130. W. Zhang; Z. Niu; K. Yin; P. Liu; L. Chen, "Quick Identification and Quantification of Proteus Mirabilis by Polymerase Chain Reaction (Pcr) Assays". *Annals of Microbiology* **2013,** *63* (2), 683-689.

131. M. D. Island; H. L. Mobley, "Proteus Mirabilis Urease: Operon Fusion and Linker Insertion Analysis of Ure Gene Organization, Regulation, and Function". *J Bacteriol* **1995,** *177* (19), 5653-60.

132. S. D. Braun; S. Monecke; A. Thurmer; A. Ruppelt; O. Makarewicz; M. Pletz; A. Reibetaig; P. Slickers; R. Ehricht, "Rapid Identification of Carbapenemase Genes in Gram-Negative Bacteria with an Oligonucleotide Microarray-Based Assay". *PLoS One* **2014,** *9* (7), e102232.

133. C. Yin-Ching; S. Jer-Horng; L. Ching-Nan; C. Ming-Chung, "Cloning of a Gene Encoding a Unique Haemolysin from Klebsiella Pneumoniae and Its Potential Use as a Species-Specific Gene Probe". *Microb Pathog* **2002,** *33* (1), 1-6.

134. H. Shi; Q. Trinh; W. Xu; B. Zhai; Y. Luo; K. Huang, "A Universal Primer Multiplex Pcr Method for Typing of Toxinogenic Pseudomonas Aeruginosa". *Appl Microbiol Biotechnol* **2012,** *95* (6), 1579-87.

135. D. S. Toder; S. J. Ferrell; J. L. Nezezon; L. Rust; B. H. Iglewski, "Lasa and Lasb Genes of Pseudomonas Aeruginosa: Analysis of Transcription and Gene Product Activity". *Infect Immun* **1994,** *62* (4), 1320-7.

136. S. M. Naser; F. L. Thompson; B. Hoste; D. Gevers; P. Dawyndt; M. Vancanneyt; J. Swings, "Application of Multilocus Sequence Analysis (Mlsa) for Rapid Identification of Enterococcus Species Based on Rpoa and Phes Genes". *Microbiology* **2005,** *151* (Pt 7), 2141-50.

137. M. Zuker, "Mfold Web Server for Nucleic Acid Folding and Hybridization Prediction". *Nucleic Acids Res* **2003,** *31* (13), 3406-15.

138. J. SantaLucia, Jr., "A Unified View of Polymer, Dumbbell, and Oligonucleotide DNA Nearest-Neighbor Thermodynamics". *Proc Natl Acad Sci U S A* **1998,** *95* (4), 1460-5.

139. C. E. Musial; L. S. Tice; L. Stockman; G. D. Roberts, "Identification of Mycobacteria from Culture by Using the Gen-Probe Rapid Diagnostic System for Mycobacterium Avium Complex and Mycobacterium Tuberculosis Complex". *J Clin Microbiol* **1988,** *26* (10), 2120-3.

140. S. L. Moseley; I. Huq; A. R. Alim; M. So; M. Samadpour-Motalebi; S. Falkow, "Detection of Enterotoxigenic Escherichia Coli by DNA Colony Hybridization". *J Infect Dis* **1980,** *142* (6), 892-8.

141. Y. W. Tang; G. W. Procop; D. H. Persing, "Molecular Diagnostics of Infectious Diseases". *Clin Chem* **1997,** *43* (11), 2021-38.

142. U.S. Food and Drug Administration Clia Categorizations. http://www.fda.gov/MedicalDevices/DeviceRegulationandGuidance/IVDRegulatoryAssistance/ucm393229.htm (accessed September 20, 2014).

143. S. S. Ehrmeyer; R. H. Laessig, "Point-of-Care Testing, Medical Error, and Patient Safety: A 2007 Assessment". *Clin Chem Lab Med* **2007,** *45* (6), 766-73.

144. B. A. Forbes, "Introducing a Molecular Test into the Clinical Microbiology Laboratory: Development, Evaluation, and Validation". *Arch Pathol Lab Med* **2003,** *127* (9), 1106-11.

145. E. A. Mothershed; A. M. Whitney, "Nucleic Acid-Based Methods for the Detection of Bacterial Pathogens: Present and Future Considerations for the Clinical Laboratory". *Clin Chim Acta* **2006,** *363* (1-2), 206-20.

146. M. A. Dineva; L. MahiLum-Tapay; H. Lee, "Sample Preparation: A Challenge in the Development of Point-of-Care Nucleic Acid-Based Assays for Resource-Limited Settings". *Analyst* **2007,** *132* (12), 1193-9.

147. S. Raja; J. Ching; L. Xi; S. J. Hughes; R. Chang; W. Wong; W. McMillan; W. E. Gooding; K. S. McCarty, Jr.; M. Chestney; J. D. Luketich; T. E. Godfrey, "Technology for Automated, Rapid, and Quantitative Pcr or Reverse Transcription-Pcr Clinical Testing". *Clin Chem* **2005,** *51* (5), 882-90.

148. S. Tanriverdi; L. Chen; S. Chen, "A Rapid and Automated Sample-to-Result Hiv Load Test for near-Patient Application". *J Infect Dis* **2010,** *201 Suppl 1*, S52-8.

149. M. A. Poritz; A. J. Blaschke; C. L. Byington; L. Meyers; K. Nilsson; D. E. Jones; S. A. Thatcher; T. Robbins; B. Lingenfelter; E. Amiott; A. Herbener; J. Daly; S. F. Dobrowolski; D. H. Teng; K. M. Ririe, "Filmarray, an Automated Nested

Multiplex Pcr System for Multi-Pathogen Detection: Development and Application to Respiratory Tract Infection". *PLoS One* **2011,** *6* (10), e26047.

150. G. Desoubeaux; C. Franck-Martel; E. Bailly; C. Le Brun; E. Gyan; A. Goudeau; J. Chandenier; P. Lanotte, "Prospective Assessment of Filmarray(R) Technology for the Rapid Identification of Yeast Isolated from Blood Cultures". *J Microbiol Methods* **2014,** *106c*, 119-122.

151. M. M. Bhatti; S. Boonlayangoor; K. G. Beavis; V. Tesic, "Evaluation of Filmarray and Verigene Systems for Rapid Identification of Positive Blood Cultures". *J Clin Microbiol* **2014,** *52* (9), 3433-6.

152. M. Paolucci; C. Foschi; M. V. Tamburini; S. Ambretti; T. Lazzarotto; M. P. Landini, "Comparison between Maldi-Tof Ms and Filmarray Blood Culture Identification Panel for Rapid Identification of Yeast from Positive Blood Culture". *J Microbiol Methods* **2014,** *104*, 92-3.

153. K. H. Rand; J. P. Delano, "Direct Identification of Bacteria in Positive Blood Cultures: Comparison of Two Rapid Methods, Filmarray and Mass Spectrometry". *Diagn Microbiol Infect Dis* **2014,** *79* (3), 293-7.

154. O. Altun; M. Almuhayawi; M. Ullberg; V. Ozenci, "Clinical Evaluation of the Filmarray Blood Culture Identification Panel in Identification of Bacteria and Yeasts from Positive Blood Culture Bottles". *J Clin Microbiol* **2013,** *51* (12), 4130-6.

155. W. Y. Jin; S. J. Jang; M. J. Lee; G. Park; M. J. Kim; J. K. Kook; D. M. Kim; D. S. Moon; Y. J. Park, "Evaluation of Vitek 2, Microscan, and Phoenix for

Identification of Clinical Isolates and Reference Strains". *Diagn Microbiol Infect Dis* **2011,** *70* (4), 442-7.

156. C. R. Woese; G. E. Fox, "Phylogenetic Structure of the Prokaryotic Domain: The Primary Kingdoms". *Proc Natl Acad Sci U S A* **1977,** *74* (11), 5088-90.

157. J. M. Janda; S. L. Abbott, "16s Rrna Gene Sequencing for Bacterial Identification in the Diagnostic Laboratory: Pluses, Perils, and Pitfalls". *J Clin Microbiol* **2007,** *45* (9), 2761-4.

158. L. Carrara; F. Navarro; M. Turbau; M. Seres; I. Moran; I. Quintana; R. Martino; Y. Gonzalez; A. Brell; O. Cordon; K. Diestra; C. Mata; B. Mirelis; P. Coll, "Molecular Diagnosis of Bloodstream Infections with a New Dual-Priming Oligonucleotide-Based Multiplex Pcr Assay". *J Med Microbiol* **2013,** *62* (Pt 11), 1673-9.

159. O. Kommedal; K. Simmon; D. Karaca; N. Langeland; H. G. Wiker, "Dual Priming Oligonucleotides for Broad-Range Amplification of the Bacterial 16s Rrna Gene Directly from Human Clinical Specimens". *J Clin Microbiol* **2012,** *50* (4), 1289-94.

160. H. Y. Wang; S. Kim; J. Kim; S. D. Park; Y. Uh; H. Lee, "Multiplex Real-Time Pcr Assay for Rapid Detection of Methicillin-Resistant Staphylococci Directly from Positive Blood Cultures". *J Clin Microbiol* **2014,** *52* (6), 1911-20.

161. A. Dmitriev; M. Bhide; I. Mikula, "Cpn60 Gene-Based Multiplex-Pcr Assay for Simultaneous Identification of Streptococcal Species". *Acta Veterinaria Brno* **2006,** *75* (2), 235-240.

162. M. C. Thaller; F. Berlutti; S. Schippa; G. Lombardi; G. M. Rossolini, "Characterization and Sequence of Phoc, the Principal Phosphate-Irrepressible Acid Phosphatase of Morganella Morganii". *Microbiology* **1994,** *140 (Pt 6)*, 1341-50.

163. P. G. Higgins; F. J. Perez-Llarena; E. Zander; A. Fernandez; G. Bou; H. Seifert, "Oxa-235, a Novel Class D Beta-Lactamase Involved in Resistance to Carbapenems in Acinetobacter Baumannii". *Antimicrob Agents Chemother* **2013,** *57* (5), 2121-6.

164. A. Roggenkamp, "Phylogenetic Analysis of Enteric Species of the Family Enterobacteriaceae Using the Oric-Locus". *Syst Appl Microbiol* **2007,** *30* (3), 180-8.

165. M. Otto, "Staphylococcus Epidermidis--the 'Accidental' Pathogen". *Nat Rev Microbiol* **2009,** *7* (8), 555-67.

APPENDIX I - CLINICAL SAMPLES USED IN FILMARRAY STUDY

#	DATE	ID#	FILM ARRAY RESULTS	CULTURE RESULTS	CONCORDANCE/PARTIAL CONCORDANCE
1	1/24/2014	422187	*Candida glabrata*	No pathogens	YES
2	1/24/2014	348268	*K. pneumoniae, Proteus*	Mixed with genital flora	
3	1/24/2014	196582	NONE DETECTED	NO GROWTH	YES
4	1/24/2014	426239	*E. coli, K. pneumoniae*	NO PATHOGENS	
5	1/24/2014	295267	NONE DETECTED	NO GROWTH	YES
6	1/24/2014	213965	*E. coli*	NO GROWTH	
7	1/24/2014	204290	*E. coli, Proteus*	*E. coli*	YES
8	1/24/2014	149387	NONE DETECTED	NO GROWTH	YES
9	1/27/2014	466915	*K. pneumoniae*	*K. pneumoniae*	YES
10	1/24/2014	468179	*E. coli, P. aeruginosa, Candida glabrata*	*E. coli*	YES
11	1/24/2014	349220	*K. pneumoniae*	*K. pneumoniae*	YES
12	1/24/2014	460990	NONE DETECTED	NO GROWTH at 24 hours; <10,000 CFU/mL-rods	YES
13	1/24/2014	405665	*E.coli, Proteus, Candida glabrata*	*P. mirabilis*	YES
14	1/24/2014	429754	*Candida albicans*	NO GROWTH	YES
15	1/24/2014	306194	NONE DETECTED	NO GROWTH	YES
16	1/24/2014	94231	NONE DETECTED	NO GROWTH	YES
17	1/26/2014	473305	*Enterococcus*	NO GROWTH	
18	1/27/2014	472923	NONE DETECTED	NO GROWTH	YES
19	1/26/2014	486828	*E. coli, Proteus, Staphylococcus* (*mecA*)	*E. coli*	YES
20	1/26/2014	230976	NONE DETECTED	NO GROWTH	YES

21	1/27/2014	207049	NONE DETECTED	NO GROWTH	YES
22	1/26/2014	456777	NONE DETECTED	NO GROWTH	YES
23	1/26/2014	473268	*E. coli, S. agalactiae, Candida*	*E. coli*	YES
24	1/27/2014	445095	*E. coli*	*E. coli, Enterococcus*	YES
25	1/26/2014	113931	*S. agalactiae, Proteus*	*P. mirabilis*	YES
26	1/26/2014	339926	*E. coli, Proteus, Candida*	*E. coli*	YES
27	1/26/2014	636363	*Enterococcus, Proteus, S. aureus*	*Enterococcus, P. mirabilis*	YES
28	1/26/2014	365298	*E. coli*	*E. coli*	YES
29	1/26/2014	280435	NONE DETECTED	NO GROWTH	YES
30	1/26/2014	135100	NONE DETECTED	E.coli, Enterococcus	
31	1/26/2014	94072	*K. pneumoniae*	*K. pneumoniae*	YES
32	1/26/2014	445470	*Streptococcus, Van A/B Enterococcus*	*Enterococcus*	YES
33	1/26/2014	231730	*Enterococcus, E. coli*	*E. coli*	YES
34	1/26/2014	355322	NONE DETECTED	NO GROWTH	YES
35	1/26/2014	463054	*Candida albicans*	NONE DETECTED	YES
36	1/26/2014	473275	NONE DETECTED	NO GROWTH	YES
37	1/26/2014	387185	*E. coli*	NO GROWTH	
38	1/31/2014	453240	INVALID	Group D. Not *Enterococcus*	
39	1/31/2014	414763	*E. coli*	Organism mixed with urogenital flora	
40	1/31/2014	452542	*E. coli, P. aeruginosa, Candida glabrata*	*Enterococcus, E. coli*	YES
41	1/31/2014	385312	NONE DETECTED	*Enterococcus*, 20,000CFU	
42	1/31/2014	123349	NONE DETECTED	*Streptococcus, Staphylococcus* <10,000	

43	1/31/2014	467440	NONE DETECTED	NO GROWTH	YES
44	1/31/2014	250960	*E. coli, K. oxytoca, K. pneumoniae, Proteus, Candida*	*P. mirabilis, Enterococcus*	YES
45	1/31/2014	174305	*K. pneumoniae*	*K. pneumoniae*	YES
46	1/31/2014	408921	NONE DETECTED	Staph coagulase positive	
47	2/3/2014	138875	*Enterococcus, E. coli, Proteus*	*P. stuartii*	
48	2/3/2014	473474	*Enterococcus, K. pneumoniae*	Multiple organisms	
49	2/3/2014	473506	*E.coli*	*E.coli*	YES
50	2/3/2014	423224	NONE DETECTED	*Enterococcus*	
51	2/3/2014	473543	*Enterococcus, E. coli*	Multiple organisms	
52	2/3/2014	115939	*K. pneumoniae*	*K. pneumoniae*	YES
53	2/3/2014	372471	*E. coli*	*E. coli*	YES
54	2/3/2014	235144	*K. pneumoniae*	*K. pneumoniae*	YES
55	2/3/2014	461585	*Proteus, E. coli*	*Proteus, E. coli*	YES
56	2/4/2014	256874	*S. agalactiae*	*S. agalactiae*	YES
57	2/4/2014	18266	NONE DETECTED	NO GROWTH	YES
58	2/4/2014	174118	*S. agalactiae, Enterobacter cloacae, K. pneumoniae*	Multiple organisms	YES
59	2/4/2014	367653	*Enterococcus, Proteus*, VAN A/B	*Enterococcus*	YES
60	2/4/2014	468609	*Candida albicans, Candida tropicalis*	Yeast	YES
61	2/4/2014	475387	*P. aeruginosa*	*Acinetobacter lwoffii*	
62	2/4/2014	173335	*E. coli, P. aeruginosa*	*E. coli*	YES
63	2/4/2014	329444	*E. coli, K. oxytoca*	*E. coli*	YES
64	2/4/2014	128147	*E. coli*	*E. coli*	YES
65	2/4/2014	325900	*E. coli*	*E. coli*	YES
66	2/4/2014	418698	*P. aeruginosa, Enterococcus, S. aureus*	*P. aeruginosa*	YES

67	2/5/2014	474182	*Candida glabrata*	*P. aeruginosa*	
68	2/5/2014	475764	*Proteus*	*P. mirabilis*	YES
69	2/5/2014	343608	NONE DETECTED	*Enterococcus* 10,000-19,999	
70	2/5/2014	468235	*P. aeruginosa, S. aureus mecA*	*P. aeruginosa, Enterococcus*	YES
71	2/5/2014	419765	*Enterococcus, Streptococcus*	*Enterococcus*	YES
72	2/5/2014	95368	*E. coli, K. pneumoniae, P. aeruginosa, S. aureus*	*K. pneumoniae*	YES
73	2/5/2014	125336	*Proteus*	*P. mirabilis*	YES
74	2/5/2014	469306	*Enterococcus VAN A/B, Candida glabrata*	*Enterococcus*	YES
75	2/5/2014	127969	*Proteus*	*P. mirabilis*	YES
76	2/6/2014	98339	*E. coli*	*E. coli*	YES
77	2/6/2014	467973	*P. aeruginosa, E. coli*	*E. coli*	YES
78	2/6/2014	478177	*E.coli, S. aureus mecA*	*E.coli, S. aureus*	YES
79	2/6/2014	402178	*Enterococcus*	NO GROWTH	YES
80	2/6/2014	475981	NONE DETECTED	NO GROWTH	YES
81	2/6/2014	346187	*Proteus*	*P. mirabilis*	YES
82	2/6/2014	284076	NONE DETECTED	NO GROWTH	YES
83	2/6/2014	384988	*E. coli, S. agalactiae*	*E. coli*	YES
84	2/6/2014	396692	*Candida albicans*	NO GROWTH	YES
85	2/6/2014	414881	*E. coli, C. albicans*	*E. coli*	YES
86	2/12/2014	201371	*E. coli*	*E. coli*	YES
87	2/12/2014	130283	*Enterococcus VAN A/B, Streptococcus*	*Enterococcus*	YES
88	2/12/2014	478351	*Candida albicans, Candida glabrata*	NO GROWTH	
89	2/12/2014	253473	NONE DETECTED	NO GROWTH	YES

90	2/12/2014	479190	*K. pneumoniae*	*K. pneumoniae*	YES
91	2/12/2014	478663	*Proteus, C. albicans*	*P. mirabilis*	YES
92	2/12/2014	459587	*Enterococcus, P. aeruginosa, K. pneumoniae*	*P. aeruginosa, K. pneumoniae*	YES
93	2/12/2014	242525	*E. coli*	*E. coli*	YES
94	2/12/2014	477616	*Staphylococcus mecA*	*Enterococcus*	
95	2/12/2014	449575	*Enterococcus, E.coli, K. pneumoniae, Proteus*	Mixed with urogenital flora	
96	2/12/2014	469264	*K. pneumoniae*	*E. faecalis, K. pneumoniae*	YES
97	2/12/2014	392331	*E. coli*	*E. coli*	YES
98	2/12/2014	466832	*E. coli*	*E. coli*	YES
99	2/12/2014	472906	*Enterococcus, Proteus, P. aeruginosa*	*Enterococcus, P. mirabilis*	YES
100	2/12/2014	422796	*E.coli, K. pneumoniae, Candida glabrata*	*E. faecalis, E. coli*	YES
101	2/12/2014	128266	*S. aureus mecA, E. coli*	S. *aureus*	YES
102	2/12/2014	401192	*Proteus*	*P. mirabilis*	YES
103	2/12/2014	439610	*P. aeruginosa*	*P. aeruginosa*	YES
104	2/12/2014	479060	NONE DETECTED	Enterococcus	YES
105	2/12/2014	386180	*E. coli*	*E. coli*	YES
106	2/12/2014	128245	*E. coli*	*E. coli*	YES
107	2/12/2014	370668	*Enterococcus*	*Enterococcus*	YES
108	2/12/2014	94477	*E. coli*	*E. coli*	YES
109	2/12/2014	148868	*K. pneumoniae*	*K. pneumoniae*	YES